Universität Potsdam
Universitätsverlag Potsdam

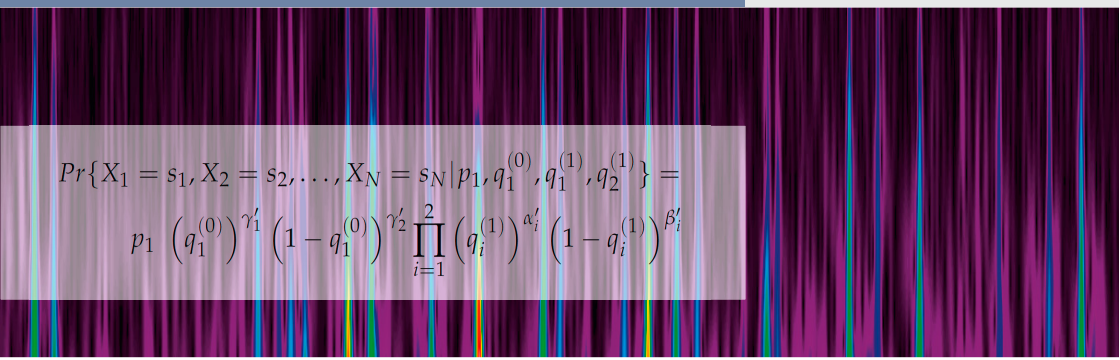

Mario Bettenbühl

Microsaccades

Symbols in fixational eye movements

Potsdam Cognitive Science Series | 5

Potsdam Cognitive Science Series | 5

Mario Bettenbühl

Microsaccades

Symbols in fixational eye movements

Universitätsverlag Potsdam

Bibliografische Information der Deutschen Nationalbibliothek
Die Deutsche Nationalbibliothek verzeichnet diese Publikation in der Deutschen Nationalbibliografie; detaillierte bibliografische Daten sind im Internet über http://dnb.dnb.de/ abrufbar.

Universitätsverlag Potsdam 2015
http://verlag.ub.uni-potsdam.de/

Am Neuen Palais 10, 14469 Potsdam
Tel.: +49 (0)331 977 2533 / Fax: 2292
E-Mail: verlag@uni-potsdam.de

Die Schriftenreihe **Potsdam Cognitive Science Series** wird herausgegeben von Johannes Haack, Dr. Christiane Wotschack und Michael Dambacher

Zugl.: Potsdam, Univ., Diss., 2012
Gutachter: Prof. Dr. Matthias Holschneider
Tag der mündlichen Verteidigung: 23.10.2012

ISSN (print) 2190-4545
ISSN (online) 2190-4553

Druck: docupoint GmbH Magdeburg
Satz: le-tex publishing services GmbH, Leipzig

Online veröffentlicht auf dem Publikationsserver der Universität Potsdam
URN urn:nbn:de:kobv:517-opus-72622
http://nbn-resolving.de/urn:nbn:de:kobv:517-opus-72622

Zugleich gedruckt erschienen im Universitätsverlag Potsdam
ISBN 978-3-86956-122-6

Acknowledgments

I am very grateful to my advisors Prof. Matthias Holschneider and Prof. Ralf Engbert who provided me with an inspiring environment and supported me in discussions and questions related to the work in this thesis. Being part of this overwhelmingly interdisciplinary research group on mind and brain dynamics at the University of Potsdam was an irreplaceable opportunity which I am most thankful to have been granted. I learned a lot in the frequent exchanges of opinion and methods in different scientific fields.

Likewise, I thank the members of the research group, the department of psychology and biological psychology and the focus area for dynamics of complex systems for animated discussions, talks and seminars. In particular, I thank Petra Sinn for her collaboration on the test lens experiment design as well as Konstantin Mergenthaler and Hans A. Trukenbrod for the offer to use their acquired data. I thank Marco Rusconi for the many sessions on our blackboard and Hannes Matuschek for his help in programming.

I am thankful to Stefan Schinkel, Udo Schwarz, Hannes Matuschek, Michael Hayn and Marcel Fuhrmann for the many style suggestions and Jessica Mann for proof-reading and correcting numerous errors.

I wish to thank all my friends who kept in touch with me throughout the years despite my being an only occasional presence in their lives. I want to express my deepest gratitude to my family, my mum, my sister and my grandparents and I am very happy that they were able to witness the path I chose. I wish to honor my father, who could not witness my path but provided me with the attitude to go my own way.

With all my heart, I thank my love Carolina, who provided me with balance during these recent years, showed her everlasting belief in me, supported me and was patient with me.

Contents

Abstract

The first thing we do upon waking is open our eyes. Rotating them in our eye sockets, we scan our surroundings and collect the information into a picture in our head. Eye movements can be split into saccades and fixational eye movements, which occur when we attempt to fixate our gaze. The latter consists of microsaccades, drift and tremor. Before we even lift our eye lids, eye movements – such as saccades and microsaccades that let the eyes jump from one to another position – have partially been prepared in the brain stem. Saccades and microsaccades are often assumed to be generated by the same mechanisms. But how saccades and microsaccades can be classified according to shape has not yet been reported in a statistical manner. Research has put more effort into the investigations of microsaccades' properties and generation only since the last decade. Consequently, we are only beginning to understand the dynamic processes governing microsaccadic eye movements.

Within this thesis, I aim to assess the dynamics governing the generation of microsaccades and model the underlying processes. I will use eye movement trajectories from different experiments, recorded with a video-based eye tracking technique, and propose a novel method for the scale-invariant detection of saccades (events of large amplitude) and microsaccades (events of small amplitude). Using a time-frequency approach, I examined the method with different experiments and validated it against simulated data. I suggest a shape model that allows for a simple estimation of saccade- and microsaccade related properties. For sequences of microsaccades, I conclude this thesis by the proposal of a time-dynamic Markov model, with a memory horizon that changes over time and which can best describe sequences of microsaccades.

1 Introduction

The complexity of the human brain and nervous system is the subject of many different research areas. Attempts have been made to at least partially model its complex, often nonlinear behavior. Vision research focuses on reading, perception, and visual attention. Every human executes eye movements to read, for example, this thesis and is half-aware of the movements because, while each word needs to be read, some words are unconsciously skipped. To investigate these movements and, for example, understand why some words are skipped, recordings of *eye movements* and/or *electroencephalography* (EEG) measurements are studied. Whereas eye movements allow a direct access to the eyes' trajectories during different tasks, eye movements in EEG are measured by electrical potentials which occur whenever the eye is moved.

In natural viewing, two different patterns continually alternate: *saccades* and *visual fixations*. A *saccade* moves the eye from one position to another and can be identified by its high-velocity. In a *fixation*, the eyes appear to be motionless at a single spot. They seem to be at rest, however almost three centuries ago Jurin (1738) proposed the existence of eye movements during fixation on a tiny target. Darwin and Darwin (1786) were the first to empirically show that our eyes move during fixations. Paradoxically, this continuous motion during fixation is called *fixational eye movements* (FEM). In Adler and Fliegelman (1934), three different components were identified and Ratliff and Riggs (1950) gave a widely-accepted classification that was dependent upon different sizes of amplitude:

- small-scale oscillations
- a slow, diffusive-like movement
- a ballistic jump-like movement

These three components are referred to as *tremor*, *drift*, and *microsaccades* (Martinez-Conde, Macknik & Hubel, 2004; Rolfs, 2009; Liversedge, Gilchrist & Everling, 2011).

In this thesis, I set out to understand the stochastic aspect of generating mechanisms of microsaccades. Using a wavelet based approach for saccade and microsaccade detection, I will be able to detect both movements at once. A statistical analysis of microsaccade and saccade shapes can return the characteristics of both and simplify subsequent analyses. In the last two decades, eye movement research focused on the last component of fixational eye movements – microsaccades. There is an ongoing debate regarding whether they serve a specific purpose (Kowler & Steinman, 1979; Collewijn & Kowler, 2008) and how a process could possibly generate them (Desbordes & Rucci, 2007; Engbert, Mergenthaler, Sinn & Pikovsky, 2011; Hafed, Goffart & Krauzlis, 2009; Otero-Millan, Macknik, Serra, Leigh & Martinez-Conde, 2011; Rolfs, Kliegl & Engbert, 2008). Whether they play any important role in fixational eye movements or not, might be answered by an explanation of the generating process of microsaccades. Often, approaches to understand natural phenomena include mathematical models. Well-suited to describe the observations, they offer an optimal description of the data, allowing researchers to test different hypotheses against a well-defined theoretical model. Additionally, to arrive at "the best" fitting model for the data, the data analysis should also be optimal. For microsaccade detection, velocity-based algorithms (Engbert & Kliegl, 2003b) and detection by hand are the most prominent methods, with the former dominating because of the huge data sets recently available from video-based eye trackers (cf. Chapter 1.5).

For the purpose of my investigation, I will provide a brief introduction in the first chapter to human eye movements, which follow multiple nonlinear rules which will be disentangled step by step. In the second chapter, I present a scale-free saccade detection method for saccades of all amplitudes, based on the continuous wavelet transform (Holschneider, 1995). A statistical (micro)saccade shape model yields a simple way to investiate microsaccade properties.

The third chapter presents how to arrive at such a model with the principal component analysis (Jolliffe, 2002). Finally, in the fourth chapter, I represent microsaccades as particular symbols which can be investigated using Markov processes (Taylor & Karlin, 1984), Bayes factor model selection (Kass & Raftery, 1995) and symbolic dynamics (Lind & Marcus, 1995). Finally, a stochastic model for the generation of microsaccade directions is proposed. The thesis will be concluded in the fifth chapter and the new findings will be discussed in the context of previous findings. At the beginning of every chapter, I will briefly introduce the mathematical concepts used for the particular chapter and review existing concepts.

Although the methods proposed and developed in this work are primarily used for data from eye movements, they might prove to be useful for a broad class of complex systems. The method for distinguishing different Markov orders through the use of a discrete-time symbol mapping and Bayes factor also allows the characterization of underlying generating processes for biological or neurological data such as neural spike trains (Rieke, Warland & Bialek, 1997). The detection method demonstrated its applicability to be used as "black-box" for the detection of microsaccades and saccades. Particularly for EEG studies, the eye movements cause artifacts in recordings of electric potentials. The wavelet method could be used by researchers whose main interest is not the study of eye movements but who are currently "cursed" to optimize a threshold multiplier to optimally detect (micro)saccades in the velocity space (Engbert & Kliegl, 2003a; Engbert & Mergenthaler, 2006).

1.1 Eye movements and fixational eye movements

Since ancient times, vision has been considered one of the five human senses (Aristotle, 384 BC–322 BC). The human eyes move constantly to perceive the surrounding visual world, explore scenes, read or perceive of surroundings. Most activities of our visual

system require our eyes to be moved from one point to another point in a scene or from one word to another.

Studies in both *passive* and *active vision* examine eye movements. Yet, studies in passive vision investigate the duration or appearance of movements whereas active vision looks into the generation and integration of these movements at the physiological level by e. g., muscle contraction (J. M. Findlay & Gilchrist, 2003). In this thesis, eye movement trajectories are examined in the context of passive vision.

Under laboratory conditions, with an immobile viewer looking at a scene in a fixed position, the eye movement can be separated into two major and disjunct modes: *saccadic eye movement* and *fixation* (Land, Mennie & Rusted, 1999; Land & Nilsson, 2002). Below or above conscious awareness, these small-sized (see Land et al., 1999, between 18–20° visual angle in daily tasks), ballistic movements occur at approximately the same time, conjugated in both eyes. *Saccades* are present in both movement directions of the eyes: the *horizontal* and *vertical* dimensions and oblique directions in a mixture of both. Their amplitude and peak-velocity are measures which are mutually linked in a linear fashion and referred to as *main sequence* (Zuber, Stark & Cook, 1965). Importantly, this relationship holds for saccades of all scales of amplitude.

The time intervals between saccades are referred to as *fixation*, in which the eye stationary rests at one point. Photoreceptors of the retina, the cells that transform visual input into electrical potentials processable by the brain (cf. Figure 1.1), continuously receive activation during saccades and fixations, while visual processing during saccades is suppressed (Thilo, Santoro, Walsh & Blakemore, 2004). A saccade moves the eye such that, while visually inspecting something, the point of interest the visual input is reflected to one spot on the retina with highest resolution, the *fovea centralis* or *foveal region*.[1]

[1]The *foveal region* refers to that part of the retina (cf. Figure 1.1) with highest spatial resolution, originating from the highest density of cone photoreceptors (those secondary receptors to "convert" visual input to electrical potentials).

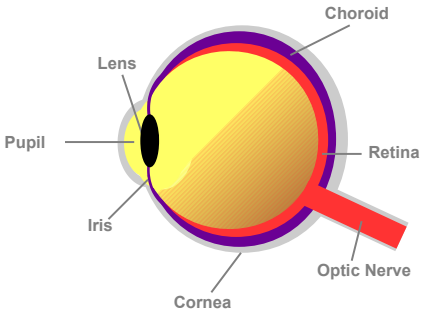

Figure 1.1: Illustration of the anatomy of the eye. *An image-at-view is upside-down and reversely projected onto the retina.*

Visual fixation is the basis for perception of a stationary target object. Jurin (1738) proposed the existence of tiny eye movements during fixation. Then, von Helmholtz (1867) showed that our eyes constantly move during fixation to continually produce input and proposed that these movements are essential to prevent retinal fatigue. In the 1950s and early 1960s, the eyes were artificially stabilized in a laboratory experiment and it was demonstrated that stationary objects rapidly fade from perception (Ditchburn & Ginsborg, 1952; Pritchard, 1961; Riggs, Ratliff, Cornsweet & Cornsweet, 1953). The adaptation of retinal receptor systems to constant input causes such perceptual bleaching and can occur rapidly (Coppola & Purves, 1996). Therefore, while our eyes fixate a stimulus to visually analyze fine details, miniature eye movements have to be produced to counteract the described perceptual fading. The term *fixational eye movements* was introduced to describe this seemingly paradoxical behavior. The perceptual performance, a function of self-generated noise, is an unimodal function which lends support to the underlying nonlinear mechanisms (Starzynski & Engbert, 2009).

Fixational eye movements consist of three components: *tremor*, *drift* and *microsaccades* (e. g., Ciuffreda & Tannen, 1995; Martinez-Conde et al., 2004; Rolfs, 2009). *Tremor* is a rapid irregular movement, which is superimposed on the drift in fixational eye move-

ments. Tremor was reported by Adler and Fliegelman (1934) for the first time and nowadays is reported with amplitudes between 1.6×10^{-3} to 8.3×10^{-3} degree visual angle (Ratliff & Riggs, 1950). Tremor occurs at very high frequencies, varying between 0–100 Hz (Eizenman & Hallett, 1985), between 30–100 Hz (Adler & Fliegelman, 1934; Higgins, 1953; Ratliff & Riggs, 1950) and more recently from 70–103 Hz (Bolger, Bojanic, Sheahan, Coakley & Malone, 1999), as governed by the different recording techniques used through the studies. Not the frequency but instead the small extent of this micromovement of the eye demands a technique with high spatial resolution. Piezoelectronic devices are used to measure these tiniest of eye movements, which includes eye contact with the apparatus. For non-contact recordings, setups like the Purkinje eye trackers which use reflections from the front of the cornea and the back of the lens to track the eye position (Crane & Steele, 1985), or laser interferometry are chosen (for an overview of different devices, see Collewijn, 1998). The video-based eye tracking device used to record the trajectories this thesis investigated for eye movements are not capable of recording these movements. Instead, the video-based eye tracking can – in addition to microsaccades – record the *drift* movements on which tremor is superimposed. This slow eye movement is erratic and occurs in the intermicrosaccadic intervals in the trajectory of fixational eye movements, i. e., recordings with the video-based system contain intervals of drifts and microsaccades. In a fixation task, the amplitude of drift movements ranges from 0.016° to 0.13° at slow velocity of $0.5^\circ/s$ whereas in natural viewing conditions, higher velocities have been measured (Deubel & Bridgeman, 1995). Mostly, drift was described as completely random process (Cornsweet, 1956) and random walk (Matin, Matin & Pearce, 1970). Investigations by Ditchburn and Ginsborg (1952) and Nachmias (1959) suggested that drift movements are – at least with regard to direction – not random. J. Findlay (1971) modeled both tremor and drift as a white-noise like signal. More recently, Mergenthaler and Engbert (2007) modeled fixational eye movements and, in particular, the drift movement by a fractional

Brownian motion in two different time regimes. For short time scales (< 100 ms), in order to counteract visual fading, persistent behavior enhances retinal image slip whereas on longer time scales (> 100 ms) fixation is stabilized by antipersistent behavior. The behavior of this model for short time scales and the work by Engbert and Kliegl (2004) motivated a successive work from Engbert et al. (2011), in which fixational eye movements altogether are modeled by a self-avoiding random walk model that includes drift and microsaccadic eye movements.

The fastest component of fixational eye movements, up to 1° visual angle (Rolfs, 2009), is produced by *microsaccades* which are high-velocity movements with the largest amplitudes. Microsaccades are movements sharing a fixed relation between amplitude and peak velocity. Furthermore, they do – alongside saccades – appear in the *main sequence* (Zuber et al., 1965) which constitutes a linear relation between the peak velocity and amplitude of the events and saturation of velocities for saccades larger than 10° (Bahill, Clark & Stark, 1975; M. Harris & Wolpert, 2006). This thesis deals in particular with microsaccades, their detection, shape classification and dynamics and I will review their characteristics, findings and importance for fixational eye movements in an extra section but first review findings on saccades, which are closely related to microsaccades.

1.2 Saccades

The term "*saccade*" can be credited to Louis Émile Javal (Javal, 1879; Wade & Tatler, 2005), who was the first to call a jump-like movement during reading that way. He was referring to an experiment performed by Lamare and published years later in Lamare (1892). In the English translation given in Wade and Tatler (2005, p. 137), the first experiment he performed to investigate saccades is described as follows: "[...] The first method was based on counting: he counted the number of letters he could read in one minute and divided that by the estimated number of pauses made. The average

value he arrived at was ten letters per saccade. [...]". Nowadays, having high-precision techniques to track eye movements, we know that a normal saccade amplitude ranges between 18–20° during an everyday task (Land et al., 1999). In a condition reproducible in the laboratory, saccades are typically of 2° amplitude for reading and 5° amplitude for scene perception (Abrams, Meyer & Kornblum, 1989; Rayner, 1978). These ballistic, binocularly-occurring eye movements have a particular shape which can occur in both directions, horizontal and vertical, and be illustrated as a jump in the trajectory of the eye movement, i. e., an abrupt change in position across time (Kowler, 2011). Investigating the trajectory of the eye movements, the oculomotor system can indirectly be studied. Saccades, occurring 3 to 4 times each second in most natural viewing tasks, have a strong relationship between their peak-velocity and amplitude, the *main sequence* (Zuber et al., 1965). The latter also determines the typical duration of a saccadic eye movement. A typical saccade shape is described as follows: "After an initial stationary rest of the eye, it accelerates to a maximal velocity just before it rapidly reduces its pace to again rest at the new position" (adapted from J. M. Findlay & Gilchrist, 2003). Furthermore, a saccade can directly reach the intended target position (a *normometric* or *orthometric* saccade) or move the eye too short (*hypometric*) or beyond the target position (*hypermetric*) (Ciuffreda & Tannen, 1995). Typically, saccades show another type of overshoot, a so-called *dynamic overshoot*. The eye surpasses the target position and then quickly reverses to the former to arrive at the final target position. Ciuffreda and Tannen (1995) suggested that "[...] this latter movement may represent a 'time optimal' behavior that places the target within the general foveal region as rapidly as possible [...]" – referring to the dynamical overshoot (see also C. M. Harris & Wolpert, 1998). We will now see, how many of these properties also apply to microsaccades or "saccades during fixation" and how they vary in their shape, with respect to microsaccades.

1.3 Microsaccades

The largest component of fixational eye movements is produced by *microsaccades*, which are high-velocity movements with small amplitudes (compared to saccades). Their name originates from their resemblance to saccades, which are present in eye movements and which, in principle, separate single fixations. I will call saccades during fixation the *microsaccades* and I will refer to saccadic eye movements of all amplitudes as *saccades*. Later, we will see that a separation in size between both different scale saccadic eye movements is not easily done and discussed through the whole vision research community. The sizes of microsaccades were reported by Adler and Fliegelman (1934) for the first time. They vary between 0.01° to 2° but their main range is from 0.1° to 0.5° (Engbert, 2006b; Otero-Millan, Troncoso, Macknik, Serrano-Pedraza & Martinez-Conde, 2008; Hermens & Walker, 2010). Microsaccades occur 1 to 2 times per second and, with similar direction and amplitude, occur at approximately the same time in both eyes (Møller, Laursen, Tygesen & Sjølie, 2002; Schulz, 1984).

Following Zuber et al. (1965), a prototypical microsaccade shape is given in Figure 1.2. Here, the horizontal eye movement is plotted versus time. Upward and downward deflections denote rightward and leftward directed eye movements. In this example, the trajectory shows that, after an initial period of rest, the eye moves quickly towards the right, which then is followed by a small leftward movement before arriving at the new horizontal position. The illustration depicts three important characteristics of microsaccades: *amplitude*, *displacement*, and *overshoot*. The last is also often called dynamic overshoot (Kapoula, Robinson & Hain, 1986), referring to a small saccade immediately following a large saccade during "normal viewing." These dynamic overshoot saccades are mostly considered part of the preceding saccade (Møller et al., 2002; Otero-Millan et al., 2008; Troncoso, Macknik & Martinez-Conde, 2008) and do not count as another saccadic movement. I will solely use the term *overshoot* as depicted in Figure 1.2 and, if not clear by context, name

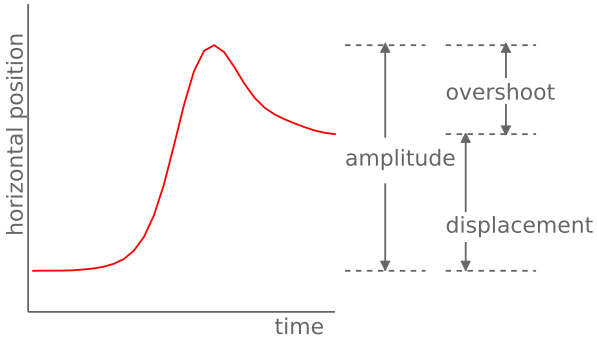

Figure 1.2: Illustration of microsaccades' properties. *A trajectory of a microsaccade plotted over time has three distinctive measures: displacement, overshoot and, as sum of both, the amplitude.*

its origin. The maximum deflection is referred to as *amplitude*; the difference between amplitude and overshoot the *displacement*. Thus, the distinction between amplitude and displacement is due to variations in the overshoot component and is relevant to kinematic as well as functional aspects of microsaccades.

Recent findings demonstrated various neural, perceptual and behavioral functions of microsaccades (Martinez-Conde et al., 2004; Martinez-Conde, Macknik, Troncoso & Hubel, 2009; Rolfs, 2009). The relevance of microsaccades for various neural and cognitive systems offers a possible explanation for the difficulties in identifying a specific function for microsaccades (for recent overviews see Martinez-Conde et al., 2004; Rolfs, 2009; Liversedge et al., 2011). I will now provide in a short list a brief review of recent findings about the functions of microsaccades (adapted from Bettenbühl et al., 2010):

Perception
Microsaccades are important for peripheral vision. During the perception of bistable visual scenes, microsaccades induce tran-

sitions to visibility and counteract transitions to perceptual fading (Engbert, 2006a; Martinez-Conde, Macknik, Troncoso & Dyar, 2006; Rucci, Iovin, Poletti & Santini, 2007). Moreover, fixational eye movements and microsaccades present noise sources that enhance perception (Starzynski & Engbert, 2009). Also during fixation, microsaccades support second-order visibility (Troncoso et al., 2008).

Attention
Microsaccades can be suppressed voluntarily with focused attention (Bridgeman & Palca, 1980; Gowen, Abadi & Poliakoff, 2005). They are also modulated by crossmodal attention with a pronounced signature in both rate and orientation (e. g., Engbert & Kliegl, 2003b; Galfano, Betta & Turatto, 2004; Hafed & Clark, 2002; R. Laubrock, Engbert & Kliegl, 2005; Rolfs, Engbert & Kliegl, 2005). The hypothesis that microsaccades represent an index of covert attention has been criticized by Horowitz, Fine, Fencsik, Yurgenson and Wolfe (2007) (but see Horowitz, Fencsik, Fine, Yurgenson & Wolfe, 2007; J. Laubrock, Engbert, Rolfs & Kliegl, 2007). However, new work by J. Laubrock, Kliegl, Rolfs and Engbert (2010) lends support to the coupling between attention and microsaccades.

Saccadic latency
Microsaccades interact with upcoming saccadic responses, which can result in prolonged as well as shortened latencies for saccadic reactions (Rolfs, Laubrock & Kliegl, 2006). Recently, Sinn and Engbert (2011) demonstrated that this effect contributes to the saccadic facilitation effect in natural backgrounds.

Neural activity
Microsaccades are correlated with bursts of spikes across the visual pathway (Martinez-Conde, Macknik & Hubel, 2000; Martinez-Conde et al., 2004, 2009). Theoretical analyses suggest that they help to decorrelate neural responses in natural viewing (Rucci & Casile, 2004).

Oculomotor control of fixation
Microsaccades enhance retinal image slip (to counteract retinal fatigue) on a short time scale and control fixational errors on a long time scale (Engbert & Kliegl, 2004). Moreover, recent evidence suggests that microsaccades are triggered on perceptual demand based on estimation of retinal image slip (Engbert & Mergenthaler, 2006).

The list of results demonstrates the importance of understanding the generating mechanisms for microsaccades. Another type of microsaccade studies focused on the patterns of successive microsaccades. Hypotheses on the generating mechanism for microsaccades are potentially relevant for the analysis of correlations within sequences of microsaccades.

Since sequences of microsaccades appear to have a non-random structure, isolated microsaccades are often distinguished in *saccadic intrusions* (SI) (Abadi, Scallan & Clement, 2000) or from square-wave jerks (SWJ) (Sharpe & Fletcher, 1986; Otero-Millan, Serra et al., 2011). Abadi and Gowen (2004) exploited the direction dissimilarity of microsaccadic events and their temporal proximity to define different types of SIs with characteristic kinematic properties (amplitude, displacement) and rate-of-occurrence. They separated four different types in their study on shapes and sequences of conjugate, horizontal saccadic eye movements during fixation. I handpicked representative parts of a horizontal eye movement's trajectory for each type of saccadic intrusion in Figure 1.3. The types are described as:

Single Saccadic Pulse (SSP)
A single saccade which has a slow return component (Abadi, Clement & Gowen, 2003).

Double Saccadic Pulse (DSP)
A single saccade whose second part of movement returns the eye to the initial velocity baseline.

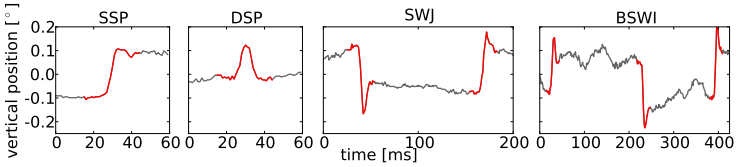

Figure 1.3: Illustration of the four types of *saccadic intrusions*. *Hand-picked sequences of microsaccadic eye movements. The time intervals between the successive events are not representative and the vertical position is, for visualization purposes, not on the same scale.*

Monophasic Square Wave Intrusion (MSWI)
A sequence of two subsequent events where a primary saccade moves the eye away from the initial eye position, followed by a short period in which the eye only drifts and a secondary saccade to return the eye to its initial position.

Biphasic Square Wave Intrusion (BSWI)
A sequence of three subsequent events with a primary saccade to leave the initial position of the eye, followed by a short time interval of rest. The second saccade overshoots the initial position and after another short period of rest, a third saccade returns the eye to its initial position.

In their study, Abadi and Gowen (2004) reported amplitude ranges of $0.4 \pm 0.2^\circ$ and $0.3 \pm 0.4^\circ$ which agrees with ranges of 0.4° (Mergenthaler & Engbert, 2010) and 0.46° for microsaccades (Otero-Millan, Serra et al., 2011) for the SIs which consist of only one single saccadic event (SSP and DSP).

Recently, Otero-Millan, Serra et al. (2011) introduced an advanced treatment of microsaccade sequences. Based on the velocity-threshold algorithm by Engbert and Kliegl (2003b), they used direction dissimilarity, magnitude dissimilarity, and temporal proximity to calculate an index to decide whether a pair of events is a SWJ or not. In Figure 1.4, I illustrate their decision-making properties (adapted from Otero-Millan, Serra et al., 2011).

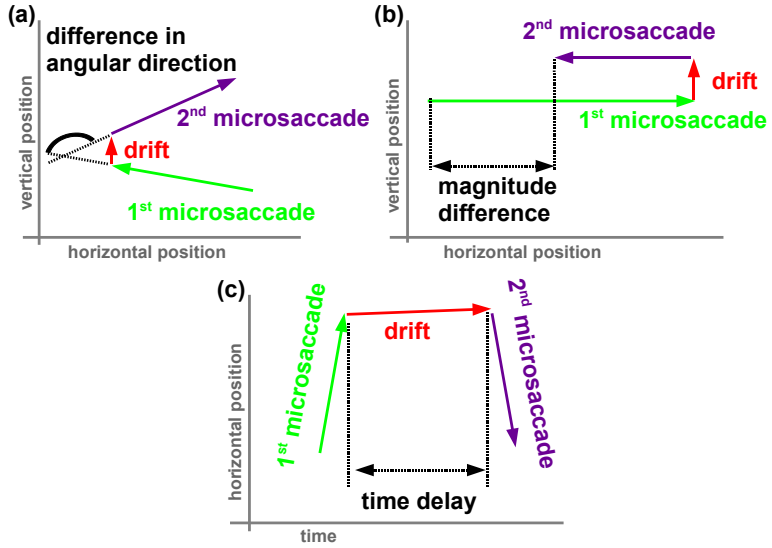

Figure 1.4: Illustration of the properties used to calculate the square-wave jerk index in Otero-Millan, Serra, et al. (2011). *Shown are the used properties from* (a) *the angular difference*, (b) *the magnitude dissimilarity*, (c) *the time delay.* The figure is adapted from Otero-Millan, Serra, et al. (2011).

Studying the relationship between microsaccades and SWJs in healthy subjects and Progressive Supranuclear Palsy (PSP) patients, Otero-Millan, Serra et al. (2011, pp. 4386) concluded "that microsaccades and SIs are essentially the same phenomena and that SWJs are generated by a common coupling mechanism in PSP patients and healthy observers."

All the above-listed results contain issues: in general, microsaccades are detected by their high-velocity and hence bound to their amplitude scale. That brings up the question of whether a scale-free detection, based on other microsaccade properties, delivers similar or equal results. Furthermore, the identification of a statistical model for microsaccade sequences can influence future investigations on the patterns of microsaccades or even serve as

a base-model to establish a model for the generation of microsaccades.

1.4 Saccade and microsaccade generation

Saccades, microsaccades, and all other eye movements are executed from the oculomotor system by contraction and relaxation of the six extraocular muscles that rotate the eye in the eye socket. The muscles are arranged as presented in Figure 1.5. The muscles $M1$ and $M2$ are responsible for the rotation along the horizontal axis; the other four, denoted by $M3, \ldots, M6$, rotate the eye in the vertical axis or produce torsions.

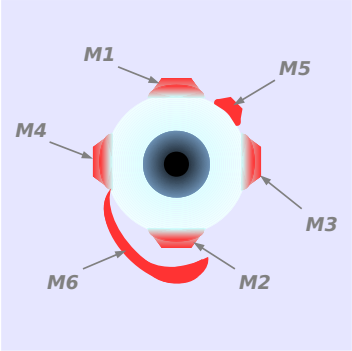

Figure 1.5: Illustration of the positions of the six extraocular muscles, frontal view. *The interplay of contraction and relaxation rotates the eye in its socket.*

The neural mechanisms for generating saccades is the focus of diverse neurophysiological studies (Munoz & Everling, 2004; Schall & Thompson, 1999; Sparks & Mays, 1990) and saccade-related activity in the different components of the neural pathway is reported in different works (Otero-Millan, Macknik et al., 2011; Scudder, Kaneko & Fuchs, 2002). For microsaccades, no different neural generation mechanism is proposed but, instead, results suggest the sharing of the neural pathway for large-amplitude

saccade generation (Hafed et al., 2009; Hafed, 2011; Otero-Millan, Macknik et al., 2011).

The works of Otero-Millan, Macknik et al. (2011) and Hafed (2011) summarized that three different brain areas can be separated according to their different functional role in the generation of saccades. The first brain area, for the target selection, is the *superior colliculus* (SC). The SC integrates input from the *frontal eye field* (FEF), *lateral parietal area* (LIP), and *supplementary eye field*, and *dorsolateral prefrontal cortex* (DLPFC) as well as *basal ganglia* (BG) and other sensory systems (Leigh & Zee, 1999; Moschovakis, Scudder & Highstein, 1996; Sparks, 2002; Wurtz & Goldberg, 1989). The FEF, SEF, DLPFC, and LIP load the SC with excitatory input whereas the BG inhibits the SC. With this combined information, the SC encodes the position of the aimed target into a *retinotopic map*, which is also often referred to as *priority map* or *saliency map*, encoding the stimuli with behavioral relevance (Krauzlis, 2005; Schall & Thompson, 1999; Wurtz, Goldberg & Robinson, 1982). Interestingly, when only the SC or the FEF were deactivated, saccades were generated but the shutdown of both resulted in the loss of any saccadic activity (Schall & Thompson, 1999). The SC is the main actor in the saccade generation mechanism. The second brain area forwards the signal to execute saccades and is represented by the neural network of the *burst generator* (nBG) in the brain stem. The spatially-encoded command, originating from the SC to trigger a saccade, is converted into a temporally encoded motor signal in the nBG. The required change of eye position is translated into muscle contraction or relaxation in order to perform an eye movement. Finally, the third brain area does the final adjustments of the movement, providing the accuracy of the saccadic eye movement. At this stage, the *cerebellum* fixes the variation, accruing from the different integrations along the three brain areas (Robinson & Fuchs, 2001). The whole neural pathway is illustrated in Figure 1.6.

Now, one important aspect in the neural mechanism for saccade generation is the connection between SC and nBG. While rostral SC neurons strongly fire excitatory signals to the *omnipause neurons*, the

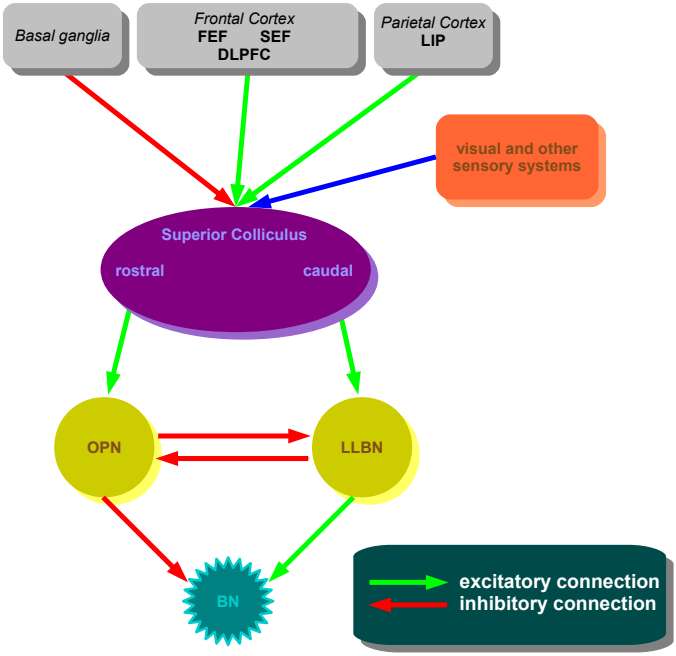

Figure 1.6: Illustration of the neural pathway for saccade generation. *The influences of each single element of the pathway are more complex then illustrated. Yet, for the purpose of my thesis, I abbreviate the most important parts. Green arrows indicate excitatory signals, red arrows inhibitory signals. The abbreviations are FEF = frontal eye field, SEF = supplementary eye field, DLPFC = dorsolateral prefrontal cortex, LIP = lateral parietal area, BG = basal ganglia, SC = superior colliculus, OPN = omnipause neurons, LLBN = long-lead burst neurons, BN = burst neurons. The last three build the neural network of the burst generator. For references, please see (Otero-Millan, Macknik et al., 2011; Scudder et al., 2002).*

caudal SC neurons – firing excitatory signals – indirectly influences the nBG through *long-lead burst neurons* (LLBN). In this circle of mutual interaction, the activity before, during and after saccades of all these three elements have proven to be equivalent or similar during microsaccades (Brien, Corneil, Fecteau, Bell & Munoz, 2009; Hafed, 2011; Munoz & Wurtz, 1993; Van Gisbergen, Robinson & Gielen, 1981; Van Horn & Cullen, 2012).

Three different qualitative models exist which try to explain the triggering mechanism for microsaccades and sometimes incorporate it with the triggering mechanism for normal, large-scale saccades. Based on the results that the peak of neural activity is located around the center in the SC map, a microsaccade is triggered whenever the peak surpasses a certain threshold distance from the center (Hafed et al., 2009; Hafed, 2011). For Rolfs et al. (2008), the firing rate at the center of the SC map has to exceed an activity threshold. Away from the SC map, Otero-Millan, Macknik et al. (2011) proposed a model in which the balance in the inhibitory circuit between OPN and LLBN spills over to the one or other opponent such that microsaccades are triggered. In the last proposal, microsaccades and saccades can be triggered by the same causes.

In the model by Hafed (2011), neurons from the rostral SC prove to be selective for microsaccade directions and amplitudes. Whereas Hafed (2011) suggests that a deviation from the center of the SC map will be the source of a microsaccade trigger, in their work, Rolfs et al. (2008) suggest that the direction of deviation of the peak of neural activity from the center of the SC map relates to the microsaccade direction. The last assumption for the selection of the direction of microsaccades is also assumed in the proposed model by Otero-Millan, Macknik et al. (2011).

1.5 Video-based eye tracking

The experimental data from the three different experiments whose data I will be using in this thesis were recorded with the EyeLink II and EyeLink 1000 video-based eye tracking devices from SR Research, Osgoode, ON, Canada and one iViewX system from SensoMotoric Instruments, Teltow, Brandenburg, Germany. I will briefly introduce the systems and setup used for the experiments.

The EyeLink II system sampled the data at 500 Hz with a spatial resolution better than 0.01° (RMS; root-mean square). Three sensitive (to infrared light) cameras are mounted on a device fastened to the head, two recording the eye movements with a third on

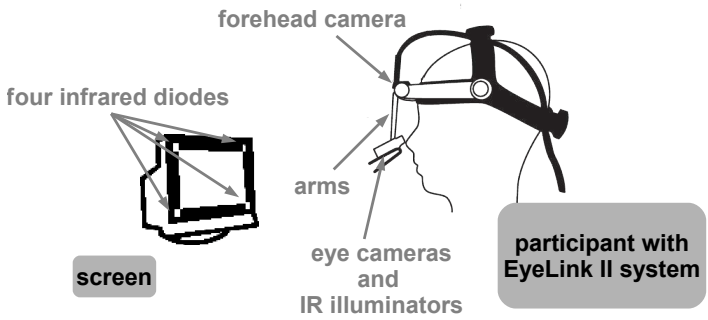

Figure 1.7: Illustration of the EyeLink II setup. *This device is fastened on the participant's head, eyes are illuminated with the infrared diodes on either side of the cameras. Adapted from the EyeLink II manual.*

the forehead to account for head movement corrections onto the trajectory. The setup is shown in Figure 1.7. The cameras measuring the eyes are seated on an arm which reaches from the temple to a position below the eye at a distance of about 5 cm.

Beside each of these cameras, one infrared diode illuminates the eye at 925 nm and another at 880 nm, the latter allowing detection of the corneal reflex. The forehead camera identifies head movements through displacement measurements to four 880 nm infrared markers fastened around the screen. The recording of eye movements is threshold-based and adaptable for each participant. A participant's pupil appears more dark than its surrounding. The threshold reduces the recorded video to a video of a disk, representing the pupil. The detected center of this disk at every time point is recorded as the trajectory of the eye. Optionally, the corneal reflex can be used for a more accurate identification of the eye position. Recorded data are filtered for random outliers with an heuristic filter by Stampe (1993).

Additionally, the EyeLink 1000 from SR Research was used. This system operates without any fixed apparatus on the participant's

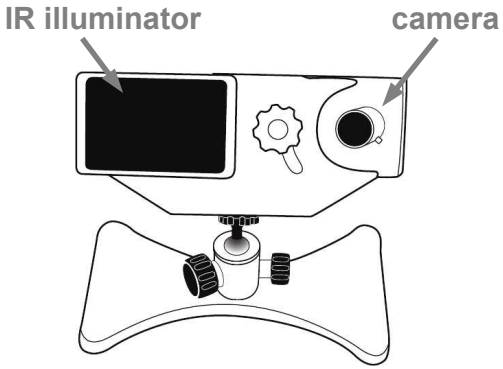

Figure 1.8: Illustration of the EyeLink1000 device. *This device is situated below the stimulus screen, illuminating the eye with infrared light and recording it with an high-speed camera. Adapted from the EyeLink 1000 manual.*

head. The EyeLink 1000 systems sits below the stimulus screen and features the 890 nm infrared illuminator and camera for binocular recording in desktop mount mode (illustrated in Figure 1.8).

No further equipment was required for a recording. A participant stabilizes his or her head on a chin rest. The eye position was processed the same way as with the EyeLink II system. Also here, the corneal reflex was optionally available for a measurement. The recordings were sampled at 1000 Hz with a spatial resolution of 0.01° RMS.

Furthermore, the iViewX Hi-Speed system from SensoMotoric Instruments, Teltow, Brandenburg, Germany was used in an experiment. The system consists of a tracking column with a head fixture, a mirror and high-speed camera. The camera is situated above the participant's head, focusing the mirror in front of the participant's eyes. For an illustration, see Figure 1.9. The mirror, coated on one side, reflects infrared light and allows the transmission of visible light. The camera records the infrared illuminated image in the mirror. The pupil is detected and computer-based image processing

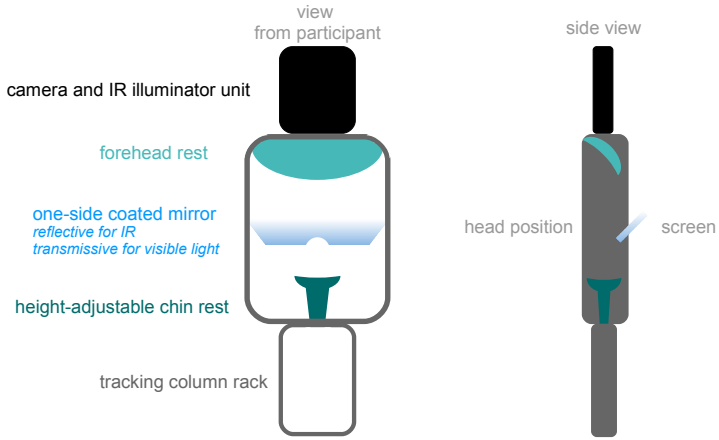

Figure 1.9: Illustration of the iViewX Hi-Speed setup. *Adapted from the iViewX manual.*

calculates the position of the eye by detection of the pupil center. This system also allows for optional tracking with corneal reflex. Data were acquired binocularly at 500 Hz at a typical tracking resolution of 0.01°.

2 Detection of saccades and microsaccades

In particular, in studies of scene perception (J. M. Findlay & Gilchrist, 2003) and reading (e. g., Cunitz & Steinman, 1969; Liversedge et al., 2011), the focus of interest is often not only on saccades and fixations but additionally on the microsaccades occurring during a fixation. Then both *saccades* and *microsaccades* appear in the trajectory of the eye. If both types of ballistic eye movements (cf. Chapter 1.3) are of interest in a particular study, the detection of both at the same time is a complex problem. In this chapter, I will present a novel detection method, which is capable of identifying saccades and microsaccades at the same time, is scale-invariant and uses the representation of the time series in the time-frequency domain. Until now, if saccades and microsaccades co-occur, they are either detected by hand (e. g., Abadi & Gowen, 2004) or, in the majority of cases, automatically detected through the first derivative or its alterations, i. e., the routines based on their property of high velocity (Engbert & Kliegl, 2003b; Mergenthaler, 2009). All extant detection approaches are either not objective or crucially dependent upon the amplitude scale. Saccades can be seen as large-scaled versions of microsaccades or microsaccades as small-scale saccades. Many times, small involuntary saccades that occur during fixation are even called *microsaccades*, expressing the close relation between both (Otero-Millan et al., 2008; Mergenthaler & Engbert, 2010). To extract saccades of all scales of amplitude from the horizontal and vertical trajectory of the eye, their time series is examined with the continuous wavelet transform (Holschneider, 1995; Mallat, 1998). Through the scale-invariance of the continu-

ous wavelet transform, both saccades and microsaccades can be detected as singularities in the time series.

In the following, I will briefly review the most prominent existing method for saccade detection, and after a mathematical preamble, I will show its applicability for detecting saccades and microsaccades in an eye movement and fixational eye movement experiment. In contrast to derivative-based methods, I use structural properties of the trajectory in this novel detection method. Furthermore, the proposed method is tested against surrogate data that mimic the unknown properties of the fixational eye movements' time series. Parts of the results have been published in Bettenbühl et al. (2010) during the preparation of this thesis.

2.1 Existing concepts

As mentioned above, two different approaches exist to determine saccades and microsaccades in eye and fixational eye movements. Reviewing hand-picking would mostly rely on the skills of a human observer to determine shapes in the trajectories of the eye movements, as in Figure 1.2. I will focus my review on the velocity-based threshold method, which has been shown to assist in the detection of saccadic eye movements in different modifications.

2.1.1 Velocity-based detection of saccadic events

With the introduction of video-based eye tracking, the amount of data available to study saccades and microsaccades increased exceptionally and detection by human observers (Adler & Fliegelman, 1934; Ratliff & Riggs, 1950; Nachmias, 1959) needed to be (semi-) automatized. Several algorithms have been proposed (Boyce, 1967; Kohama & Usui, 2002; Martinez-Conde et al., 2000; Møller et al., 2002; Mould, Foster, Amano & Oakley, 2011; Nyström & Holmqvist, 2010) to deal with the huge amount of available data and detect saccadic eye movements – e. g., in fixation tasks, reading or scene perception experiments. In vision research, most of the detection

algorithms used one main property shared between saccades and microsaccades: the high velocity (or its derivative, acceleration).

For the first time, Boyce (1967) used a method that was based on the statistics of the increments of the trajectory, the first derivative of the time series. Engbert and Kliegl (2003b) introduced an algorithm that accounts for different velocities of saccades of individual participants. This method is still widely used in the field of eye movement research. Basically, the method uses an ellipse in the velocity space of the eye movements' trajectories. An individual threshold multiplier then determines the radii of the ellipse in the space of the horizontal and vertical eye movement's velocities. The threshold multiplier is set according to the data's standard deviation in horizontal and vertical eye movement directions. As a result, parts of the trajectory that leave the ellipse for a short period of time are detected and considered saccadic eye movements (Engbert & Mergenthaler, 2006). In order to acquire the best detection results for every participant and experiment, a so-called threshold multiplier needs to be optimized such that the radius of the ellipse is individually adapted.

A challenge for the velocity threshold method is the detection of microsaccades and saccades at the same time. The velocity threshold method offers three possibilities for detecting both event types – saccades and microsaccades. First, optimization of the threshold multiplier by visual inspection of the results in order to obtain an optimal value, which then is sensitive enough to detect microsaccades and thereby also large-scale saccades. Second – if recording a secondary dataset of fixational eye movements – the determination of a proper threshold multiplier through the former. Third, successive computations in order to primarily detect saccades and, after removal of the former and adjustment of the threshold multiplier, the detection of microsaccades.

2.2 Mathematical background

Mathematically, both microsaccades and saccades can be seen as singularities in a time series. I will give a primer on *singularities* and the *continuous wavelet transform* for *real-valued* and *complex-valued time series* as well as the *method of maximum modulus lines*, a numerical method for detecting singularities in time series through the continuous wavelet transform.

2.2.1 Singularities, onsets and cusps

A time series is a function $s(t)$ which at each time point t associates the observed quantity $s(t)$ with a number. Now suppose that a time series $s(t)$ is differentiable at all time points t except for a denumerable number of time points. At these time points, the time series is irregular. In mathematical terms, the term *pointwise regularity* refers to the local behavior of a function or time series at an individual time point. The lower the pointwise regularity is at a time point t_0, the stronger the *singularity* at t_0. More than one singularity can occur in a time series. A complex time series can appear as a superposition of singularities. One way to characterize and detect singularities is to measure the *Hölder regularity* of the time series $s(t)$. A time series $s(t)$ is called α-Hölder regular in t_0 if a polynomial $P_n(t)$ of degree n exists such that

$$|s(t_0 + \Delta t) - P_n(\Delta t)| \leq c|\Delta t|^\alpha \tag{2.1}$$

with $\Delta t \to 0$, a constant $c > 0$, and $n = \lfloor \alpha \rfloor$ the integer part of $\alpha \in \mathbb{R}$ (adapted from Farge, Schneider, Pannekoucke & Nguyen van yen, submitted 09/2010). An example of a stochastic process[1] whose realizations are almost always singular is the fractional

[1] To give a brief definition of the term *stochastic process*, it is sufficient to note that a stochastic process is a collection of random variables $X(t) = X_t$ on an index set $t \in \mathbb{T}$. The random variables are drawn from a specifiable probability distribution, which, in the case of a fractional Brownian motion, is the normal distribution. One finite-length realization is one set of random variables $X(t)$ ordered according to their index $t = 1, \ldots, N$. This realization presents us a time series.

or fractal Brownian motion (Mandelbrot & Van Ness, 1968). Fractals have structure at all length scales and display self-similar behavior, i. e., zooming to smaller scales inside the function, the same pattern will appear over and over again (Mandelbrot, 1982). Normalized fractional Brownian motion $B_H(t)$ is, in terms of probability distributions, self-similar since

$$B_H(\lambda t) \approx |\lambda|^H B_H(t) \tag{2.2}$$

with $\lambda \in \mathbb{R}$ and $H \in (0,1)$ the Hurst exponent (Hurst, Black & Simaika, 1965) as a measure of intensity of the self-similarity. A self-similar time series $B_H(t)$, which was achieved as one realization from a fractional Brownian motion process, is everywhere non-differentiable and is composed of dense singularities. The time series $B_H(t)$ has the same Hölder regularity (the same Hölder α) everywhere and is called *monofractal* (Mandelbrot, 1982).

In contrast to these dense singularities, a typical example of a function that contains an isolated singularity is an *onset*, presented in Figure 2.1a as singularity at $t_0 = 0$. The equation of a local cusp as in (Holschneider, 1995) is given by

$$s(t_0 + t) = s(t_0) + c_- |t|_-^\alpha + c_+ |t|_+^\alpha \tag{2.3}$$

with $\alpha \in \mathbb{R}$, $c_\pm \in \mathbb{R}$ and $|t|_\pm = \frac{1}{2}(|t| \pm t)$. An onset is obtained by eliminating one of the summands $c_- = 0$ or $c_+ = 0$. Additionally, different values for α are illustrated in Figure 2.1b.

For $\alpha \to 0$, the trajectory of the time series looks steplike if presented over time. For $\alpha \to 1$ the trajectory after the onset point $t_0 = 0$ increases (almost) linearly. If both c_+ and c_- are nonzero as in Figure 2.1b, different slopes are obtained on the left and right side of the singularity.

In Figure 2.2, a trajectory of a fractional Brownian motion and inserted cusps is presented. The trajectory is singular almost everywhere but differs in the type of singularity. The dense singularities of the fractional Brownian motion and the isolated singularities inserted through the cusps differ. Both the dense and isolated sin-

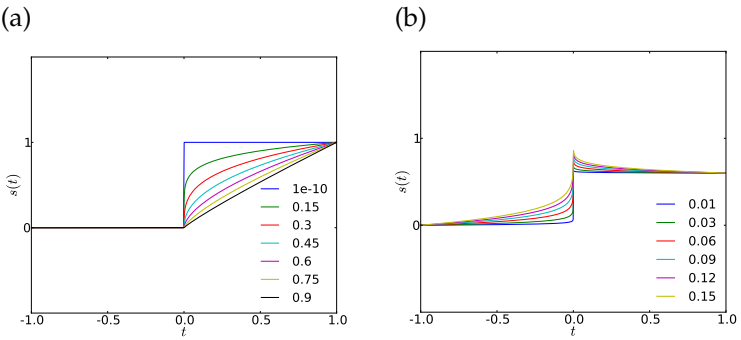

Figure 2.1: Different shapes of singularities at $t_0 = 0$ for different α. *Trajectories of the time series defined by Equation (2.3) with* (a) $c_- = 0$, $c_+ = 1$ *and* (b) $c_- = -1.0$, $c_+ = -0.4$ *and different* α.

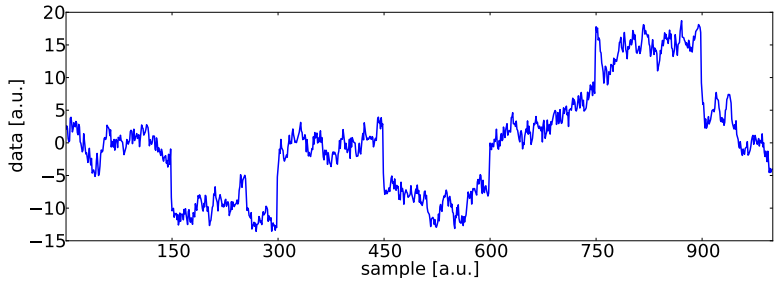

Figure 2.2: The generated trajectory of a fractional Brownian motion with inserted isolated singularities. *Six singularities were inserted at positions* $t = n \times 150$ *for* $n = 1, \ldots, 6$. *The Hurst exponent of the fractional Brownian motion is* $H = 0.35$.

gularities are scale-invariant. Here, a scaling of the amplitude does not change the local regularity in the time series. We will see how it is possible to detect the latter although dense singularities occur in the time series. The continuous wavelet transform offers the most suited tool to this purpose.

2.2.2 Continuous wavelet transform

To analyze local regularity in a time series and detect local singularities, the continuous wavelet transform has proven to be a powerful tool (Arneodo, Grasseau & Holschneider, 1988; Holschneider & Tchamitchian, 1991; Mallat & Hwang, 1992). Analyses of a time series in its time-frequency representation found several applications in signal processing and time series analysis (see e. g., Daubechies, 1992; Holschneider, 1995; Quiroga, Nadasdy & Ben-Shaul, 2004; Daubechies & Teschke, 2005; Diallo, Holschneider, Kulesh, Scherbaum & Adler, 2006).

The transform for a real-valued time series

For a time series $s(t) \in \mathbb{R}$, the *Fourier transform* is given by

$$\widehat{s}(\omega) = \int_{-\infty}^{\infty} s(t)\, \overline{g}(t,\omega)\, dt \;=\; \langle g(t,\omega) \mid s(t) \rangle \tag{2.4}$$

with $g(t,\omega) = e^{i\omega t}$ and the complex conjugate $\overline{g}(t,\omega) = e^{-i\omega t}$. Interpreting ω as frequency, the function $\widehat{s}(\omega)$ is the *frequency representation* of the time series $s(t)$ at frequency ω. The integral equals the scalar product if and only if the integral converges absolutely.

The *continuous wavelet transform* of a time series $s(t) \in \mathbb{R}$ with respect to a wavelet Ψ is defined by the integral transform

$$\mathcal{W}_s(a,b) = \frac{1}{a} \int_{-\infty}^{\infty} s(t)\, \overline{\Psi}\left(\frac{t-b}{a}\right) dt \;=\; \langle \frac{1}{a}\Psi\left(\frac{t-b}{a}\right) \mid s(t) \rangle \tag{2.5}$$

such that $\mathcal{W}_s(a,b)$ is a complex-valued function of two parameters a and b. Its values are referred to as *wavelet coefficients*. Here, the bar at $\overline{\Psi}$ denotes the complex conjugate of *the wavelet* or *wavelet function* Ψ. Again, the integral needs to converge absolutely such that the second equal sign is true. The parameter b is called

translation parameter such that a variation of b shifts the wavelet along the time axis, whereas a is the *dilation parameter* to scale the wavelet. For the analysis of singularities, the L^1-normalization is used by applying prefactor $1/a$ to the dilated wavelet in Equation (2.5). This emphasizes small scales, i. e., high frequencies (Antoine, 2004). The dilated wavelet Ψ has its Fourier spectrum concentrated around $\omega = \omega_0/a$ such that the real *frequency* ω is present through $\omega = \omega_0/a$ with ω_0 the (characteristic) center frequency of the wavelet Ψ. The Fourier transform of the dilated wavelet is localized around ω_0/a.

In wavelet analysis, the time series is transformed into its time-frequency representation, which indicates when (parameter b) which frequency (parameter ω_0/a) occurs. Other time-frequency transformations exist, for example, the short-time Fourier transform (Oppenheim, Schafer, Buck et al., 1989) or Gabor transform (Feichtinger & Strohmer, 1998), which is a special case of the former. But only wavelet analysis is able to characterize *local singularities*, as it has fewer a priori limits to its time-resolution.
If the origin of the time series is a measurement, the time series will no longer be continuous but discrete in time. Then, the integral transform (Equation 2.5) for a time series $s(t_i) \in \mathbb{R}$ will be calculated by a sum (Torrence & Compo, 1998)

$$W_s(a,b) = \frac{1}{a} \sum_{i=1}^{N} s(t_i) \overline{\Psi} \left(\frac{(t_i - b)}{a} \right) \tag{2.6}$$

with t_i the discrete time and N the number of time points of the time series $s(t_i)$. Transforming $s(t)$ or $s(t_i)$ into its time-frequency representation, the wavelet transform contains information about the distribution of amplitude and phase of the time series in time and frequency such that

$$\mathcal{W}_s(a,b) = A_s(a,b)\, e^{i\Phi_s(a,b)} \tag{2.7}$$

where the modulus $|\mathcal{W}_s(a,b)| = A_s(a,b)$ is the amplitude and $\Phi_s(a,b) = \arg(\mathcal{W}_s(a,b))$ is the phase.

Not every function can be used as *mother wavelet* Ψ but the function has to respect three major properties (Holschneider, 1995):

1. localization in time or space,
2. localization in frequency space,
3. function of zero mean or, in more general, some consecutive moments must vanish.

In mathematical terms, the condition on localization in time and space is given by

$$|\Psi(t)| \leq c(1+|t|^2)^{-\nu/2} \tag{2.8}$$

for some $c > 0$ and $\nu > 1$. Denoting with $\widehat{\Psi}(\omega)$ the Fourier transform of $\Psi(t)$, the second condition is written as

$$|\widehat{\Psi}(\omega)| \leq c(1+|\omega|^2)^{-\mu/2} \tag{2.9}$$

with some $c > 0$ and $\mu \geq 0$. The last condition is for some consecutive moments defined as

$$\int_{-\infty}^{\infty} \Psi(t)\, t^m dt \;= 0 \qquad \text{for} \;\; m = 0, \ldots, n \tag{2.10}$$

with a positive integer $n \geq 0$. With reference to the vanishing of the first moment it is called *admissibility condition*.

The Morlet wavelet

To detect singularities, even if they are superimposed, the best choice is a complex-valued wavelet (Farge et al., submitted 09/2010). The Morlet wavelet (Grossmann & Morlet, 1985) is a

complex-valued wavelet and is presented in time-space domain through (Holschneider, 1995, p. 30)

$$\Psi(t) = e^{i\omega_0 t} e^{-t^2/2} \tag{2.11}$$

and in frequency domain through (Holschneider, 1995, p. 30)

$$\widehat{\Psi}(\omega) = \sqrt{2\pi} e^{-(\omega-\omega_0)^2/2} \tag{2.12}$$

with $a = \omega_0/\omega$ and ω_0 as center frequency. The oscillating wavelet is enveloped by a Gaussian function that is given by $e^{-t^2/2}$. In a strict mathematical sense, the Morlet wavelet is not a wavelet because the first moment does not vanish (cf. Equation 2.10) and it is called *pseudo-wavelet*. However for large enough $\omega_0 > 0$, the Fourier coefficients of the negative frequency components are small compared against those of the positive frequency components of $\widehat{\Psi}(\omega)$ and $\widehat{\Psi}(0) \approx 0$ or, what amounts to the same, the wavelet is over zero mean and the admissibility condition is fulfilled. For practical purposes, values of $\omega_0 > 5$ are chosen to avoid problems

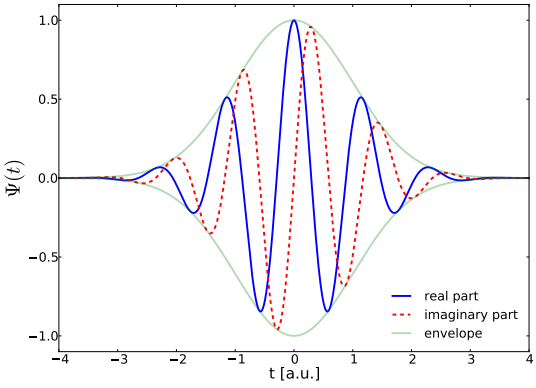

Figure 2.3: The Morlet wavelet at center frequency $\omega_0 = \pi\sqrt{2/\ln 2}$. The oscillations of the real and imaginary part of the complex-valued wavelet $\Psi(t)$ are enveloped by the positive and negative modulus of $\Psi(t)$.

with smallest frequency components. The illustration in Figure 2.3 (adapted from Holschneider, 1995) presents the Morlet wavelet at a center frequency $\omega_0 = \pi\sqrt{2/\ln 2} \approx 5.336$. At this value, the real part of the Morlet wavelet touches the Gaussian envelope at half its height and the value has proven to be particularly useful in signal processing (Grossmann, Kronland-Martinet & Morlet, 1989).

For what follows, it is essential to review the definition of the terms *progressive* and *regressive* function (from Holschneider, 1995). If and only if the Fourier transform of a function $f(t) \in L^2(\mathbb{R})$ is supported by positive frequencies only,

$$\text{supp } \widehat{f}(\omega) \subseteq \mathbb{R}_+ \tag{2.13}$$

then the function $f(t)$ is called *progressive*. Here, $\widehat{f}(\omega)$ denotes the Fourier transform of the function $f(t)$. In contrast, a function $g(t) \in L^2(\mathbb{R})$ is called *regressive* if and only if

$$\text{supp } \widehat{g}(\omega) \subseteq \mathbb{R}_- \tag{2.14}$$

or, what amounts to the same, if the time-reversed function $g(-t)$ is progressive.
The Morlet wavelet becomes a progressive wavelet with a real-valued frequency representation $\widehat{\Psi}(\omega) \in \mathbb{R}$ by adding a corrective term $\eta(t)$ such that

$$\Psi(t) = e^{i\omega_0 t} e^{-t^2/2} + \eta(t) \tag{2.15}$$

The fact that the Morlet wavelet is a progressive wavelet allows, for example, the study of phase shifts in the complex-valued part of the wavelet transform $\mathcal{W}_s(a, b)$ and simplifies the application to a complex-valued time series.

The transform for a complex-valued time series
Applying the wavelet transform with a complex-valued wavelet function Ψ on a time series $s(t) \in \mathbb{C}$ and considering Equation (2.5), attention has to be paid to the absence of symmetry in frequency.

This symmetry exists for $s(t) \in \mathbb{R}$. If $s(t) \in \mathbb{C}$, then the full wavelet transform for all frequencies is separated into the progressive component $\mathcal{W}_s^+(a,b)$ and regressive component $\mathcal{W}_s^-(a,b)$ (Kulesh, Diallo & Holschneider, 2005) such that

$$\mathcal{W}_s(a,b) = \mathcal{W}_s^+(a,b) + \mathcal{W}_s^-(a,b) \tag{2.16}$$

with

$$\mathcal{W}_s^+(a,b) = \begin{cases} W_s(a,b) & a^{-1}\omega_0 \geq 0 \\ 0 & a^{-1}\omega_0 < 0 \end{cases} \tag{2.17}$$

$$\mathcal{W}_s^-(a,b) = \begin{cases} 0 & a^{-1}\omega_0 \geq 0 \\ W_s(a,b) & a^{-1}\omega_0 < 0 \end{cases} \tag{2.18}$$

with dilation and translation parameters $a = \omega_0/\omega$ and b and the characteristic center frequency ω_0. In contrast to the physical frequency ω, the dimensionless dilation parameter a can take both positive and negative values.

Now, to represent a time series $s(t) \in \mathbb{R}$ or $s(t) \in \mathbb{C}$ in its time-frequency representation, the dilation parameter a has to be scaled such that it covers the frequency range that is of interest for the time series. For every different dilation parameter a, the wavelet transform $W_s(a,b)$ contains the frequency information of the time series $s(t)$ up to the frequency $\omega = \omega_0/a$. Selecting a specific frequency range of interest for the wavelet transform is called a *zoom* of the wavelet transform. Using different dilation parameters obtained through $a = a_0 + n\Delta a$ with a_0 the maximum scale, corresponding to minimum frequency, $n = 1, \ldots, N$ the number of *voices* (frequency steps) and Δa selected such that the frequency zoom can be covered, one obtains the wavelet transform that represents the time series at N voices over time.

Now, to perform the full wavelet transform as in Equation (2.16), two transforms have to be computed. The N voices can be differently distributed for a given frequency range. A logarithmic scaling in the frequency range is particularly useful for the characterization of singularities as we will see below.

2.2.3 Detection of singularities

In Chapter 2.2.1, the onset was presented as an example of an isolated scale-invariant singularity. Now, the time series $s(t)$ might be given through Equation (2.3) with $c_- = 0$, $c_+ = 1$ and $\alpha = 0.15$. In Figure 2.4, at different frequencies $\omega = \omega_0/a$ the modulus and the phase $\Phi(a, b)$ (cf. Equation 2.7) of the wavelet transform are shown. The wavelet transform is calculated for 128 voices in the frequency range between 20 and 50 Hz. The frequency range, on which the time series was analyzed, is logarithmically sampled. Then, the Morlet wavelet was dilated with these parameters a. In time-frequency representation, the singularity at time point t_0

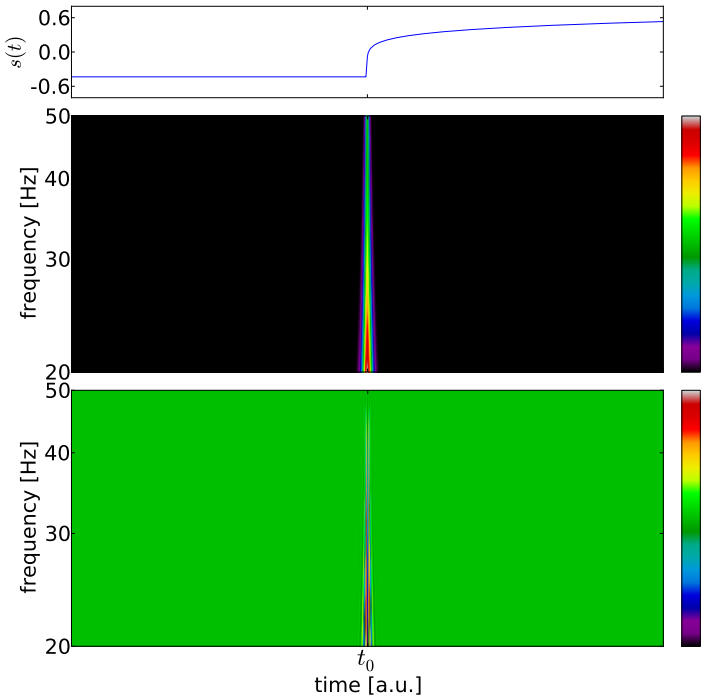

Figure 2.4: Modulus and phase of the wavelet transform of an onset. *The onset was calculated by Equation (2.3) with $c_- = 0$, $c_+ = 1$, and $\alpha = 0.15$.*

appears as a cone-like structure in the modulus of the wavelet transform. At lower frequencies, the wavelet is broader such that the width of the cone scales with the width of the wavelet function at each voice a. The latter is only true for low variance in the time series before and after the singularity. The wavelet focuses the whole variance at time points of singularities into the cone, whose maximum at each voice corresponds to the position of the singularity in the time series.

Now, singularities can be detected in the modulus of the wavelet transform (Mallat & Hwang, 1992; Tu, Hwang & Ho, 2005). The slope of the wavelet coefficients over all analyzed frequencies at the time point of the singularity characterizes the singularity (Holschneider, 1988; Jaffard, 1989). In Figure 2.4, one single cone, centered around t_0, is present for the isolated singularity at t_0. The slope of the wavelet coefficients of the time series $s(t)$ characterizes the Hölder α regularity such that at time point t_0 the singularity is characterized through

$$\mathcal{W}_s(a, b_0) \approx c\ a^{\alpha}\ e^{i\Phi_s(a,b_0)} \tag{2.19}$$

with the overall amplitude c and $\Phi_s(a, b_0)$ the phase of the wavelet transform – the local geometry of the singularity (Holschneider, 1995). In Figure 2.5, the wavelet coefficients at point t_0 from Figure 2.4 are plotted against frequency in green color. The other lines correspond to the other onsets which were illustrated in Figure 2.1. The slope of every line identifies the Hölder α.

Building on this, singularities can be characterized and detected in the modulus of the wavelet transform. Numerically, the detection is usually done with the so-called *method of maximum modulus lines* (Marr & Hildreth, 1980; Witkin, 1983). Mallat and Hwang (1992) gave a precise definition of a maximum modulus line, which I adapted as follows:
If $\mathcal{W}_s(a, b)$ is the wavelet transform of a time series $s(t)$, then

- Any point (a_0, b_0) is called *local extremum* if $\partial\mathcal{W}_s(a_0, b)/\partial b$ has a zero-crossing at $b = b_0$,

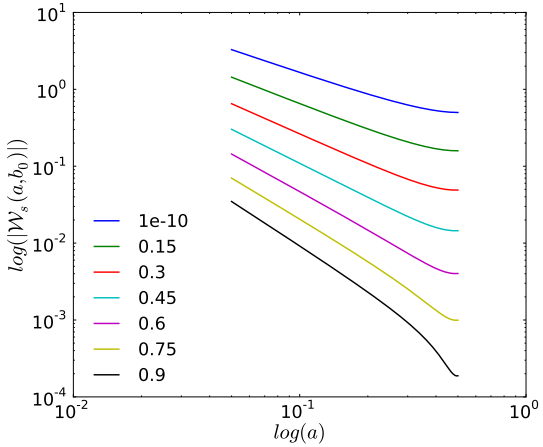

Figure 2.5: The asymptotic behavior of $|\mathcal{W}_s(a,b_0)|$ of a scaling singularity in a log-log-plot. *The slope of every single line identifies the α value used for the onsets presented in Figure 2.1.*

- Any point (a_0, b_0) is called *maximum modulus* if $|\mathcal{W}_s(a_0, b \pm \varepsilon)| < |\mathcal{W}_s(a_0, b_0)|$ for some $\varepsilon > 0$.

Then, any curve, which connects the maximum modulus at each single voice a as such that the curve passes the whole analyzed frequency range, is called a *maximum modulus line*. It is called a *line* because, for a singularity as exemplified in Figure 2.4, the line would be on top of the cone through the maxima of each voice. We will see later that, for real-world time series, it might not be a straight line every time but instead a curve with slight variations in b_0.

For a real-valued time series $s(t) \in \mathbb{R}$, the maximum modulus line $\mathcal{L}(a, b_0)$ contains for $\varepsilon > 0$ the wavelet coefficients over all a at b_0 such that

$$|\mathcal{W}_s(a, b_0 \pm \varepsilon)| < |\mathcal{W}_s(a, b_0)| = A_s(a, b_0) = \mathcal{L}(a, b_0)\ . \tag{2.20}$$

The parameter ε can be scaled with the frequencies $1/a$ to account for the cone-like structure of the singularity in the modulus of the

wavelet transform. Each singularity occurring in the time window of 2ε produces a cone-like structure in the modulus of the wavelet transform. For dense singularities, the overlapping of the cones forms a smooth surface such that isolated singularities can be detected by the maxima in the modulus. According to Mallat and Hwang (1992), a maximum modulus line converges at small scales to the location of the singularity such that

$$\mathcal{L}(a, b_0) \to \mathcal{L}(0, t_0) \quad \text{for} \quad a \to 0 \tag{2.21}$$

and t_0 defines the position of a singularity in the time series $s(t)$.

In Chapter 2.2.1, we have seen that a time series originating from a fractional Brownian motion process is singular (almost) everywhere. Now, only if a time series has few isolated singularities, can the singularities be identified by their asymptotic behavior along the frequency (Equation 2.21) and the values of Equation (2.19) estimated. The wavelet coefficients of the dense singularities of fractional Brownian motion are rarely local maxima. Using the Morlet wavelet and transforming a time series as presented in Figure 2.2, only isolated singularities can be detected by the cone they produce in the wavelet transform (Farge et al., submitted 09/2010). In Figure 2.6, the isolated singularities are visible on all scales but are influenced by the cones of the surrounding singularities of fractional Brownian motion such that the identification through the method of maximum modulus lines will detect the time points of isolated singularities in the time series.

Analyzing a time series $s(t) \in \mathbb{C}$ with the Morlet wavelet, the wavelet transform for all frequencies is separated into progressive and regressive wavelet transform. Recapitulating Equation (2.19), the slope of the wavelet coefficients identifies the Hölder α regularity. For a singularity, it identifies the type of singularity by α. Now, for the purpose of this thesis, no interest is turned into the type of singularity indicated by α but instead, a singularity should, using the *maximum modulus lines* be detected irrespectively of its contribution of positive or negative frequencies. Instead of using a pre-defined threshold to separately detect the time points

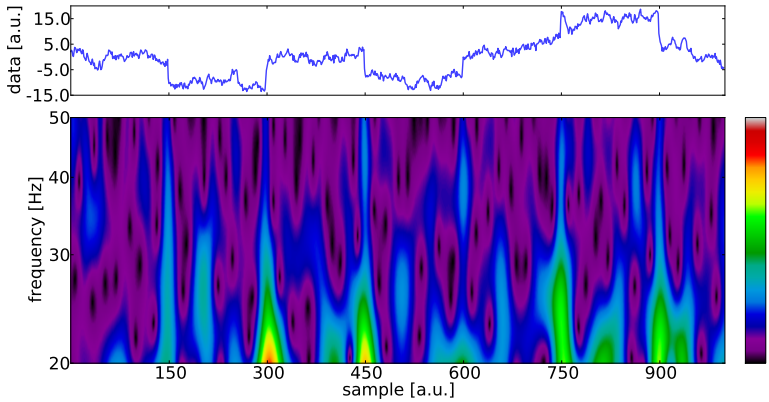

Figure 2.6: Modulus of the wavelet transform for a trajectory of fractional Brownian motion with inserted isolated singularities. *The six singularities were inserted at positions $n \times 150$ for $n = 1, \ldots, 6$. Their corresponding cones are visible in the wavelet transform.*

of singularities in both transforms, I overestimated the modulus of the wavelet transform to detect maximum modulus lines such that

$$\begin{aligned} |\mathcal{W}_s(a, b_0 \pm \varepsilon)| \quad < |\mathcal{W}_s(a, b_0)| \quad &= |\mathcal{W}_s^+(a, b_0) + \mathcal{W}_s^-(a, b_0)| \\ &\leq |\mathcal{W}_s^+(a, b_0)| + |\mathcal{W}_s^-(a, b_0)| \\ &= \mathcal{L}(a, b_0) \end{aligned} \tag{2.22}$$

Considering real world data, "perfect" singularities are physiologically impossible because they would require infinite accelerations. Thus, a more realistic model of singularities might be to consider smoothed singularities. Then, the maximum modulus line may end at a scale related to the smoothing scale of the singularity. For this reason, I only considered those maximum modulus lines which go from a fixed highest frequency ($\widehat{=}$ smallest scale) to smallest frequency ($\widehat{=}$ largest scale). The estimated position t_0 of the singularity is then simply the small-scale end of the corresponding maximum modulus line.

2.3 Novel detection method for saccades

We have seen how the continuous wavelet transform allows the detection of isolated singularities, even in a time series of superimposed dense singularities. Now in vision research, the time series of eye movements during a sequential scanning task experiment can be divided into time periods of saccades and fixations. Simultaneously, fixations are again subdivided into tremor, drift and saccades during fixation (cf. Chapter 1.1). Mergenthaler and Engbert (2007) showed that fixational eye movements can be modeled by a fractional Brownian motion process. According to this, if the time series of a sequential scanning task experiment can be divided into saccades and fixational eye movements, the latter containing microsaccades, and if the continuous wavelet transform can scale-invariantly detect isolated singularities in time series of superimposed dense singularities, then the proposal to define saccades and microsaccades as singularities in the time series of eye movements leads to a novel detection method for both.

To examine this proposed novel detection method, I used data from a Landolt-C-maze experiment (Snellen & Landolt, 1874b, 1874a). Saccades of all scales appear in these eye movements through the jumps between stimuli and within stimuli fixations. The specifications of the video-based eye tracking setup are given in Chapter 1.5 and the Landolt-C-maze experiment was performed as follows: Each participant was required to perform a visually guided search through a maze of Landolt-Cs with a closed circle as a target. The start position was marked with a bold font Landolt-C. The gap position indicated the search direction, the proposed movement direction for the eye.

The Landolt-C stimuli were black of 1.12° size (when presented centrally), 0.27° width and with a gap of 0.07° in one of four cardinal positions at 0°, 90°, 180°, or 270°. The 9×11 stimulus maze was plotted on an invisible grid. Symbols placed in a distance of 3° were presented on a light gray background to account for illuminance homogeneity. The resolution of the screen

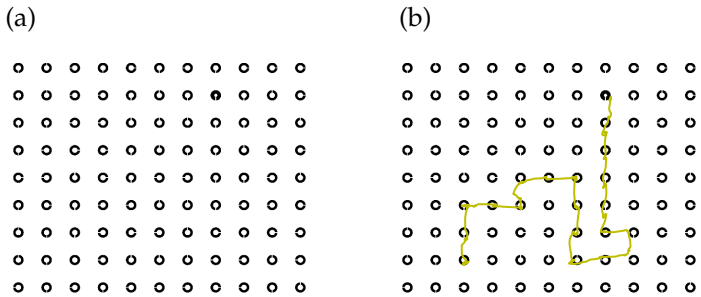

Figure 2.7: Illustration of the Landolt-C-maze and an eye movement trajectory on the Landolt-C-maze. (a) *A path, given by the sequence of open sides of the Landolt-C stimuli, needed to be followed by a participant with their eyes. The path started at the bold font C and stopped when the participant reached the closed symbol.* (b) *A representative eye movement trajectory observed from one participant through video-based eye tracking.*

was 1280×1024 pixels. Positions of gaps for Landolt-Cs outside the search path have been chosen at random. Eye movements were recorded using a video-based eye tracking system (cf. Chapter 1.5). Each of the 38 participants performed 100 trials. For each trial, a randomly chosen Landolt-C-maze was used. For the scale-free detection with the wavelet method, a set of 2574 randomly chosen trials was used. The experiment was designed and performed by Hans A. Trukenbrod at the University of Potsdam (Trukenbrod & Engbert, 2007, 2012) with the iViewX Hi-Speed eye tracking device (cf. Chapter 1.5). The optional corneal reflex was used in the experiment to compensate head-camera-related position changes.

By using the complex-valued Morlet wavelet, I aimed to detect saccadic events in more than one movement direction. Saccades occur more prominently in horizontal and vertical direction but also in oblique direction (cf. Chapter 1.2). The time series $h(t)$ and $v(t)$ are recorded for the horizontal and vertical eye movements. To detect singularities irrespectively of movement direction with

the continuous wavelet transform, I constructed a complex-valued time series $\tilde{s}(t)$ such that

$$\tilde{s}(t) = \tilde{h}(t) + i\tilde{v}(t) \tag{2.23}$$

with

$$\tilde{h}(t) = \frac{h(t) - \hat{\mu}_h}{\hat{\sigma}_h} \quad \text{and} \quad \tilde{v}(t) = \frac{v(t) - \hat{\mu}_v}{\hat{\sigma}_v} \tag{2.24}$$

with $\hat{\mu}_h$ and $\hat{\mu}_v$ the estimated mean and $\hat{\sigma}_h$ and $\hat{\sigma}_v$ the estimated standard deviations of the values in time series $h(t)$ and $v(t)$, respectively. The time series $\tilde{h}(t)$ and $\tilde{v}(t)$ are standard-normalized such that variances are equal. No influence exists in the selection of which time series is taken to represent real or imaginary part of $\tilde{s}(t)$.

For the detection of singularities in the time series $\tilde{s}(t)$ with the continuous wavelet transform as given in Equation (2.5) and the Morlet wavelet (Equation 2.11), a frequency range from 20 to 50 Hz was chosen. As the left and right eye are well-correlated over this range. Additionally, this allowed for working above a threshold of 20 Hz, considering that below this threshold, the wavelet transform gets influenced by other structures that might mask the data. Above 50 Hz, the wavelet transform identifies more and more singular points. The filtering effect by the superposition of the single cone and those related to each time point is reduced. Additionally, the number of voices has to be chosen for the wavelet, i. e., the number of different dilation parameters a. On the logarithmic scale, 128 voices have been used, i. e., 128 logarithmically sampled frequencies between 20 and 50 Hz.

Singularities are visible at all frequencies such that I detected those time points of singularities at which the maximum modulus lines passed through the whole analyzed frequency range. In Figure 2.8, the modulus of the wavelet transform $\mathcal{W}_{\tilde{s}}(a, b)$ together with both dimensions of the eye movement trajectory is shown. The positions of occurrence of a singularity are marked with dots.

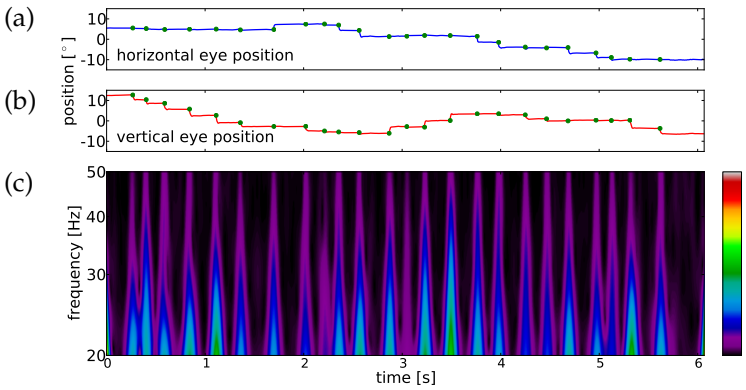

Figure 2.8: Time-frequency representation of an eye's trajectory performing the visual search path. (a) *First 6 seconds of a representative horizontal and* (b) *vertical component of the eye trajectory with detected singularities (green dots).* (c) *Modulus of the wavelet transform. The maximum modulus lines (cf. section 2.2.3) are apparent during visual inspection.*

Having detected the saccadic eye movement at all scales, I show in Figure 2.9 a representative eye's trajectory of one trial of one participant on a Landolt-C-maze. The wavelet method is a point estimator for t_0, the time point of the occurrence of the singularity – the saccadic eye movement. In Figure 2.9, a time window of ± 60 ms around these time points of singularities is used to mark the saccade. In the inset figure, the part of the trajectory that belongs to a saccade (in green) or fixation (in yellow) is marked.

Both the saccades that separate fixations and the microsaccades inside the fixations have been identified by the wavelet method. Thus, the proposed wavelet method proves to be a scale-free detection method for saccades and microsaccades. No optimizing computation steps need to be performed to detect both at the same time. I computed the detection for all participants and trials. The detection of singularities using the continuous wavelet transform and definition of saccades and saccades during fixation as isolated smoothed singularities has been proven to be an appropriate method for their detection. We will now see how the detection

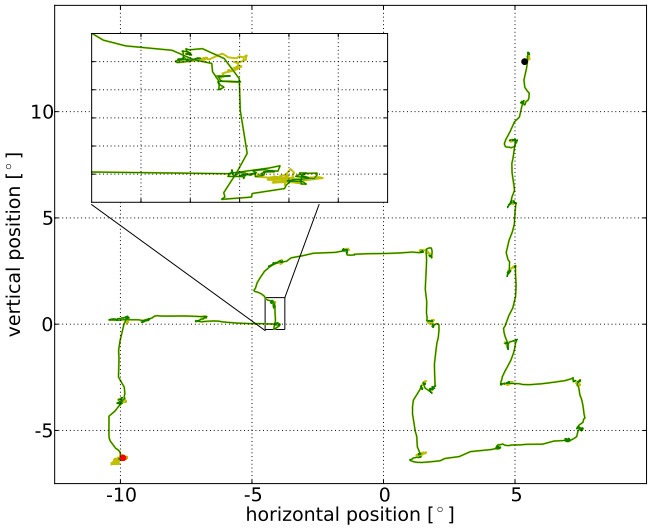

Figure 2.9: Detection of saccadic eye movements in the trajectory of the left eye, following a path on a Landolt-C-maze. *Trajectory parts in green depict a 0.12 seconds time window around the detected time point of a singularity. The yellow parts are the rest of the trajectory, i. e., for this type of task the fixations. The inset figure is a zoom into the trajectory. Start and end point of the search task are marked as black and red dot, respectively.*

method performs on time series acquired from a fixational eye movement experiment.

2.4 Detection of microsaccades

We have seen how the wavelet method allows us to detect saccades of all amplitude scales in the two time series of horizontal and vertical eye movements in a sequential scanning task experiment. Time series with smaller variances in their amplitude distribution are the time series recorded in a fixation task experiment. During fixational eye movements, the amplitudes of the drift and microsaccadic movement are smaller. This reflects itself in the velocity distribution and complicates the detection through the latter.

First, I will give a brief introduction into the fixation task experiment. Participants with an average age of 22 years and normal or corrected to normal vision performed a fixation task. A black square on a white background (3×3 pixels, spatial extent of 7.2 arcmin) was presented. Participants were asked to remain focused on this point and to prevent blinking during each record. An online check for blinks assured the completion of trials. Skipped trials were repeated. To avoid false detection of blinks, trajectories were checked by hand and skipped if a blink occurred. Each subject was required to finish 30 trials of 20 seconds each. Every fixation trial was followed by the presentation of a photograph for 10 seconds, allowing participants to relax and perform inspection saccades or blinks. The horizontal and vertical position of the eye was examined by the position of the center of mass of the recorded dark area of the pupil.

This experiment was designed and operated (cf. Chapter 1.5) by Konstantin Mergenthaler on the EyeLink II eye tracking device at the University of Potsdam (Engbert & Mergenthaler, 2006; Mergenthaler & Engbert, 2007; Mergenthaler, 2009).

As mentioned in the previous section, fixational eye movements have been modeled as fractional Brownian motion and we saw how the wavelet method is capable of detecting isolated singularities inside these dense singularities. In fact, it is more convenient to define microsaccades as smoothed versions of isolated singularities. The trajectory of microsaccades and the evolution of an onset over time look highly similar, when considering the notion of defining microsaccades as smoothed singularities (compare Figures 1.2 and 2.1).

In Figure 2.10, the trajectories of both eyes in a fixation task experiment are plotted. The dot in the center of each axes marks the position of the visual target the participants were asked to fixate. For illustration purposes, the size of the target was not changed such that it is a direct representation of the eye movements on the target. Furthermore the scale of the movements in comparison to the target is proportional.

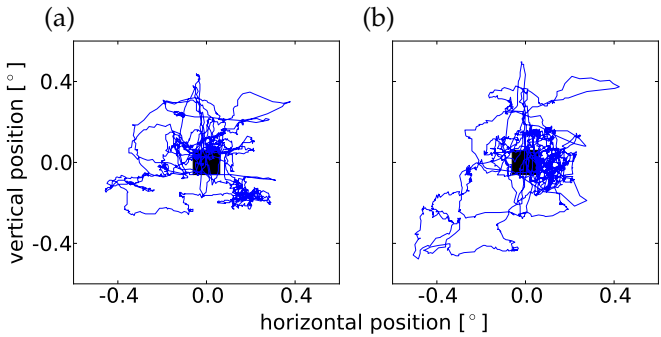

Figure 2.10: First five seconds of the time series representing the trajectory of both eyes fixating a small spot on a computer display. (a) *shows the trajectory of the left eye and* (b) *the trajectory of the right eye. The target is displayed at the center of the screen.*

Previous results (Engbert & Kliegl, 2003b, 2003a) have shown that microsaccades in fixational eye movements are highly pronounced in the horizontal movement direction. And Liang et al. (2005) have shown that the horizontal component dominates the vertical component in microsaccades. Using only the time series $h(t)$ of the horizontal eye movements, the detection of singularities reduces to the detection of maximum modulus lines in the modulus of $\mathcal{W}_h(a,b)$. The only preprocessing needed for $h(t)$ is the subtraction of the mean. Figure 2.11c shows a typical example of the modulus of $\mathcal{W}_h(a,b)$, the wavelet transform of the time series of the horizontal fixational eye movements. The frequency range and number of voices is the same as for the Landolt-C-maze experiment data (20 to 50 Hz and 128 voices). Again, the time points of each maximum modulus line at the highest frequency analyzed refers to the position of the singularity in the time series (cf. Equation 2.21). The trajectories in 2.11a and 2.11b for horizontal and vertical fixational eye movements are presented together with the marks at the detected time points of singularities.

The detection of singularities was performed for both eyes separately. In the total number of 682 trials, 35531 and 35066 singularities have been detected in the left and right eye, respectively.

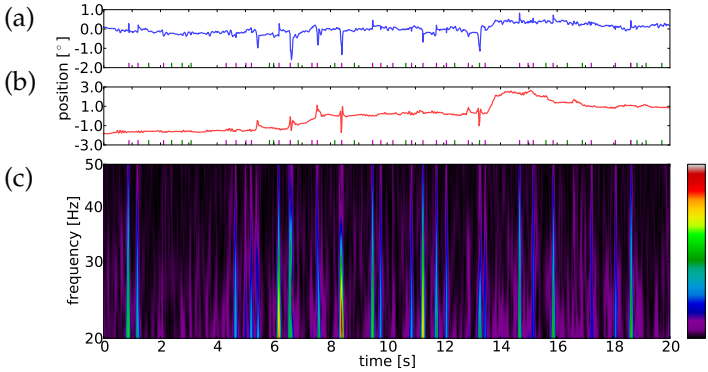

Figure 2.11: Representation of a fixational eye movement trajectory in time-position and time-frequency space. (a) *Horizontal and* (b) *vertical trajectory is plotted together with markers indicating the detected time points. Green markers refer to detected singularities and magenta markers refer to singularities that satisfied the binocularity criterion.* (c) *Modulus of the wavelet transform of the horizontal component of the fixational eye movements trajectory. Maximum modulus lines are identified because they connect local maxima through the frequency range.*

The difference in the number of detections between the eyes is lower than 1.3 %, yielding good agreement for the microsaccadic processes in both eyes.

Taking previous works into consideration (Ditchburn & Ginsborg, 1952; Krauskopf, Cornsweet & Riggs, 1960), microsaccades are generally binocular and conjugated eye movements. For the further analysis on microsaccades in this thesis, I restrict myself to the analysis of those singularities which occurred within a given time window of $\pm$ 15 ms around the point of a singularity in both eyes ($\tau = 15$ ms). Microsaccades in one eye have to have their simultaneously appearing microsaccades in the other eye in a time window $[t_0 - \tau, t_0 + \tau]$. I will refer to this as *binocularity criterion*. In Figure 2.11a and 2.11b, the magenta-colored marks identify binocular singularities and green marks correspond to the remaining singularities. Table 2.1 provides a summary of the detection results. After application of the binocularity criterion as described above, a total number of 16947 time points of binocular

Table 2.1: Rates of detected singularities in the horizonal eye movement in the fixation task experiment. *The total rates are given as mean ± standard deviation.*

Participant	Number of trials	Detected singularities rate of $[\frac{1}{s}]$		Binocular singularities rate of $[\frac{1}{s}]$
		left	right	
1	30	2.6	2.7	1.5
2	29	3.3	3.3	2.4
3	30	2.7	2.8	1.4
4	30	2.2	2.1	0.3
5	22	2.3	2.3	0.6
6	30	2.8	2.9	1.8
7	30	2.8	2.8	1.7
8	30	2.9	2.8	1.7
9	30	2.1	2.0	0.5
10	17	2.6	2.5	1.0
11	28	2.5	2.4	1.0
12	30	2.4	2.4	0.8
13	29	2.3	2.3	0.6
14	30	2.6	2.5	1.2
15	29	3.1	2.9	1.8
16	30	2.7	2.5	1.2
17	29	2.4	2.4	0.8
18	23	2.6	2.5	1.4
20	29	2.8	2.7	1.7
21	29	2.9	2.9	1.9
22	30	2.1	2.1	0.3
23	29	2.6	2.5	1.2
24	30	2.8	2.7	1.7
25	29	2.5	2.5	1.2
Total	682	2.6±0.3	2.6±0.3	1.2±0.5

singularities remains. The mean rate of binocular singularities is 1.2 ± 0.5 events per second, given as mean ± standard deviation. This is in good agreement with Engbert and Mergenthaler (2006)

on trials of the same experiment, using a threshold multiplier of $\lambda = 5$ in the velocity method.

2.5 Test of the detection method against surrogate data

In fixational eye movement studies, a persistent behavior on a short time scale (Engbert & Kliegl, 2004; Engbert & Mergenthaler, 2006) is observed. This is reflected in a positive autocorrelation function of the velocities for small lags. Additionally, it has been shown that microsaccades only influence the persistence behavior of fixational eye movements. Detecting saccadic eye movements as isolated singularities in the time series of fixational eye movements, the approach has to be tested against the possibility that drift movements might have been identified as isolated singularities. Then, the null hypothesis that positively autocorrelated samples in the drift are the reason for the observation of high-velocity epochs in fixational eye movements, may be rejected. Drift or fixational eye movements have been described as a time series that consists of dense singularities. Indeed, autocorrelated samples could be identified by the wavelet method to be isolated singularities. To obtain a measure for false detections of singularities in the fixation task experiment, a time series is generated which preserves properties of the velocity distribution of fixational eye movements but shuffles the time indices. One specific type of surrogate data allows us to test the null hypothesis. It is the amplitude-adjusted phase-randomized surrogate data (Theiler, Galdrikian, Longtin, Eubank & Farmer, 1992), which keeps the velocity distribution and approximates the autocorrelation function of the original dataset. The velocity $\vartheta(t)$ of the time series $h(t)$ of horizontal fixational eye movements is calculated as in (Engbert & Kliegl, 2003b). The generation of amplitude-adjusted surrogates is split into the following steps (adapted from Bettenbühl et al., 2010):

1. Sort $\vartheta(t)$ and obtain a rank series $r(\vartheta(t))$.

2. Generate a series $g(t)$ of Gaussian distributed random numbers with the same length as $\vartheta(t)$, sort it and rearrange it according to the rank series $r(\vartheta(t))$. This way, a time series $\breve{\vartheta}(t)$ is generated that is a rescaled time series of $\vartheta(t)$ with the property that the amplitude samples are normal distributed.

3. Transform $\breve{\vartheta}(t)$ to the Fourier space: $(\mathcal{F}\breve{\vartheta})(t) = \tilde{\vartheta}(\omega)$.

4. Randomize the phase: $\tilde{\vartheta}_{rand}(\omega) = \tilde{\vartheta}(\omega)\ e^{i\varphi(\omega)}$. The series $\varphi(\omega)$ contains equally distributed random numbers between $-\pi$ and π with identical values for positive and negative frequency.

5. Calculate the inverse of the Fourier transform: $(F^{-1}\ \tilde{\vartheta}_{rand})(\omega) = \breve{\vartheta}_{rand}(t)$.

6. Obtain a rank series of $\breve{\vartheta}_{rand}(t)$ and rearrange $\vartheta(t)$ according to the new rank series.

To again achieve a position-time series, the velocities, each divided by the sampling frequency, are summed up. In the following, I will refer to the obtained position-time series as surrogates or surrogate data of fixational eye movements. All 682 trials of surrogates are included and the wavelet method is applied the same way as for the original time series of fixational eye movements. The results for the detected singularities are shown in Table 2.2. The rates of binocular singularities significantly differ from the results on fixational eye movements and surrogates (two-sided t-test for independent samples, $p < 10^{-7}$).

High velocity epochs in the data of fixational eye movements that correspond to microsaccades can be split into more than one interval containing a singularity. But this is true only for monocular singularities. However, a high number of binocular singularities is observed, an average of 10 detections per trial. To explain this high number, a short calculation on the probability of randomly co-occurring extended events of length 2τ is to be performed. Here, co-occurrence is defined as: A singularity is detected in one eye within the time window of τ milliseconds before or after a singularity

Table 2.2: Rates for the detected monocular and binocular singularities in the surrogates of horizontal fixational eye movement data sets. *The total rates are given as mean±standard deviation.*

Participant	Number of trials	Detected singularities rate of $[\frac{1}{s}]$		Binocular singularities rate of $[\frac{1}{s}]$
		L	R	
1	30	2.5	2.6	0.4
2	29	3.1	3.1	0.6
3	30	2.8	2.7	0.4
4	30	2.4	2.2	0.4
5	22	2.7	2.5	0.5
6	30	2.9	2.9	0.5
7	30	3.1	3.0	0.6
8	30	3.2	3.2	0.7
9	30	2.5	2.5	0.4
10	17	2.7	2.6	0.4
11	28	3.1	3.0	0.6
12	30	3.0	3.2	0.6
13	29	2.3	2.3	0.3
14	30	2.8	2.4	0.5
15	29	3.1	3.0	0.6
16	30	2.7	2.5	0.4
17	29	2.4	2.3	0.4
18	23	3.3	3.3	0.7
20	29	3.2	3.2	0.7
21	29	3.4	3.3	0.7
22	30	2.5	2.4	0.4
23	29	3.3	3.3	0.7
24	30	2.8	2.7	0.4
25	29	3.4	3.3	0.7
Total	682	2.9±0.3	2.8±0.4	0.5±0.1

in the other eye. To estimate the probability of this co-occurrence, I will refer to the length of a monocular time series as T and number of monocular singularities as N. As each 2τ millisecond

time window frames the singularity in the center and singularities are at least Δt apart, a significant number of samples in the time series remain that can cause the co-occurrence of singularities. The probability of observing an event at approximately the same time in two time series by chance, i. e., two events satisfying the binocularity criterion, is given by

$$p(E) = \frac{(2\tau + \Delta t) \cdot N}{T} \tag{2.25}$$

which is the ratio of time, belonging to points of possible co-occurring candidates in the full trajectory.

For the presented data the values are: $\tau = 0.03\,\mathrm{s}$, $\Delta t = 0.002\,\mathrm{s}$, $T = 20\,\mathrm{s}$, and as average number for detected monocular singularities from all surrogates $N = 57$. Thus, the average number of events, co-occurring in both surrogate time series is $p(E) \cdot N \approx 10$ and agrees with the numbers of observed binocular events in the surrogates: 10 binocular events (cf. Table 2.2) on average. I can close the analysis on surrogates by stating that the detected number of binocular events mainly depends on the probability $p(E)$ of random co-occurrence. This probability is given by the parameter used in the binocularity criterion.

In the next chapter, I will analyze the shapes occurring in the time series at the time points of detected singularities in order to tackle the problem of false-detections by the continuous wavelet transform and the binocularity criterion, and to understand the shape relation between saccades and microsaccades as well as to verify possibly significant properties of saccade or microsaccade shapes if compared to surrogates.

3 A mathematical model for microsaccade shapes

The ballistic, jump-like event occurring in both eyes at almost the same time, is often described the following way: having a trajectory over time, the eye – after an initial period of rest – starts to accelerate to its maximum velocity and rapidly decelerates to attain its future (steady) position (J. M. Findlay & Gilchrist, 2003). A microsaccade, as already mentioned in Chapter 1.3, is often referred to as a small-amplitude saccade during visual fixation. The structural properties, the shape of saccades and microsaccades, are usually observed in studies but lack a detailed, statistical investigation.

In this chapter, I will propose a model for saccade and microsaccade shapes. Using this model, the suggested pattern of single-saccadic and double-saccadic pulse (cf. Chapter 1.3) can be completely parameterized. Furthermore, the model allows for the study of microsaccades, describing the events through individual parameter sets, and to get closer to a general model for fixational eye movements.

After a brief review of existing characterization approaches for (micro)saccades, I will introduce a method from multivariate statistics used in this chapter, the *principal component analysis* (Jolliffe, 2002), and propose a shape model. Then, using this data-based shape model, the prominent properties of saccades and microsaccades can easily be evaluated. An investigation on surrogate data (Chapter 2.5) will reveal that the presented shape properties are linked between saccades and microsaccades, which both have been detected with the wavelet method. Additionally, I will present an iris lens experiment whose analysis reveals that the video-based eye tracking device indeed – as often hypothesized (Collewijn

& Kowler, 2008) – overestimates the overshoot for saccades during visual fixation. The chapter closes with the application of the proposed shape model to examine important saccade and microsaccade properties. Parts of the results have been published in Bettenbühl et al. (2010) during the preparation of this thesis.

3.1 Existing concepts

Although the main sequence and different types of saccade patterns can be found in literature to vaguely parameterize saccades and microsaccades, no statistical model for the shape of saccades and microsaccades exists. I will briefly review two of the most-used characterization attempts for saccades and microsaccades before I present a statistical model in this thesis.

3.1.1 Characterization through the main sequence

Since the ground-breaking work of Zuber et al. (1965), a well-known concept for astronomers (Hertzsprung, 1911; Russell, 1913) has explained the nonlinear relationship between the velocity of a saccadic eye movement, its amplitude, and its duration: the *main sequence*. The amplitude and peak velocities of saccades of all amplitude scales are plotted against each other in a log-log-scatter plot. They show a power law relation, i. e., the points are located on a line in log-log presentation, showing their nonlinear dependence between duration, average velocity, peak velocity and saccade sizes (Bahill et al., 1975). In the work by Zuber et al. (1965), microsaccades have been demonstrated to share this characteristic relationship between peak velocity and amplitude, though in another range of the logarithmic scale than large-amplitude saccades which separate fixations. This shared aspect of saccades of all amplitudes and microsaccades allows them to conclude that a common physiological system produces both, the voluntary saccadic and involuntary microsaccadic eye movements, with the latter occurring in fixational eye movements. Other results also have suggested a common generator for saccades and microsaccades (Otero-Millan et al., 2008; Rolfs

et al., 2006, 2008). Additionally, the results suggested a common shape for both saccades and microsaccades.

3.1.2 Saccadic intrusions

With the beginning of the last decade and growing interest in microsaccades, Abadi et al. (2000) investigated the so-called *saccadic intrusions* (SI) in fixational eye movements as – with regard to the three components reviewed in Chapter 1.1 – an additional class of involuntary eye movements. The term SIs originates from studies on large-scale saccadic eye movements. This pattern of saccadic eye movement has been of interest in ophthalmology and medicine (Dell'Osso & Daroff, 1975; Dell'Osso, Abel & Daroff, 1977; Doslak, Dell'Osso & Daroff, 1983; Feldon & Langston, 1977; Jung & Kornhuber, 1964; Shallo-Hoffmann, Petersen & Mühlendyck, 1989). We already saw the classification scheme in Chapter 1.3. Two classes exist for single-standing microsaccades: *Single Saccadic Pulse* (SSP) and *Double Saccadic Pulse* (DSP). Whether these shapes are part of the proposed fourth type – the saccadic intrusions – or can be considered a specific shape of microsaccades, is a reasonable question that has to be answered.

3.2 Mathematical background

To investigate the main features of a shape or structure in a time series, a multivariate statistics tool, the *principal component analysis* (Pearson, 1901) can be used. Different observations of the same kind of structure, for example, the interval around a singularity in a time series can be averaged to obtain a "mean-value based structure". But the observations may, and will usually, deviate from the expected mean. Then the question arises regarding the measure of these differences. The *principal component analysis* determines the principal dimension or, in this case, the principal structural variations or *principal shape* of the observed structures. Additionally, it offers the possibility of breaking the number of microsaccade-

describing shapes down to the essential, most important ones. I will review in the following the mathematical basis of this analysis.

3.2.1 Principal component analysis

For N different observations $Y_1, Y_2, \ldots, Y_N$ of possibly interrelated variables, each observation of length m, the general purpose of using the principal component analysis (Jolliffe, 2002; Smith, 2002) is the transformation to a new, linearly uncorrelated set of variables through the orthogonal transformation to a new coordinate system with dimensions which explain most of the observed variance. The unbiased sample variance of two observations Y_k and Y_l is given by

$$\mathrm{Cov}(Y_k, Y_l) = \frac{1}{m-1} \sum_{i=1}^{m} \left(Y_{ki} - \bar{Y}_k\right)\left(Y_{li} - \bar{Y}_l\right) \tag{3.1}$$

and $\bar{Y}_k$ and $\bar{Y}_l$ are the mean of the m values for Y_k and Y_l, respectively. The autocovariance or variance is $\mathrm{Var}(Y_k) = \mathrm{Cov}(Y_k, Y_k)$.

Now, the dimension which contains the most variance of all N observations is of interest. Any observation Y_k can be represented by its m-dimensional vector y_k for $k = 1, \ldots, N$. A vector p_0 is sought which maximizes

$$\mathrm{Var}(\langle p_0, y_i \rangle) = \frac{1}{N-1} \sum_{k=1}^{N} \left(\langle p_0, y_i \rangle - \langle p_0, \bar{y} \rangle\right)^2 \quad \text{for } i = 1, \ldots, N \tag{3.2}$$

under the constraint that $\langle p_0, p_0 \rangle = 1$ and $\bar{y}$ denoting the mean of all vectors. The term $\langle u, v \rangle$ expresses the vector scalar product of two vectors u and v. Doing the subtraction

$$\widetilde{y}_k = y_k - \bar{y}_k \quad \text{for all } k = 1, \ldots, N \tag{3.3}$$

the value $\bar{y}$ will equal 0 and the product $\langle p_0, \bar{y} \rangle$ will vanish. Now, taking the $(m \times m)$-sized covariance matrix C which contains in its elements c_{ij} for $i \neq j$ all covariances between different vectors $\widetilde{y}_i$ and

$\widetilde{y}_j$ and which contains in its diagonal elements c_{ii} for $i = 1, \ldots, m$ the variances, one can rewrite Equation (3.2) as:

$$\mathrm{Var}(\langle p_0, y_i \rangle) = p_0' \; C \; p_0 \tag{3.4}$$

with p_0' denoting the row transpose of p_0. Now, the vector p_0 that maximizes the sample variance, is the eigenvector of C, corresponding to the largest eigenvalue λ_0 (Jolliffe, 2002). For this pair of eigenvalue and eigenvector, the sample variance is maximized. If arranged in descending order, the eigenvector p_1 of the second largest eigenvalue λ_1 maximizes the remaining sample variance of the data and so forth. Repeating this, we obtain m descendingly-ordered, different eigenvectors corresponding to m different eigenvalues describing the sample variance in m dimensions. These eigenvectors aligned in descending order are called *principal components* and are also *empirical orthogonal functions*. Under the given constraint of unit length, the obtained components are even *empirical orthonormal functions*.

The importance or score of every single principal component is measured as the amount of sample variance described by this principal component, which can then be calculated as

$$\widetilde{\lambda}_k = \frac{\lambda_k}{\sum_{i=0}^{m} \lambda_i} \tag{3.5}$$

with $\widetilde{\lambda}_k \in [0, 1]$. In Figure 3.1, the principal component analysis was performed on a dataset of two random normal distributed sets which were brought into linear relation. The resulting principal components represent a new orthogonal coordinate system, along which the first dimension accounts for the highest amount of variance, the second for the highest amount of variance of the remaining and so on.

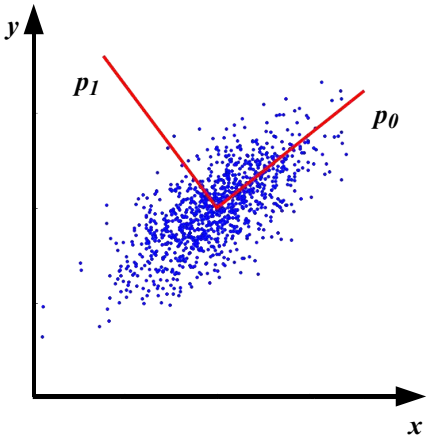

Figure 3.1: Illustration of the principal component analysis for two linearly dependent sets of numbers drawn from normal distribution. *The two dimensions p_0 and p_1 explain the most variance in the data.*

3.3 Characterization of saccade shapes

In Chapter 2.3, we have seen how to detect saccades of all amplitude scales in a time series recorded for the horizontal and vertical eye movements for both eyes. The saccades and microsaccades were defined as singularities in the time series. Both show a strikingly common property: their high velocity. To obtain a statistical model for the shape of saccades, the principal component analysis is performed for a 120 ms time interval (corresponding to 61 data samples at 500 Hz sampling rate) around the center of the detected singularity. I selected this time interval according to reported durations for large- and small-scale saccadic eye movements (Collins, Semroud, Orriols & Doré-Mazars, 2008). Furthermore, using such an interval, I accounted for possible detected positions of singularities which might, due to numerical computation errors, not be in the center of the interval every time. The detected time point of a singularity could, in principle, be detected at the start or end point of the saccade. Each single time period is taken as one indepen-

dent observation of the same natural phenomenon: a saccadic eye movement.

Before performing the principal component analysis, the time intervals need to be preprocessed to account for Equation (3.3). A set of time points is obtained which refers to the position of singularities for every participant, every trial and each eye. The interval around the lth singularity will be denoted with the vector $m^{(l)}$. First, the mean value is subtracted from every vector

$$\widetilde{m}^{(l)} = m^{(l)} - \frac{1}{61}\sum_{i=1}^{61} m_i^{(l)} \tag{3.6}$$

with $m_i^{(l)}$ for $i = 1, \ldots, 61$ denoting the ith element of the vector $m^{(l)}$. The vector $m^{(l)}$, representing the 120 ms interval around the singularity, is 61-dimensional (the sampling rate of the eye tracking device in the Landolt-C-maze experiment was 500 Hz, cf. Chapter 1.5 and 2.3). The subtraction of the mean is needed to center the observations around the origin. In a second step, the vectors $m^{(l)}$ of all trials and all participants were used to perform the principal component analysis, separately for each eye. This way, the main shapes for a shape model will be based on major variations. In a third step, before the application of the principal component analysis, the overall mean was subtracted, compared to Equation (3.2), then $\bar{y} = 0$.

Table 3.1: Scores of the principal shapes for both eyes and movement directions. *The first two principal components can explain at least 94 % of the variance in the observations.*

direction	$\widetilde{\lambda}_0^{left}$	$\widetilde{\lambda}_1^{left}$	$\widetilde{\lambda}_0^{right}$	$\widetilde{\lambda}_1^{right}$
horizontal	0.93	0.05	0.9	0.04
vertical	0.94	0.04	0.92	0.04

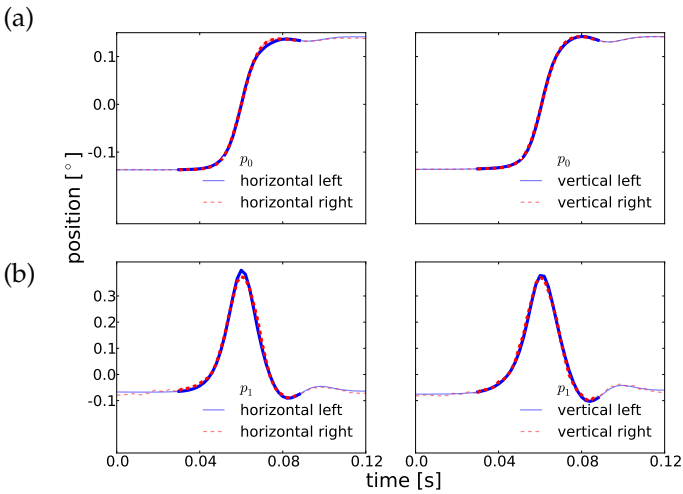

Figure 3.2: The first two principal components for both eyes and both movement directions. *The shapes of p_0 and p_1 are plotted as results of the principal component analysis of saccadic eye movements.* (a) *Presents p_0 for both movement directions and* (b) *the vertical movement. The step-like p_0 presents itself as sigmoidal for the highlighted part of the trajectory whereas p_1 is a bump with a tiny oscillation at the right tail. The highlighted part will be used to compare the shapes versus results from the fixational eye movements.*

Figure 3.2 shows the results for p_0 and p_1 for both eyes and both directions. Their scores are presented in Table 3.1. A 60 ms time interval around the center of the singularity is emphasized by bold lines. To describe above 94 % of the observed variance, I selected the first two principal components for the shape model. To obtain the minimal set of shapes for the shape model of saccadic eye movements, it is sufficient to use only p_0 and p_1. This model is able to represent the shape of saccades of all amplitude scales. But this model might not be representative of saccades during fixations – microsaccades – because most detected saccades in the Landolt-C-maze experiment have been of large amplitude scale, as a result of the task performed in this experiment. A shape model for the saccades during fixations might differ. With the data at hand from the fixation task experiment (cf. Chapter 2.4), another analysis can be performed for saccades during fixation.

3.4 A microsaccade shape model

The previous section closed with the shape model for saccades of all scales. For fixational eye movements, the saccades that are expected to be detected, are microsaccades, the *saccades during fixation* (cf. Chapter 1.3). The typical minimum duration of microsaccades is reported to be of 6 ms (Engbert & Mergenthaler, 2006) and 12 ms duration (Engbert & Kliegl, 2003b). I use these results to define the time period around the time points of singularities. These periods are the set of observations for the principal component analysis. As with saccades, the detected time point of the singularity could be at the start or end of a microsaccadic eye movement. Thus, I selected a time interval of 30 ms before and after the time point of the lth singularity for the vector of observations, denoting it again with $m^{(l)}$. Differently than for the saccades detected in the Landolt-C-maze experiment, I used only the time points of those singularities which occurred in both eyes at approximately the same time (*binocularity criterion*, cf. Chapter 2.4). In doing so, I accounted for results regarding microsaccades, which are described as binocular events (Rolfs et al., 2008).

The vectors $m^{(l)}$ are preprocessed as described in Chapter 3.3. One typical shape of a time interval around the binocular singularity is presented in Figure 3.3, together with its representation by the linear combination of the principal components. Importantly, I used all binocular singularities of all participants in all trials to

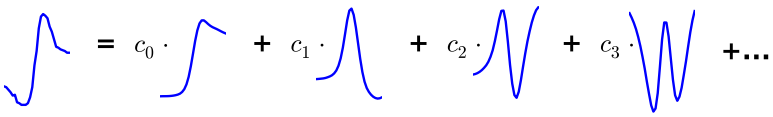

Figure 3.3: Illustration of the 60 ms time interval around a binocular singularity as linear combination of the computed principal components. *The shape on the left presents one typical 60 ms horizontal trajectory of one participant around the time point of a singularity. The shapes on the right present the results of the principal component analysis. The factors c_i for $i = 0, \ldots, 30$ are factors that present the contribution of every shape to the variance of the original trajectory.*

Table 3.2: Scores of the principal shapes, analyzed for the microsaccades in fixational eye movements. *For both eyes, the first two principal componets can explain at least 94 % of the variance in the observations.*

	$\widetilde{\lambda}_0$	$\widetilde{\lambda}_1$
left eye	0.82	0.12
right eye	0.80	0.14

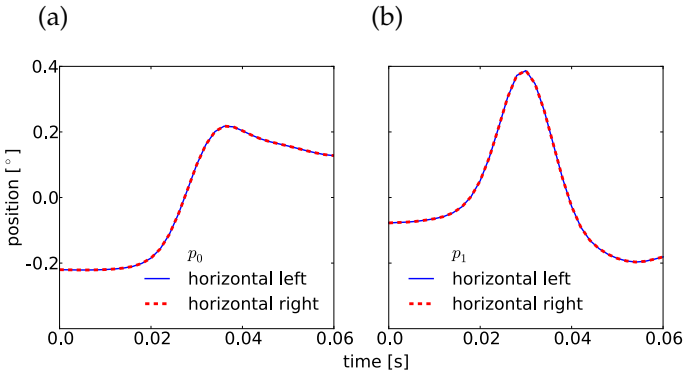

Figure 3.4: The first two principal components in the left and right eye, obtained for the fixation task experiment. (a) *Shows a steplike shape as first principal component p_0, which has the tendency to return after it reaches the maximum amplitude. This overshoot, typical for microsaccades, dominates together with the almost linearly increasing part of this shape.* (b) *The shape of the second component p_1 is bump-like. It identifies how much overshoot each microsaccade has. The left (blue solid line) and right (red dashed line) eyes agree in the shape of the first two principal components. The scores are $\lambda_0 = 0.82$ and $\lambda_0 = 0.8$ as well as $\lambda_1 = 0.12$ and $\lambda_1 = 0.14$ for the analysis done for the left and right eye, respectively.*

perform the principal component analysis of the time intervals $m^{(l)}$ separately for the left and right eye.

The principal component analysis of time intervals $m^{(l)}$ revealed that the first two principal components p_0 and p_1, presented in Figure 3.4, account for more than 94 % of the variability of microsaccadic shapes. The scores are reported in Table 3.2. For further analyses, it is therefore sufficient to restrict analyses to these first two principal shapes.

A single microsaccade $m^{(l)}$ is decomposed into the following five terms:

- a first principal shape p_0,
- a second principal shape p_1,
- a scalar $\bar{m}^{(l)}$ returning the mean of the observations in the time interval around the singularity,
- a vector ν_{eye} to represent the mean of all vectors $\widetilde{m}^{(l)}$ for one eye,
- a small residual vector ζ to account for numerical errors.

All these components are directly computed from the observations (except the residual vector which enters through the numerical computation). A model for a typical microsaccade shape can therefore be expressed as

$$m^{(l)} = c_0^{(l)} p_0 + c_1^{(l)} p_1 + \bar{m}^{(l)} + \nu_{eye} + \zeta \tag{3.7}$$

with $c_0^{(l)}$ and $c_1^{(l)}$ the shape coefficients of every individual microsaccade m^l, obtained through projection, i. e., the scalar products $\langle p_0, m^{(l)} \rangle = c_0^{(l)}$ and $\langle p_1, p_1^{(l)} \rangle = c_1^{(l)}$. Clearly, for the saccades in the Landolt-C-maze experiment, a shape model can be constructed as well. In that model, the principal shapes obtained in the analysis of the saccades in the Landolt-C-maze experiments have to be chosen. But it cannot present a generally-applicable shape model for saccades because saccades in different tasks might also differ in their shapes. Comparing the results of the principal component analysis for saccades in the Landolt-C-experiment – being of all scales – and for microsaccades in the fixation task experiment, clear similarities are revealed. Both present a step-like first and bump-like second component. In fixational eye movements, the horizontal dominates the vertical direction for microsaccades such that a shape model for the horizontal eye movements during microsaccades is sufficient. In contrast, in the Landolt-C-experiment, the principal shapes for

horizontal and vertical saccades are similar in that the shape model must account for the possibility of oblique directions. However, it seems that the overshoot is more prominent in microsaccades.

3.5 Comparison of the model with simulations

The overshoot in the shape of microsaccades is quite prominent. It does not prominently emerge in the experiment, which contains saccades of all amplitude scales. To determine if the difference which is obtained for the shapes of microsaccades and saccades in their overshoot behavior is due to the detection and characterization method proposed, I performed a principal component analysis for the detected singularities in a surrogate dataset (cf. Chapter 2.5). Applying the binocularity criterion as described in Chapter 2.4, the time intervals around the singularities are preprocessed as explained in Chapter 3.3 and the data is analyzed for its principal components. Again, the first two components explain more than 95 % of the variance in the data. The principal components p_{0s} and p_{1s} will get chosen in order to obtain a representative shape model. Presented in Figure 3.5, the principal component p_{0s} is a sigmoidal function and does not show any overshoot. The second component p_{1s} is a very smooth peak-like bell curve. Both p_{0s} and p_{1s} are smoothed versions of singularities that could be represented by Equation (2.3) in Chapter 2.2.1, the local cusp.

Importantly, the p_0 and p_1 of the original data show a directionality in time: They cannot be time-reversed. The principal components p_{0s} and p_{1s} for the surrogate data can be reversed. Both of the latter satisfy the condition of symmetry such that $f(-t) = -f(t)$ for a function $f \in \mathbb{R}$ and do not show any directionality.

One can conclude that the observed binocular singularities in the time series of fixational eye movement and in the time series of the Landolt-C-experiment have a distinct shape and that the strongly pronounced overshoot in the microsaccade shape model is part of

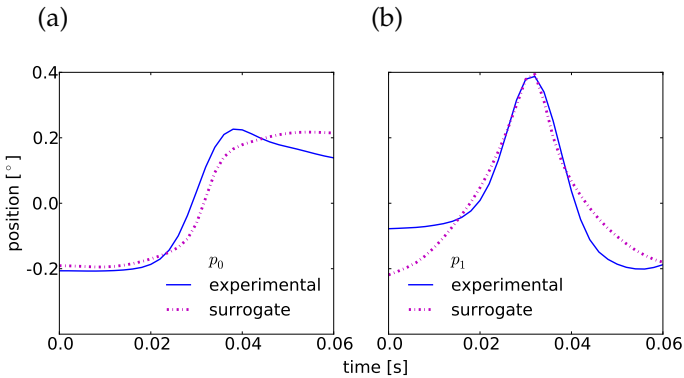

Figure 3.5: The first two principal components obtained for surrogate data vs. experimental data. (a) *Presents the p_0 and p_{0s} for fixational eye movement and surrogate data and* (b) *the p_1 and p_{1s} of the same datasets is shown. Analyses for both eyes result in the same shapes.*

microsaccades that were recorded with a video-based eye tracking device.

3.6 Iris test lens experiment

We have seen that the overshoot is a prominent property of microsaccades in the shape model for saccades during fixational eye movements. In literature, these overshoot components of microsaccades are often questioned and assumed to be artifacts which are caused by the video-based eye tracking method (Collewijn & Kowler, 2008; Drewes, Montagnini & Masson, 2011; Mammo, Kimmel & Newsome, 2011). In video-based eye tracking, one possible source for an artifact could be the dilation of the pupil. As explained in Chapter 1.5, video-based eye tracking devices calculate the position of the eye as center of the recorded disk which represents the eye pupil. A change in size of this disk affects the accuracy of the calculated eye position. Together with Petra Sinn, we designed an experiment to examine this possible artifact. To investigate the influence of the pupil dilation and fluctuations on the

recorded eye movement trajectories in the fixation task experiment, we set up the fixation task experiment as explained in Chapter 2.4, without the presentation of a photograph between subsequent fixation screen. During two sessions of 4×30 trials each, participants wore an iris lens in one of their eyes, changing the eye to wear the lens between the two different sessions.
Iris lenses are used by opticians for cosmetic or medical corrections of an injured or diseased eye ball. For humans with, for example, cataract (Spencer & Mamalis, 2010), they allow the covering of the eye's opacification through a printed or hand-painted iris lens around a transparent center. To adjust iris lenses for the radius of the eye ball and lens size, opticians use a white opaque iris lens with a clear and transparent center. Like the iris lens, the test lenses adhere more strongly to the eye ball than normal contact lenses because they need to stay in position to cover the opacificated eye, even after the occurrence of a blink. For our experiment, this induces less floating on the eye ball and the recordings of the disk are not affected by "lens floating". In Figure 3.6, I present an illustration of the test lens on the eye, showing those parts visible to the video-camera. The iris is covered by the white part of the test lens and the size of the eye's pupil is slightly reduced if compared to the other eye. The radius of the clear part for the pupil can be of different sizes. We used test lenses from Galifa Contactlinsen AG, St. Gallen, Switzerland for our experiments.

Figure 3.6: Illustration of the both eyes, the right one wearing the test lens. *Recordings of fixational eye movements might get influenced by small fluctuations of the pupil size. One eye wears a test lens which allows eye-tracking through a static, stable disc.*

The iris lens experiment was recorded with the EyeLink 1000 system at 1000 Hz for both eyes. Possible head movements have been significantly reduced through a chin rest. Participants were required to perform the same experiment as explained in Chapter 2.4, except for the presentation of the photograph for 10 s. The experiment was carried out by Petra Sinn at the University of Potsdam with the EyeLink 1000 device (cf. Chapter 1.5), using the corneal reflex if possible.
Performing a singularity detection with the wavelet method, time intervals $m^{(l)}$ of 60 ms duration around the singularities were used for the principal component analysis (Chapter 3.4). This analysis is performed for all singularities – regardless of the binocularity criterion – and for binocular singularities to account for possible influences by that criterion.

Again, the first two principal components p_0 and p_1 were sufficient to explain the variance in the observed time intervals $m^{(l)}$ to above 94 %. In Figure 3.7, the resulting principal components are presented in four different graphs, allowing investigation of all possible combinations of

- all singularities in the eye with the test lens,
- all singularities in the eye without the test lens,
- binocular singularities in the eye with the test lens,
- binocular singularities in the eye without the test lens.

This allowed for an investigation of possibly existing effects of selecting all or only binocular singularities and furthermore study the hypothesized effect of pupil dilation on the precision in the video-based eye tracking device. In this thesis, I focus only on the effect of pupil dilation on the overshoot component of the microsaccades.

From now on, I will refer to the eye, wearing the lens as *lens-eye* and for the eye without lens as the *normal-eye*. The principal shapes for the normal-eye will be referred to as p_0 and p_1 and for the lens-eye with ρ_0 and ρ_1. The superscripts a and b will denote if they

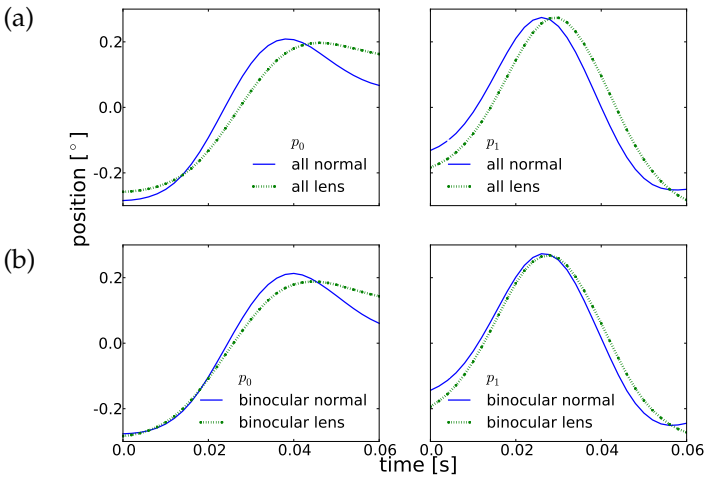

Figure 3.7: The results of the principal component analysis obtained for different data sets. *Shown are p_0 and p_1 for the data of measurements in the following setups and criterion:* (a) *all and without lens,* (b) *binocular and without lens,* (c) *all and with lens,* (d) *binocular and with lens. For each particular setup, no difference between the PCA performance on monocular or binocular singularities exists. But the overshoot is not prominent in the principal shapes obtained for the trajectories, which have been recorded for the eye which was wearing the test lens.*

are obtained by the analysis of all singularities or only binocular singularities, respectively. All vectors are normalized. Performing the analysis on all singularities or only binocular singularities revealed no differences between lens- and normal-eye. Additionally, with regard to the normal eye, the components remained the same if either all or only binocular singularities were chosen for the principal component analysis such that the selection of all singularities or binocular singularities for the principal component analysis does not alter the results for the shape model. This becomes clear if considering their projections $\langle p_0^a, p_0^b \rangle \approx 1$ and $\langle p_1^a, p_1^b \rangle \approx 1$. The same result is obtained for the lens-eye. Thus, I can refer to the principal components for the normal-eye as p_0 and p_1 and for the lens-eye as ρ_0 and ρ_1 without differentiation in the superscript a or b.

Secondly, by visual inspection of the trajectories obtained for p_0 and ρ_0, the overshoot does not present a prominent characteristic for the lens-eye. The second components, p_1 and ρ_1, only differ slightly in the slope of their right tail. The distinctiveness between the principal components for the lens- and normal-eye is a first hint that pupil dilation might indeed lead to the appearance of more pronounced overshoots for microsaccades in fixation task experiments if recorded with a video-based eye tracking system.

3.7 A (micro)saccade catalog

The previously-obtained shape model for microsaccades in fixational eye movements provides us an easy access to microsaccade properties which are of interest to study (cf. e. g., Zuber et al., 1965; Otero-Millan, Serra et al., 2011). The wavelet method used the definition of saccades and microsaccades as singularities in the time series of (fixational) eye movements. Now, with the shape model one further step allows us to refine this definition by the two shape factors

$$c_0^{(l)} = \langle \widehat{m}^{(l)}, p_0 \rangle$$

and

$$c_1^{(l)} = \langle \widehat{m}^{(l)}, p_1 \rangle$$

with

$$\widehat{m}^{(l)} = \frac{\widetilde{m}^{(l)}}{|\widetilde{m}^{(l)}|}$$

and $\widetilde{m}^{(l)}$ the time interval around a singularity in the eye movement experiments.
Now, the shape model can easily represent single saccadic and double saccadic pulse with a certain parameter set $\{c_0, c_1\}$. Both can be considered as microsaccades, only under different parameterization in the shape model. Regarding all analyses, a refinement of the definition of microsaccades as singularities in the time series can be done. With respect to the shape factors, the time periods around binocular singularities whose variance can to be described

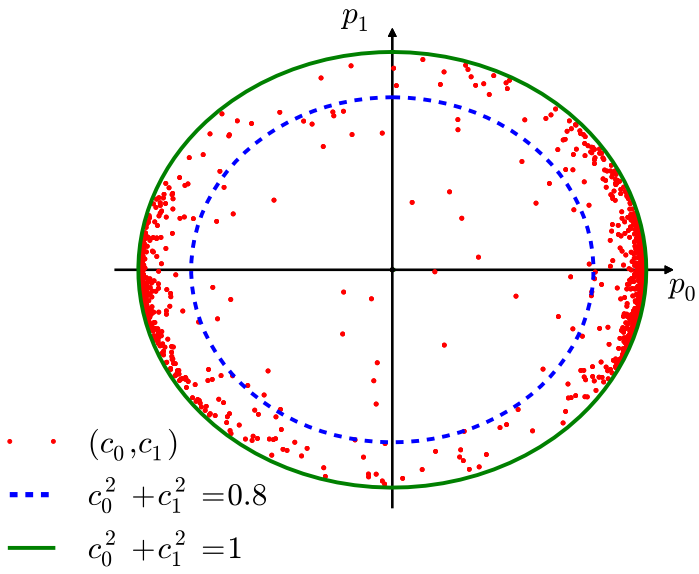

Figure 3.8: Representation of microsaccade candidates in the feature space spanned by p_0 and p_1. *Every pair (c_0, c_1) represents the contribution of the dimension to the microsaccade shape.*

by the first two principal components to at least 80 %, should be defined as microsaccade. In terms, it is

$$\left(c_0^{(l)}\right)^2 + \left(c_1^{(l)}\right)^2 \geq 0.8 \sum_{i=0}^{30} \langle \widehat{m}^{(l)}, p_i \rangle^2 \tag{3.8}$$

and illustrated in Figure 3.8 by the blue-dashed and green-solid line. I will refer to this criterion as *energy criterion*.

For further analyses, I used only the trajectories around binocular singularities that fulfilled the binocularity and energy criterion. I will refer to these time periods as microsaccades .

Because of its smooth estimation of the trajectory of a microsaccade, the model allows a simplified estimation of all important

microsaccade shape-related properties. A microsaccade property catalog will then contain for every microsaccade:

- time point of occurrence,
- direction,
- amplitude,
- overshoot,
- displacement,
- shape factors c_0 and c_1.

Having this catalog, I investigated the amplitudes for microsaccades and estimated the probability density for the distribution of measured amplitudes by Gaussian kernel density estimation, using the Silverman rule for bandwidth selection (Silverman, 1986). The results are, together with a plot of the amplitudes in the lower plot, presented in Figure 3.9. The result of 0.16° visual angle as maximum of this unimodal distribution is in strong agreement with the reported value of 0.15° by Mergenthaler (2009), who detected microsaccades with the velocity threshold method and estimated the amplitude without any model for the microsaccade shape.

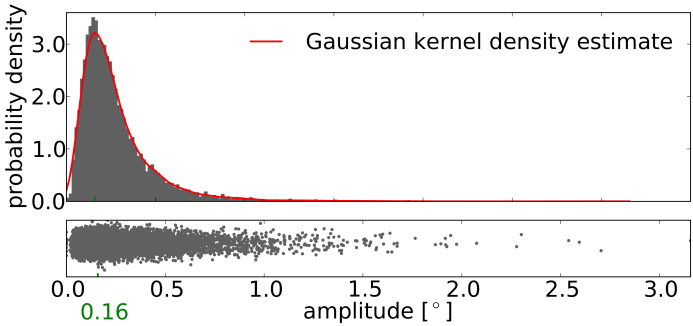

Figure 3.9: Probability density of the microsaccade amplitudes in the fixation task experiment. *The probability density was estimated by Gaussian kernel density estimation, using Silverman's rule for bandwidth selection. The position at 0.16° returns the most probable amplitude for the measured microsaccades.*

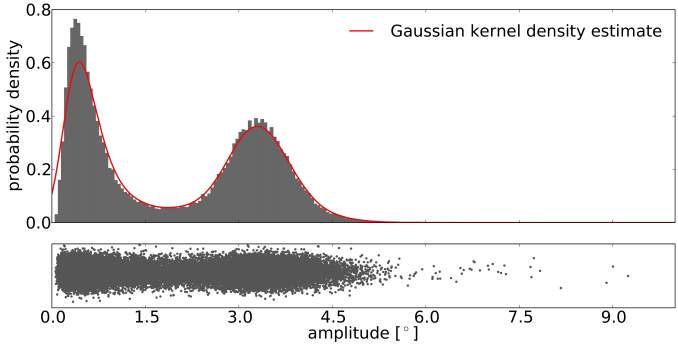

Figure 3.10: Probability density of amplitudes for all saccades detected in the Landolt-C-maze experiment. *The probability density was estimated by Gaussian kernel density estimation, using Silverman's rule for bandwidth selection. The two local maxima are at 0.45° and 3°.*

For saccades of all amplitudes as detected in the Landolt-C-maze experiment, an estimate of the amplitude distribution is presented in Figure 3.10. It is a bimodal distribution with maxima at 3° and 0.45° visual angle. The stimuli were 3° apart, which explains the one maximum. The other maximum is in a typical range of microsaccade amplitudes in non-fixation task experiments (Engbert, 2006b; Otero-Millan et al., 2008).

Having arrived at a straight-forward and computable catalog of saccade and microsaccade properties, I will continue to investigate their dynamics with a focus on microsaccades by studying saccadic dynamics during fixation. In a fixation task, no external stimuli drives the eye movements and we can hope to understand the baseline of microsaccadic dynamics to gather a deeper insight into saccade dynamics.

4 Dynamics in microsaccade sequences

In the previous chapters, I presented a method for scale-free detection of saccades in different experiments and characterization of their shapes, with respect to their different behavior at different scales. Here, I want to focus on the dynamics within sequences of microsaccades.

In this chapter of my thesis, a stochastic model for symbols of discrete-events in time series, such as microsaccades in fixational eye movements, is proposed. In the last 15 years, studies started to separate certain patterns of successive saccades and single-standing saccades during fixation (Abadi et al., 2000; Abadi & Gowen, 2004; Otero-Millan, Serra et al., 2011). Again, fixation task experiments are the most controlled framework in which to investigate the underlying mechanisms of the oculomotor system. Trajectories of the eye movements indirectly allow the study of the rotation and movement of the eye (J. M. Findlay & Gilchrist, 2003). Thus, understanding the dynamics of microsaccades will broaden the knowledge for modeling eye movements in general.

I will abridge the most prominent works by Abadi and Gowen (2004) and Otero-Millan, Serra et al. (2011) before introducing definitions and background from stochastic modeling, discrete-time Markov chains, and Bayesian modeling. To select a model from a family of models that are alike, I will use the analysis of the Bayes factor. We will see how describing a sequence of symbols by Markov chains provides the best model for microsaccade sequence dynamics. I will finish the chapter by investigating the role of "continuous time". I will show its importance to distinguish in a time-dynamic Markov chain model to generate microsaccades. All

analyses and results of fixational eye movements in this chapter are obtained from the left eye. For the right eye, the analyses and results are the same.

4.1 Existing concepts

Searching for results on microsaccade sequence dynamics, I found two prominent approaches, which were communicated in different contexts. I will briefly review the main results and bring them into the context of my analysis on microsaccade sequence dynamics. Both results use many adjustable parameters to describe or distinguish microsaccade sequence patterns. We will later see that the study in this thesis does not approach sequences on this basis.

4.1.1 Saccadic intrusions

Besides the single events classified as *Single Saccadic Pulse* (SSP) or *Double Saccadic Pulse* (DSP), Abadi and Gowen (2004) introduced two types of SIs in fixational eye movements, which consist of two or three subsequent (micro)saccadic events, called *Monophasic Square Wave Intrusion* (MSWI) and *Biphasic Square Wave Intrusion* (BSWI).

Numerous definitions of MSWI for normal, large-scale saccades, exist (Jung & Kornhuber, 1964; Dell'Osso & Daroff, 1999). I will outline the definition's ambiguity. Starting from here, I will call a MSWI a pattern that is a sequence of two subsequent microsaccades in fixational eye movements, separated by a short interval of drift movement and oppositely directed in the horizontal trajectory of an eye's recording. Abadi and Gowen (2004) reported this major type of SI found in 94 % of their subjects, collected in an experiment of two 50-second binocular eye recordings during fixation of a static target. They hand-picked the events from the original raw time series. Important characteristics of the MSWI are the amplitude which ranged from 0.1° to 4.1° and the mean duration of 255 ± 147 ms between the subsequent events.

The sequence of three subsequent microsaccadic events, called BSWI, was found in 40 % of the subjects in the same experiment. The pattern was less prominent and less frequent than the MSWI. A typical duration of the set of three events was between 85 to 267 ms (calculated from Table 1, Abadi & Gowen, 2004). For both patterns, MSWI and BSWI, the direction and amplitude of the last microsaccade depend on the first event or first two events, respectively.

In another study, Gowen, Abadi, Poliakoff, Hansen and Miall (2007) investigated the influence of exogenous and endogenous attention on SIs or, more specifically, the modulation of MSWI by the former. Furthermore, they compared MSWI and microsaccades at different experimental target cues. Gowen et al. (2007, pp. 162) proposed that "the above similarities between microsaccades and SI support the conjecture that the two saccadic behaviors relate to the same phenomena" (in this context, SI refers to MSWI).

4.1.2 Square-wave jerks

Not only do microsaccades often have different names (compare Chapter 1.3) but the saccadic intrusion or, moreover, its most prominent type, the monophasic square wave intrusion, also has different names in the literature, and is often referred to as square-wave jerks[1] (Otero-Millan, Serra et al., 2011).

Recently, Otero-Millan, Serra et al. (2011) introduced an advanced treatment of microsaccade sequences. Based on the velocity-threshold algorithm by Engbert and Kliegl (2003b), they used direction dissimilarity, magnitude dissimilarity, and temporal proximity to calculate an index to decide whether a pair of microsaccadic events is a SWJ or not. Already in Chapter 1.3, I illustrated the properties and measurements they used to decide whether a pair of subsequent microsaccades presents a SWJ or two independent single-standing microsaccades.

[1] In the following, I will use the name square-wave jerk (SWJ) to avoid confusion MSWI, the other, for larger saccades, widely-accepted term.

In their calculation, an ideal intermicrosaccadic interval (IMSI) of 200 ms was reported, estimated by the fit of an ex-Gaussian distribution function of all subject IMSIs. After separation of single-standing microsaccades and SWJs by the SWJ index, the intra-SWJ time interval averaged to 280 ± 10 ms for the control group, i. e., healthy subjects. Compared to the study of Abadi and Gowen (2004), this value is larger but it is based on an automated detection routine for microsaccades and SWJs. Studying the relationship between microsaccades and SWJs in healthy subjects and Progressive Supranuclear Palsy (PSP) patients, Otero-Millan, Serra et al. (2011, pp. 4386) concluded "that microsaccades and SIs are essentially the same phenomena and that SWJs are generated by a common coupling mechanism in PSP patients and healthy observers".

I will propose a statistical model which will support the previous assumption and go beyond the proposal to deliver a model for microsaccade generation which includes direction and the intermicrosaccade interval distribution.

4.2 Mathematical background

Before I will present microsaccades as symbols in fixational eye movements, I will briefly review definitions from Markov chains, symbolic dynamics and the Bayes factor for model selection that contribute to the understanding of this chapter. A detailed treatment of definitions would go beyond the scope of this work. For further reading, I recommend, for example, Taylor and Karlin (1984) for reference.

4.2.1 Markov chains

Given a process $\mathcal{X}$ in the *state space* $\mathcal{S}$, $\mathcal{S} = \{0, 1\}$ and assuming that the process is an uncorrelated random process, then a *sequence of states* X_T for $T = 1, \ldots, k, \ldots, N$ is obtained by randomly assigning each time point X_k one state $s_k \in \mathcal{S}$. For the state space $\mathcal{S} = \{0, 1\}$, probabilities for each state are given by $Pr\{X_k = 0\} = p_1$ and

$Pr\{X_k = 1\} = 1 - p_1$ such that p_1 parameterizes the probability distribution of that uncorrelated random process.
Now, lets consider a discrete-time stochastic process with state space $\mathcal{S} = \{0, 1\}$ where the probability of the next state $j \in S$ at the next time point X_{k+1} depends only on the current state $i \in S$ at time point X_k, or in mathematical terms:

$$\begin{aligned} Pr\{X_{k+1} = j | X_k = i, X_{k-1} = s_{k-1}, \ldots, X_1 = s_1\} \\ = Pr\{X_{k+1} = j | X_k = i\} \end{aligned} \tag{4.1}$$

with $s_1, \ldots, s_{k-1} \in \mathcal{S}$. Every stochastic process with a countable set as state space $\mathcal{S}$ and this so-called *Markov property* is called a *Markov process* (Markov, 1971). A *discrete-time Markov process* is also referred to as *Markov chain*. The conditional probability in Equation (4.1) is called *one-step transition probability* and will be denoted by

$$P_{ij} = Pr\{X_{k+1} = j | X_k = i\} \; . \tag{4.2}$$

If this probability does not depend on time such that Equation (4.1) is true for $1 \leq k < N$, then the probabilities are called *stationary transition probabilities*. They affiliate with a *stationary* or *time-homogeneous Markov chain*. Now, lets expand the state space to $\mathcal{S} = \{s_1, \ldots, s_M\}$, containing M different states, then the transition probabilities in Equation (4.2) can be arranged into a *transition matrix* T of size $M \times M$, given by

$$T = \begin{pmatrix} P_{11} & P_{12} & \ldots & P_{1M} \\ P_{21} & P_{22} & \ldots & P_{2M} \\ \vdots & \vdots & \ldots & \vdots \\ P_{M1} & P_{M2} & \ldots & P_{MM} \end{pmatrix} \tag{4.3}$$

with, for example, P_{12} as a change from state s_1 to s_2 and the others accordingly. Clearly, all $P_{ij} \geq 0$ for $i, j \in \mathcal{S}$ and

$$\sum_{j \in \mathcal{S}} P_{ij} = 1 \tag{4.4}$$

for each $i \in \mathcal{S}$. For a time-homogeneous Markov chain, its *stationary probability distribution* can be identified. With the transition matrix T, the vector π contains the nonnegative probabilities of the stationary distribution of the Markov chain. A vector π solving the equation

$$\pi' T = \pi \tag{4.5}$$

is the left-handed or Perron-Frobenius eigenvector (Perron, 1907; Frobenius, 1912) with $||\pi||_1 = 1$ and all M entries $\pi_j \geq 0$ for $j = 1, \ldots, M$. Here, π' defines the transpose of column vector π. Once the process is in its stationary distribution, another transition does not alter the distribution anymore. This is expressed in Equation (4.5) in which another multiplication with T onto vector π does not change the vector π.

Under consideration of Equation (4.1), the probability measure is called an *nth-order Markov measure* if it satisfies

$$\begin{aligned} Pr\{X_{k+1} = j | X_k = i, X_{k-1} = s_{k-1}, \ldots, X_1 = s_1\} \\ = Pr\{X_{k+1} = j | X_k = i, \ldots, X_{k-n} = s_{k-n}\} \end{aligned} \tag{4.6}$$

with $i, j, s_1, \ldots, s_{k-1} \in \mathcal{S}$. Now, the probability of a certain state at time point k depends only on the sequence of the previous n time points. A discrete-time process is called an n-order Markov chain if its probabilities have this kind of memory.

4.2.2 Symbolic dynamics

From symbolic dynamics, I will only review some basic definitions which will add to the understanding of the following sections. For a more detailed introduction, see Lind and Marcus (1995). Above, the sequence of states was considered through $X_T \in \mathcal{S}$ with state space $S = \{s_1, \ldots, s_M\}$. Now, observing events in discrete time, these events might be mapped onto *symbols* or *letters* in an *alphabet* S. Under consideration of the framework of this thesis, let the alphabet or *symbol space* be $S = \{l, r\}$ with l for an eye movement to the left and r to the right. A *compound symbol*, for

example, *lr* or *lrl* is called a *word* or *block*. Then, a sequence of symbols can be separated into words of different lengths.

4.2.3 Model selection using Bayes factor

A set of *events* that represents the recorded outcomes of an experiment, can be called a *data set* D. For an observed data set D, often a collection of parameterized *stochastic models* can be proposed and the question arises regarding which model should be selected as the best descriptor. The selection criteria should not only take into account how well the data is described but also the complexity of the model that describes it. The goal is not to optimally fit existing data but to minimize the prediction error when new, unobserved data comes at hand. Optimizing only the fit leads to poor prediction performance, a phenomenon known as overfitting. In the Bayesian setting, the model selection is done by analyzing the Bayes factor (Kass & Raftery, 1995).

The *likelihood* that a hypothesized model M under parameterization θ can describe the data D, is denoted by $Pr\{D|M,\theta\}$. In Bayesian statistics, the *degree of belief* in a hypothesized model M under the parameterization θ is measured by the *prior probability* $Pr\{\theta|M\}$. Under consideration of the data set D, the prior probability for a model will then be updated through

$$Pr\{\theta|D,M\} = \frac{Pr\{D|M,\theta\}Pr\{\theta|M\}}{\int Pr\{D|M,\theta\}Pr\{\theta|M\}d\theta} \tag{4.7}$$

and $Pr\{\theta|D,M\}$ is called *posterior probability*. The denominator is called *evidence* or *integrated posterior*.

Having competing models M_i and M_j, parameterized by parameter sets θ_i and θ_j, to describe a data set D, the Bayes factor for comparison between the alternative models M_i and M_j is then defined by

$$b_{ij} = \frac{\int Pr\{D|M_i,\theta_i\}\ Pr\{\theta_i|M_i\}\ d\theta_i}{\int Pr\{D|M_j,\theta_j\}\ Pr\{\theta_j|M_j\}\ d\theta_j} \tag{4.8}$$

which is the ratio of the integrated posteriors (Kass & Raftery, 1995).
To discriminate even smaller differences between hypotheses of different models, Equation (4.8) is log-transformed to deciban scale:

$$B_{ij} = 10 \log_{10} \frac{\int Pr\{D|M_i, \theta_i\}\ Pr\{\theta_i|M_i\}\ d\theta_i}{\int Pr\{D|M_j, \theta_j\}\ Pr\{\theta_j|M_j\}\ d\theta_j} \,. \tag{4.9}$$

The value of B_{ij} provides evidence in favor of one model against the other. For consistency, I will put the model under null hypothesis in the denominator. Values of $B_{ij} < 0$ will support the model M_j under null hypothesis; otherwise, values for B_{ij} in the range $0-5$, $5-10$, $10-15$, $15-20$, and larger than 20 provide weak, substantial, strong, very strong, and decisive evidence against model M_j, respectively (cf. Jeffreys, 1998).

4.3 Estimating the order of Markov chains with Bayes factor

Motivated by the knowledge about Markov chains, probabilities, symbolic dynamics and Bayesian model comparison, I will present an approach for estimating the order of a Markov chain that is proposed for describing a countable sequence of symbols X_T with $T = 1, \ldots, N$ in this section. The outcomes of an experiment are mapped on symbols and time-ordered in X_T. In Chapter 4.2.1, I introduced the state space $\mathcal{S}$ and in Chapter 4.2.2 the alphabet S. Again, the alphabet $S = \{l, r\}$ is taken for the symbols in the sequence of symbols X_T. To allow for an estimation of the order of the Markov chain by the Bayes factor analysis and estimate the order that best describes this sequence of symbols, I introduce a state space

$$\mathbb{S}_n = \underbrace{S \times S \times S \times \ldots \times S}_{n\text{-times}}$$

with

$$\mathbb{S}_0 = \mathbb{S}_1 = \{l, r\} \tag{4.10}$$

of compound symbols, representing all possible permutations of the symbols in the alphabet $S = \{l, r\}$ as words of length n.

Now, proposing that the model for describing the sequences of symbols is a Markov chain model, the order of the Markov chains, i.e. the length of the memory horizon n, is unknown. In the following, I will consider Markov chains up to second-order – a memory horizon of two. But I will show how to present even nth order Markov chain as first-order Markov chain by using words of length n.

In case of the uncorrelated random process – also called zeroth-order Markov chain in the following – the current state has absolutely no influence on the future state, the next symbol in the sequence. Therefore, this process is described by a single number $P_l = q_1^{(0)} \in [0, 1]$, which is the probability to draw l as next symbol. Examining the Markov chain as a zeroth-order and first-order Markov chain, the alphabet or symbol space equals the state space (cf. Equation 4.10).
A transition from l to r in a time step k to $k + 1$ is then written by

$$P_{lr} = Pr\{X_{k+1} = r | X_k = l\} = q_1^{(1)} \tag{4.11}$$

and the transition matrix T_1 for a first-order Markov chain is

$$\begin{aligned} T_1 &= \begin{pmatrix} P_{ll} & P_{lr} \\ P_{rl} & P_{rr} \end{pmatrix} \\ &= \begin{pmatrix} 1 - q_1^{(1)} & q_1^{(1)} \\ q_2^{(1)} & 1 - q_2^{(1)} \end{pmatrix} . \end{aligned} \tag{4.12}$$

It is important to note that everything is parameterized in terms of the 2^1 numbers $q_1^{(1)}, q_2^{(1)} \in [0, 1]$.

For a second-order Markov chain, all transitions from the last two symbols to the new symbol have to be considered. To fix this idea, consider a transition from lr to r which then is, according to

Equation (4.6), represented by

$$P_{lrr} = Pr\{X_{k+1} = r | X_k = r, X_{k-1} = l\} \tag{4.13}$$

This defines 2×2^2 numbers of which only 2^2 are independent, since, e. g., $P_{lrr} + P_{lrl} = 1$. This process is equivalent to a first-order process in the space of words of length 2 by identifying the transition from ab to c with the compound transition ab to bc and $a, b, c \in \{l, r\}$ for all a, b, c. The state space is then $\mathbb{S}_2 = \{ll, lr, rl, rr\}$. It is impossible that a transition from rl to rl occurs – last letter of first word and first letter of second word have to be equal – such that entries equal zero in the transition matrix of the Markov chain, representing a second-order Markov chain. The transition matrix is then given by

$$T_2 = \begin{pmatrix} P_{lll} & P_{llr} & 0 & 0 \\ 0 & 0 & P_{lrl} & P_{lrr} \\ P_{rll} & P_{rlr} & 0 & 0 \\ 0 & 0 & P_{rrl} & P_{rrr} \end{pmatrix} = \begin{pmatrix} 1-q_1^{(2)} & q_1^{(2)} & 0 & 0 \\ 0 & 0 & q_2^{(2)} & 1-q_2^{(2)} \\ 1-q_3^{(2)} & q_3^{(2)} & 0 & 0 \\ 0 & 0 & q_4^{(2)} & 1-q_4^{(2)} \end{pmatrix} \tag{4.14}$$

where the second-order Markov chain is parameterized by the 2^2 numbers $q_1^{(2)}, q_2^{(2)}, q_3^{(2)}, q_4^{(2)} \in [0, 1]$. The transition matrices and parameters for higher-order Markov chains can be obtained in an equal manner such that an nth-order Markov chain can be examined as a first-order Markov chain with the state space $\mathbb{S}_n$. Every time, the rows of the transition matrices have only two non-zero entries. Thus, an nth-order Markov chain will be parameterized by 2^n numbers.

Now, the calculation of the Bayes factor, as introduced in Chapter 4.2.3, is based on the prior probability of a model and parameterization as well as the likelihood of the model, given the observed sequences of symbols. Under the assumption that a sequence of symbols can be described by an nth order stationary Markov chain

model M_n with $\theta^{(n)}$, the likelihood of a sequence X_T given the transition probabilities $q_i^{(n)} \in [0,1]$, $i = 1, \ldots, 2^n$ is

$$Pr\{X_1, \ldots, X_N | M_n, q_1^{(n)}, \ldots, q_{2^n}^{(n)}\} = \pi^{(n)}(X_1, \ldots, X_n | q_1^{(n)}, \ldots, q_{2^n}^{(n)}) \prod_{i=1}^{2^n} \left(q_i^{(n)}\right)^{\alpha_i^{(n)}} \left(1 - q_i^{(n)}\right)^{\beta_i^{(n)}} \quad (4.15)$$

Here, $\pi(X_T|\theta^{(n)})$ is the probability of finding the first n symbols as the initial word. This probability is taken from the stationary distribution which can be calculated for every transition matrix T_n through computation of the Perron-Frobenius eigenvector as described in Equation (4.5). Through the calculation as left-handed eigenvector of the transition matrix, the stationary distribution also depends on $q_1^{(n)}, \ldots, q_{2^n}^{(n)}$. On the remaining symbols $X_{n+1}, \ldots, X_N$, the exponents $\alpha_i^{(n)}$ for $i = 1, \ldots, 2^n$ count for each word (or compound symbol), enumerated by i, the number of transitions for which the new symbol that is added to the sequence was different from the last symbol in the word, whereas $\beta_i^{(n)}$ for $i = 1, \ldots, 2^n$ counts transitions from state i which preserve the last symbol. For example, for a second-order Markov chain, a transition from lr to rl would increase α_2 by the value of 1, whereas a transition ll to ll would increase β_1. Since the likelihood function of the whole sequence X_T depends only on the numbers $\alpha_i^{(n)}$, $\beta_i^{(n)}$, and the first n symbols, these numbers represent a sufficient statistic.

Now, after developing the method steps to determine the order of the Markov chain using Bayes factor and to describe the sequences of symbols by Markov chain models, the applicability of the proposed method for estimating the order of Markov chains is shown. A first validation approach is the estimation of the orders of simulated Markov chains, whose orders are given. Sequences of symbols X_T with a two-element symbol space $S = \{l, r\}$ were simulated through Monte Carlo Markov chains (MCMC) of zeroth-, first-, and second-order. A number of 532 sequences of symbols were generated for each different order, using 19 different random

transition matrices. The sequences were of random lengths between 20 and 60 symbols.[3] First, 30,000 iterates were computed to remove transients of the process, before sequences of different lengths were chosen.

Under the assumption that a given sequence X_T, $T = 1, \ldots, N$ of symbols $S = \{l, r\}$ can be described by a discrete-time, stationary nth-order Markov chain, the likelihood is calculated for zeroth-, first-, second-, and third-order Markov chains through Equation (4.15). The sufficient statistics $\alpha_i^{(n)}$ and $\beta_i^{(n)}$ are cumulated for the different sequences, generated for each individual transition matrix and the order of the Markov chain is estimated.
This was done by evaluating the Bayes factor, defined in Equation (4.9), using a flat prior, and evaluating the likelihood (Equation 4.15). Due to the hierarchical structure of the Markov models, this approach is an application of Occam's razor in ambiguous conditions: When the Bayes factor supports two alternative hypotheses with equivalent strengths, the most parsimonious model (the lowest order) would be selected. In Figure 4.1, I present the results of the Bayes factor analysis – by means of the Monte Carlo simulation – for sequences of (a) zeroth-, (b) first-, and (c) second-order Markov chains.

As mentioned in the beginning of this section, I chose a zeroth-order Markov chain as the model under null hypothesis. For simulated uncorrelated random processes, the estimation returned a zeroth-order Markov chain as best descriptor for the data. None of the higher-order Markov chain models showed evidence against the model under null hypothesis (compare Figure 4.1a), i. e., in this case all B_{i0} for $i = 1, 2, 3$ are negative. For sequences simulated from a first-order Markov chain, the estimator returned the highest evidence against the null model for the first-order Markov chain. The B_{i0} for $i = 1, 2, 3$ are all positive, yet the first-order Markov chain presents the highest evidence against the zeroth-order. Due to nesting of the Markov chains, a second- or third-order Markov

[3] How these numbers agree with the estimation performed for the real data, sequences of microsaccades, will be shown later.

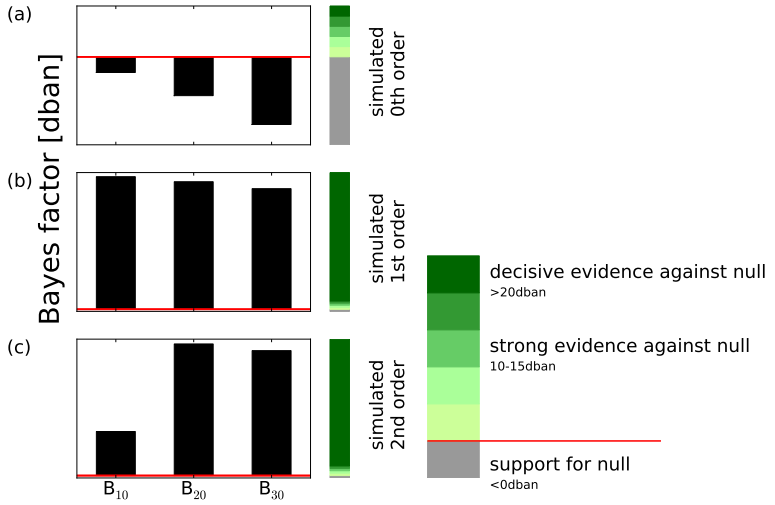

Figure 4.1: Order estimation for sequences of simulated different order Markov chains. *Using a zeroth-order Markov chain as the model under null hypothesis, the Bayes factor compares the evidences against first-, second-, and third-order Markov chain models. The sequences are generated from* (a) *an uncorrelated random process,* (b) *a first-order Markov chain, and* (c) *a second-order Markov chain, each for a two-element symbol space. In* (a), *support for zeroth-order parameterization is obtained. In* (b), *evidence against the model under null hypothesis exists for all orders. But it is highest for a first-order Markov chain. A first-order Markov chain model would be estimated.* (c) *Also for a simulated sequences from a second-order Markov chain, the second-order Markov chain would be estimated as best descriptor.*

chain has evidence against the null, as well. But the scale of interpretation of the Bayes factor allows the separation of the first-order Markov chain from the others. The Bayes factor analysis estimated the first-order Markov chain (compare Figure 4.1b). A similar result is obtained for the simulated sequences of second-order Markov chains. Here, the highest evidence against the null is given for a second-order Markov chain model (compare Figure 4.1c). Thus, here the estimator returned the correct order as well. The validity of the estimator has been shown with the simulation results. Now, I will apply the estimator on the microsaccades, detected in fixa-

tional eye movements and represented as symbols in a discrete-time sequence.

4.4 Markov chains for sequences of microsaccades

In Chapter 2, the scale-free detection method for microsaccades in the time series of fixational eye movements was introduced. In Chapter 3, I proposed a model for the microsaccade shape that lets us access major microsaccade properties. Using the catalog derived in Chapter 3.7, the direction of the microsaccadic horizontal eye movements can easily be accessed. The mapping of the directions of *L*eft and *R*ight movements on the symbols L and R is illustrated in Figure 4.2.

Under the assumption that microsaccade symbol sequences of an individual participant can be evaluated as realizations of a single

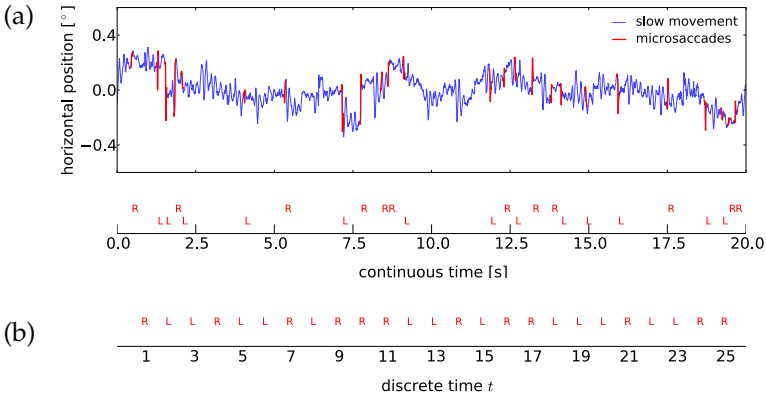

Figure 4.2: Sequences of microsaccades, detected with the wavelet method, are mapped on sequences of symbols. (a) *Only those microsaccades which fulfill the binocularity and energy criterion are marked in red in the horizontal trajectory of a sample fixational eye movements trial. Then, they are mapped on symbols* Left *and* Right *in continuous time.* (b) *The continuous time is then neglected and microsaccades are represented as symbols in fixational eye movements.*

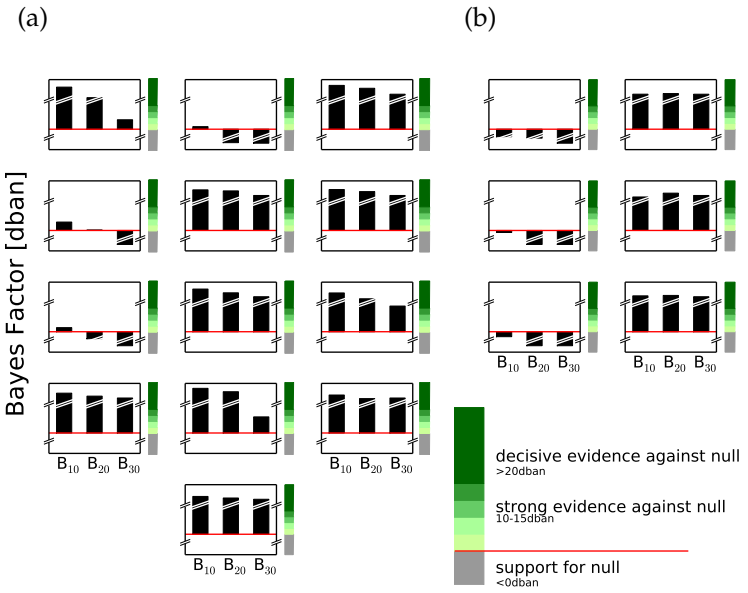

Figure 4.3: Order estimation for microsaccade sequences of nineteen participants in a fixation task experiment. *Using the zeroth-order parameterization of the Markov chain model as null, the Bayes factor is calculated to estimate the order of the Markov chain that best describes the sequences of microsaccade symbols.* (a) *Thirteen participants show evidence of different strengths against the null hypothesis. Through parsimony, a first-order parameterization of the Markov chain would be estimated as best descriptor.* (b) *For six participants, support for zeroth- (left column) or second-order (right column) is estimated. For visualization purposes, the y-scale gets broken at values > 20 or < 0 as they deliver either decisive evidence against or support for the null hypothesis. Differences above or below these values inside one subplot are marked with a proportion of their original value.*

Markov process, I summed up the counts $\alpha_i^{(n)}$ and $\beta_i^{(n)}$ from all different trials of one participant and estimated the order of the Markov chain as described in the previous section.

Again, the model under null hypothesis is the zeroth-order Markov chain, an uncorrelated random process. Higher-order Markov chains are compared by the Bayes factor (cf. Equation 4.9) against the zeroth-order Markov chain. For thirteen out of 19 participants, the estimator suggests that the sequences of symbols, are

best described by a first-order Markov chain if compared against zeroth-order. Evidence against the model under null hypothesis is shown for all thirteen cases (compare Figure 4.3a). The first-order Markov chain presents the highest evidence against the model under null hypothesis such that, through the scale of interpretation of the Bayes factor, the estimator identifies the first-order Markov chain as the best describing model. In Figure 4.3b, the analysis is presented for the remaining six participants. For three subjects, no evidence against the null hypothesis was found (Figure 4.3b, left column). The microsaccade symbol sequences for the remaining three subjects can best be described by a second-order Markov chain (Figure 4.3b, right column).

For thirteen participants, a first-order Markov chain returns the best fitting stochastic process for the microsaccade sequences. Nevertheless, for six participants, the support for zeroth- or second-order Markov chain is very close in their evidences supporting a first-order Markov chain.

Table 4.1 summarizes the estimated orders of Markov chains for all participants and the characteristic properties of microsaccades. The amplitude and displacement were evaluated for the horizontal component of microsaccades. The average rate and intermicrosaccade interval (IMSI) were calculated for binocular microsaccades. Estimated order of Markov chain and microsaccade-related properties do not show any connections.

In Figure 4.4, I illustrate the one-step transition matrices for all participants for the first-order Markov model in color code. The transition probabilities, presented in the 4 quarters of each graphic to represent one 2×2 matrix, are calculated on the maximum likelihood estimates by

$$q_i^{(1)} = \frac{\alpha_i^{(1)}}{\alpha_i^{(1)} + \beta_i^{(1)}} \,. \tag{4.16}$$

The transition matrices across participants show interindividual differences. A few participants have almost equal probabilities to

Subject	Rate [MS/s]	Ampl. [°]	Displ. [°]	order of MC	IMSI [s]
01	0.74	0.21	0.10	first	1.35
02	1.12	0.34	0.24	second	0.88
03	0.42	0.2	0.15	zeroth	2.29
04	1.26	0.23	0.15	first	0.78
05	1.34	0.24	0.16	first	0.75
06	1.48	0.37	0.29	second	0.70
07	0.73	0.16	0.12	first	1.35
08	0.84	0.40	0.34	first	1.24
09	0.60	0.51	0.34	first	1.46
10	0.72	0.13	0.08	first	1.33
11	1.37	0.22	0.16	first	0.79
12	0.78	0.16	0.11	first	1.34
13	0.37	0.17	0.11	first	2.67
14	0.99	0.39	0.21	zeroth	1.01
15	1.31	0.27	0.16	first	0.79
16	1.70	0.27	0.22	first	0.58
17	0.84	0.32	0.22	zeroth	1.23
18	1.20	0.14	0.09	second	0.82
19	0.87	0.56	0.44	first	1.01
total	0.98 $\pm$0.36	0.28 $\pm$0.12	0.19 $\pm$0.1	first	1.17 $\pm$0.52

Table 4.1: Microsaccade properties and estimated order of Markov chain. *Microsaccade and microsaccade sequence properties for microsaccades in the left eye of nineteen participants in a fixation task experiment. The order of the Markov chain (order of MC), amplitude (Ampl.), displacement (Displ.), rate and IMSI are given as average over all trials of each participant. A microsaccade was defined as binocular singularity, fulfilling the energy criterion (cf. Chapter 3.7).*

change from one symbol to another or stay with the same symbol. Although the probabilities are close to those in an uncorrelated random process, the first-order Markov chain describes their sequences the best. Furthermore, evidences against higher- or lower-order Markov chains (cf. Figure 4.3) does *not* imply that the transition matrices have to be similar, as well (cf. Figure 4.4b). Therefore, an

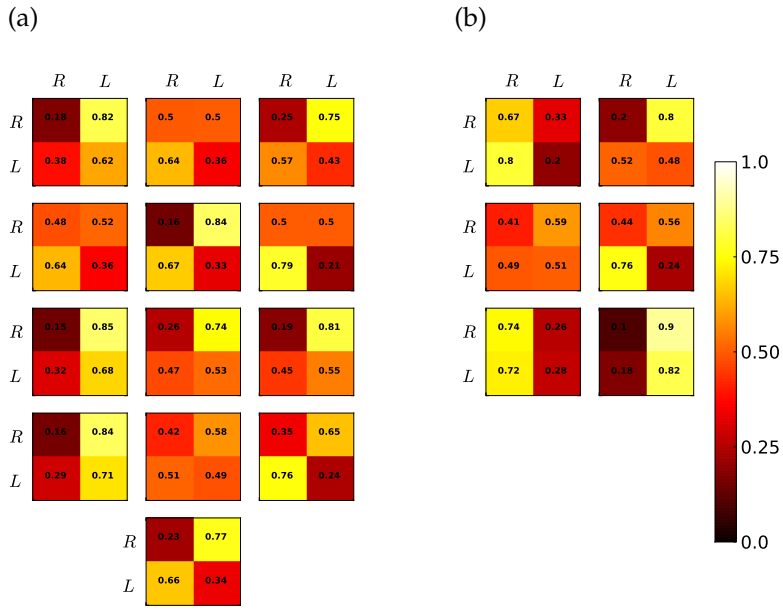

Figure 4.4: First-order Markov chain transition matrix for all participants. *The transition matrices of the participants are arranged as in Figure 4.3. The values are color-coded to facilitate reading. Only the transition matrix for a first-order Markov chain is reported.*

exclusive analysis of the transition matrices to determine the order of the Markov chain would not return correct orders.

At the end of the analysis, the data of most participants are best described by a first-order Markov chain (Bettenbühl, Rusconi, Engbert & Holschneider, 2012). A model is returned which presents microsaccades in fixational eye movements as symbols in sequences. This is compatible with recent findings of a statistical coupling of subsequent microsaccade orientations (Otero-Millan, Serra et al., 2011). It is important to note that I neglected any temporal proximity for the sequences. To investigate the effect of time for subsequent events, I continue in the next section with an analysis of the factor related to *intermicrosaccade interval*.

4.5 A model for sequences of microsaccade

Neglecting temporal proximity between microsaccadic events, I could show that a first-order Markov chain model delivers an appropriate description for the symbols l and r, representing left- and rightward directed microsaccades. In section 4.1.2, we have seen that the waiting time between first and second microsaccade played a key role in separating square-wave jerks from single-standing microsaccades.

In order to investigate the waiting times, I computed the intermicrosaccade intervals (IMSIs) for all microsaccades that are collected in the microsaccade catalog (cf. Chapter 3.7). In Figure 4.5, the probability density function of the IMSIs is estimated by the Gaussian kernel density estimation and plotted on top of the normalized histogram with 200 bins. The probability density function

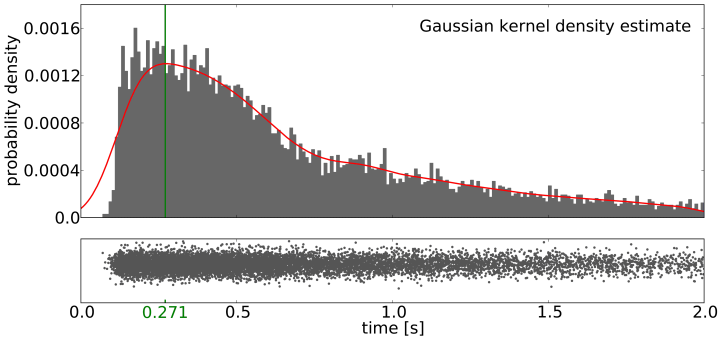

Figure 4.5: Distribution of IMSIs in the fixation task experiment. *Using Gaussian kernel density estimation, the probability density is presented in red on top of the normalized histogram of IMSIs in blue. The bottom graphic presents every single IMSI as point. The green marked time denotes the maximum of the probability density. The IMSIs exhibit a broad peak around the maximum, which seems to have two different slopes.*

of the IMSIs which are for $i = 1, \ldots, n$ denoted by Δ_i, is estimated through

$$\widehat{Pr}\{\Delta\} = \frac{1}{nh\sqrt{2\pi}} \sum_{i=1}^{n} e^{-\frac{1}{2}\left(\frac{\Delta-\Delta_i}{h}\right)^2} \tag{4.17}$$

with Δ_i the observed IMSIs, i. e., each single dot in the bottom of Figure 4.5, and h the bandwidth, given by

$$h = 1.06 \min\left(\sigma, \frac{Q_{.75} - Q_{.25}}{1.34}\right) n^{-1/5} \tag{4.18}$$

with σ the variance of the IMSIs Δ_i, n the number of IMSIs, $Q_{.75}$ and $Q_{.25}$ the 75 % and 25 % quartile, respectively (Silverman, 1986). IMSIs between 0 and 0.5 s are most probable as seen by the broad peak in Figure 4.5. Two different slopes seem to be present at either side of the maximum of the distribution (compare also Engbert & Mergenthaler, 2006). Otero-Millan, Serra et al. (2011) suggested using an ideal threshold time of around 0.2 s for the separation of single-standing microsaccades and square-wave jerks – oppositely directed pairs of microsaccades that depend upon each other.

Now, I propose a stochastic model for the generation of microsaccades, which switches between two different probability distributions, dependent upon the waiting time of each single microsaccade. The microsaccades are represented for each trial in a sequence X_T with $T = 1, \ldots, N$ by the symbols l and r for left- and rightward directed microsaccades, respectively. The symbol space is again $S = \{l, r\}$.

In this model, the probability distribution for the next symbol in the sequence changes according to the waiting time, drawn from $\widehat{Pr}\{\Delta\}$. Now suppose that, with waiting time $\Delta_1 = 0$, the start symbol $s_1 \in S$ of the sequence X_T is known such that

$$p_1 = Pr\{(X_1 = s_1)\} = 1 \tag{4.19}$$

for $s_1 \in \{l, r\}$. The waiting time Δ_{k+1} for the $k+1$st symbol is drawn from $\widehat{Pr}\{\Delta\}$, and the probability for the $k+1$st symbol with $k+1 \geq 2$ is determined by

$$Pr\{X_{k+1} = s_{k+1}\} = \begin{cases} Pr\{X = s_{k+1}\} & \text{for } \Delta_{k+1} > \tau \\ \\ Pr\{X_{k+1} = s_{k+1} | X_k = s_k\} & \text{for } \Delta_{k+1} \leq \tau \end{cases} \tag{4.20}$$

for a threshold time $\tau > 0$ and $s_k, s_{k+1} \in \{l, r\}$. The probability $Pr\{X = s_{k+1}\}$ of symbol s_{k+1} is drawn from the probability distribution of a random uncorrelated process, parameterized by $q_1^{(0)}$. The probability $Pr\{X_{k+1} = s_{k+1} | X_k = s_k\}$ is a transition probability of a first-order Markov chain, parameterized by $q_1^{(1)}$ and $q_2^{(1)}$. Thus, the probability of the next symbol – the next microsaccade direction – is drawn from the probabilities of a zeroth- or first-order Markov chain, depending upon the waiting time. Under the assumption that every symbol is independently drawn, respecting Equation (4.20), the probability of a sequence X_T of N symbols from $S = \{l, r\}$, given the parameters $q_1^{(0)}$, $q_1^{(1)}$, and $q_2^{(1)}$, to represent the N microsaccade directions of one trial is then given by

$$\begin{aligned} Pr\{X_1 = s_1, X_2 = s_2, \ldots, X_N = s_N | p_1, q_1^{(0)}, q_1^{(1)}, q_2^{(1)}\} = \\ p_1 \left(q_1^{(0)}\right)^{\gamma_1'} \left(1 - q_1^{(0)}\right)^{\gamma_2'} \prod_{i=1}^{2} \left(q_i^{(1)}\right)^{\alpha_i'} \left(1 - q_i^{(1)}\right)^{\beta_i'} \end{aligned} \tag{4.21}$$

and with $p_1 = 1$ (cf. Equation 4.19), the likelihood can be rewritten as

$$\begin{aligned} \mathcal{L}(q_1^{(0)}, q_1^{(1)}, q_2^{(1)} | X_1, \ldots, X_N) = \\ = \left(q_1^{(0)}\right)^{\gamma_1'} \left(1 - q_1^{(0)}\right)^{\gamma_2'} \prod_{i=1}^{2} \left(q_i^{(1)}\right)^{\alpha_i'} \left(1 - q_i^{(1)}\right)^{\beta_i'} \end{aligned} \tag{4.22}$$

with

$$\gamma_1' + \gamma_2' = n_0$$

the number n_0 of waiting times at which $\Delta_{k+1} > \tau$ for $1 \leq k < N$ and

$$\sum_{i=1}^{2} \alpha_i' + \beta_i' = n_1$$

the number n_1 of waiting times at which $\Delta_{k+1} \leq \tau$ for $1 \leq k < N$ and $n_0 + n_1 = N - 1$. The numbers γ_1' and γ_2' count the different symbols l and r, which have been drawn for $\Delta_{k+1} > \tau$. For first-order transitions, for $\Delta_{k+1} \leq \tau$, the numbers α_1', α_2', β_1', β_2' count the transitions as in Chapter 4.3. All six numbers represent a sufficient statistic for the sequence of symbols. For different trials of one participant, i. e., different sequences of symbols, these counts can once again be summarized.

The Bayes factor as introduced in Chapter 4.2.3 can be used to select a proper model. Neglecting time, the first-order Markov chain best describes the sequences of microsaccade directions. Under the assumption that the probability of the initial state $Pr\{X_1 = s_1\} = 1$ is known, the likelihood for the parameters $q_1^{(1)}, q_2^{(1)}$ of the first-order Markov chain model is given by

$$\mathcal{L}(q_1^{(1)}, q_2^{(1)} | X_1, \ldots, X_N) = 1 \cdot \prod_{i=1}^{2} \left(q_i^{(1)}\right)^{\alpha_i} \left(1 - q_i^{(1)}\right)^{\beta_i} \qquad (4.23)$$

with α_i, β_i counting the transitions as in Chapter 4.3. To compare both models with the Bayes factor (Equation 4.9), the *time-dynamic model*, which switches between an uncorrelated random process and a first-order Markov chain, i. e., it loses memory over time, is used as numerator and the first-order Markov chain model as denumerator. Their likelihood functions are given in Equation (4.22) and Equation (4.23); the Bayes factor is calculated again using a flat prior. The Bayes factor reduces to be the ratio of integrated

likelihoods. The integrals are given for the time-dynamic model by

$$\int_0^1 \int_0^1 \int_0^1 \mathcal{L}(q_1^{(0)}, q_1^{(1)}, q_2^{(1)} | X_1, \ldots, X_N) dq_1^{(0)}\, dq_1^{(1)}\, dq_2^{(1)} =$$

$$\mathcal{B}(\gamma_1' + 1, \gamma_2 + 1')\ \mathcal{B}(\alpha_1' + 1, \beta_1' + 1)\ \mathcal{B}(\alpha_2' + 1, \beta_2' + 1) \tag{4.24}$$

and pure first-order Markov chain model by

$$\int_0^1 \int_0^1 \mathcal{L}(q_1^{(1)}, q_2^{(1)} | X_1, \ldots, X_N) dq_1^{(1)}\, dq_2^{(1)} = \mathcal{B}(\alpha_1 + 1, \beta_1 + 1)\ \mathcal{B}(\alpha_2 + 1, \beta_2 + 1) \tag{4.25}$$

with the Beta function $\mathcal{B}(x, y)$ given by

$$\mathcal{B}(x, y) = \frac{\Gamma(x)\Gamma(y)}{\Gamma(x + y + 1)} \tag{4.26}$$

and the gamma function $\Gamma(x) = (x - 1)!$ for $x \in \mathbb{N}^+$.

The Bayes factor (Equation 4.8) for comparing both models with a flat prior is then given by the ratio of the results of Equation (4.24) in the nominator and Equation (4.25) in the denominator. I will denote it with $B_{\mathcal{D},1}$ Varying the threshold parameter τ in Equation (4.20) such that $\tau = \kappa \cdot 5\,\text{ms}$ for $\kappa = 1, \ldots, 200$ and calculating the Bayes factor for every single τ, a function $B_{\mathcal{D},1}(\tau)$ is obtained over the threshold time τ. The value for the first-order Markov chain, i. e. the model in the denominator, remains constant because no time memory is present.

In Figure 4.6, I present $B_{\mathcal{D},1}(\tau)$ for the participants. For small threshold times, the probabilities for new symbols are only drawn from the distribution of the uncorrelated random process of the time-dynamic model. As already shown in Chapter 4.4, the first-order Markov chain presents evidence against the model of an uncorrelated random process for the sequences of symbols. This is once again the case for small threshold times τ. The time-dynamic

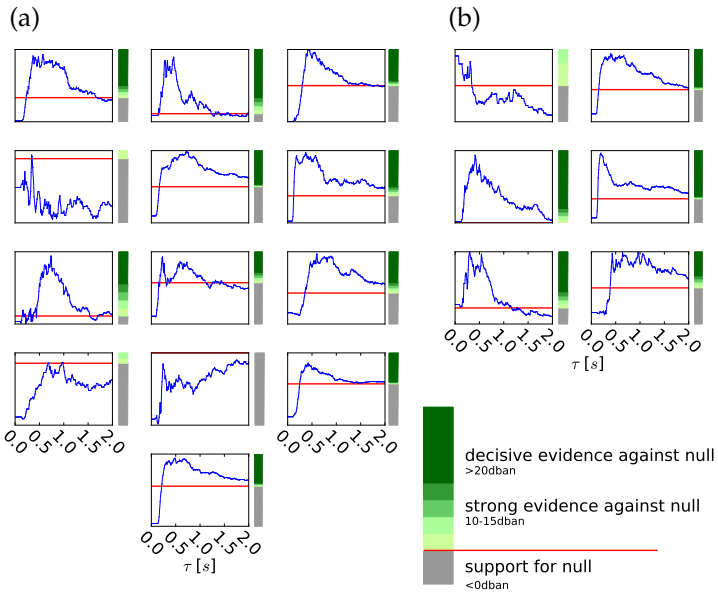

Figure 4.6: Time-dynamic model for microsaccade direction sequences. *The value of $B_{\mathcal{D},1}$ is presented for 19 participants, arranged as in Figure 4.3. At the first zero-crossing, the time-dynamic model, which is a mixture between an uncorrelated random process and first-order Markov chain, presents evidence against the pure first-order Markov chain models.*

process is then actually driven by the uncorrelated random process. If the time-dynamic model better describes the sequences of symbols, then evidence against the first-order Markov chain without time memory should be present. For three participants, no clear evidence against the pure first-order Markov chain model exists, i. e., the temporal proximity is neglectable for the description of their sequences. For three participants in Figure 4.6b, left column, a zeroth-order Markov chain model is directly estimated. If neglecting temporal proximity, the same results occurred (cf. Figure 4.3b, left column). For participants whose estimation of Markov order resulted in a second-order Markov chain (cf. Figure 4.3b, right column), the estimator favors the time-dynamic model.

For those participants where evidence against the first-order Markov chain is present, the zero-crossing of the threshold time occurs between 130 ms and 390 ms, with a mean of 214 ± 84 ms (mean $\pm$ standard deviation). In the tail, the evidence of the mixed model converges asymptotically to the evidence of the first-order Markov chain model. The meaning of the time point at which the time-dynamic model does not have any more memory effect will be part of the discussion.

5 Discussion

Eye movements and especially saccadic eye movements of small- and large-amplitudes are studied under various aspects. Starting at the source, neuroscientists investigate the coding of saccades and microsaccades in the brain structures in neurophysiological studies (Van Horn & Cullen, 2012). Neural mechanisms for microsaccade generation have been reported based on studies on the level of single neurons (Van Gisbergen et al., 1981; Hafed et al., 2009). Partially developed from this, models for the triggering mechanisms for microsaccades were proposed (Hafed, 2011; Otero-Millan, Serra et al., 2011) that lend support to existing models for saccade generations (Schall & Thompson, 1999; Sparks & Mays, 1990; Wurtz & Optican, 1994). Investigations in cognitive science include the study of eye movements at the highest level, as well as the output of the neurophysiological and oculomotor system. Psychophysical data studying microsaccade inhibitions (Rolfs et al., 2008) is used to model the generation of microsaccades. For fixational eye movements, modeling approaches taken from physics include the stochastic simulation of the eye's retina as a swamp under a potential (Engbert et al., 2011). The stochastic modeling benefits from the results obtained in both the study of eye movement generation and the trajectory of the movements.

In this thesis, a stochastic model for microsaccade shapes is proposed. This model may be of importance for studies of the executed saccadic eye movements. It allows for a well-estimated set of properties – including amplitude, duration, overshoot, shape factors – the representation of the saccadic eye movements on all amplitude scales. In contrast, the time-dynamic model of a stochastic process with memory for microsaccades adds knowledge to the understanding of microsaccade generation. Additionally, it

yields the possibility of predicting microsaccade directions under different experimental paradigms.

5.1 Detection of saccades and microsaccades

In vision research, it is important to differentiate fixations and saccades in many tasks and experiments. When studying how a person is reading a text, for example, saccades and fixations have to be separated, to understand why a certain word is skipped (Drieghe, Rayner & Pollatsek, 2005) or re-fixated (McConkie, Kerr, Reddix, Zola & Jacobs, 1989). When presenting a photograph to a participant, saccades and fixations describe dynamics present during the perception of details or of the complete image (Otero-Millan et al., 2008; Rucci, 2008). When studying saccades and microsaccades in scene perception, descriptive measures and functional characteristics lead to proposals of generating processes and comparison with pure fixation task microsaccades (Mergenthaler & Engbert, 2010). Possibly, eye movements may even be related to perceived emotions, which could be used in marketing studies of specific advertisements (Rayner, Miller & Rotello, 2008; Bannerman, Milders & Sahraie, 2009).

Studies of activity-related brain potentials with EEG, co-registered with eye movements, open another realm in which the separation of eye movements into fixations and saccades is of major interest for evaluating measured brain potentials (Dambacher & Kliegl, 2007; Dimigen, Sommer, Hohlfeld, Jacobs & Kliegl, 2011; Kliegl, Dambacher, Dimigen, Jacobs & Sommer, 2011). Furthermore, fixations and saccades need to be separated to examine behavioral characteristics of the participants not only under laboratory conditions but also with head-mounted, video-based eye tracking while walking outside ('t Hart & Einhäuser, 2011) or while driving a car (Cohen & Studach, 1977; Omori, Sato, Yamauchi, Ishikawa & Wakita, 2009). All these research fields show the importance of being able to properly distinguish saccades and fixations. The fixa-

tions yield another challenge because they contain microsaccades. These small, involuntary saccades during fixation are related to various functions in vision (compare Chapter 1.3 and Rolfs, 2009). Therefore, it would be of great benefit to detect both saccades and microsaccades at the same time, using a tool that does not require long computation times and has a parameter space that is independent of the different tasks or different subjects.

In this thesis, I investigated the hypothesis that saccades and microsaccades can be modeled as singularities in time series. The continuous wavelet transform is a tool for the vision research community and detects saccades of all amplitudes (Chapter 2.3), including microsaccades (Chapter 2.4). The method is used on a predefined minimal set of parameters: Frequency range (Chapter 2.3), length of maximum modulus line over frequencies (Chapter 2.2.3), and, especially for the collection of microsaccades into a microsaccade catalog, the binocularity (Chapter 2.4) and energy criterion (Chapter 3.7). All these parameters are independent of subject and task. The widely-used method to detect saccades and microsaccades in the velocity space (Engbert & Kliegl, 2003b) requires knowledge about an optimal threshold or the recording of secondary data in order to determine it. The wavelet method has proven to not require any tuning because the same parameter set is used for every experiment under investigation.

When performing a simple comparison of rates for binocular microsaccades detected by the velocity threshold (using a dynamical threshold multiplier as described in Mergenthaler, 2009) and wavelet method for the time series of the fixation task experiment, the rates are significantly correlated ($r=0.96$, $p<0.0001$). Rates are reported in Table 5.1 and a short time interval of a representative trajectory with detected microsaccade positions is presented in Figure 5.1.

Performing an analysis on amplitude-adjusted surrogate data for fixational eye movements (Chapter 2.5) strictly suggests that almost simultaneously occurring structures of low regularity in the trajectories of fixational eye movements cannot be explained by

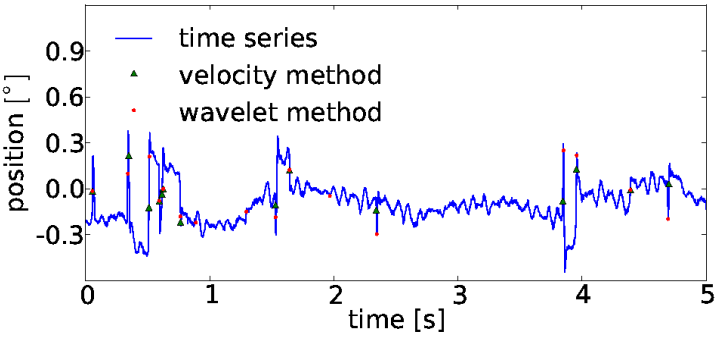

Figure 5.1: Illustration of the microsaccade detections in fixational eye movements by the velocity threshold and wavelet method. *The velocity threshold method used a dynamical threshold multiplier to detect microsaccades (Mergenthaler, 2009). The wavelet method also detects smallest microsaccades, for example, at time* $\approx 1.3\,\mathrm{s}$.

randomly co-occurring autocorrelated samples in the slow movements, or drift, in both eyes. Thus, having validated the method through the analysis of simulated data, the mathematical approach to define saccades and microsaccades as singularities proves to be a successful method for the detection of these movements. Using structural properties rather than the characteristic of high-velocity to identify time positions has two advantages: Primarily, it "verifies" the already existing approach to be a successful detection method because both methods have nearly the same results. Secondly, it presents an alternative detection approach that has less parameters to be optimized. Additionally, the proposed method might be useful for researchers who consider eye movements to only be artifacts in the measurements of their primary data source, for example in EEG studies. They can profit from the performance of this novel method because it can be used to detect artifacts such as saccadic eye movements without a priori knowledge about them.

Table 5.1: Detection of microsaccadic events with the continuous wavelet transform (WT) and velocity threshold (VT) method (with dynamical threshold multiplier) in the fixation task experiment. *Results are compared after application of the individual settings for both methods. The VT algorithm detects 5 % less binocular events. The total rates are given as mean ± standard deviation.*

Participant	**Number of trials**	**Binocular events rate of $[\frac{1}{s}]$**	
		wavelet	velocity
1	30	1.5	1.1
2	29	2.4	2.4
3	30	1.4	1.4
4	30	0.3	0.1
5	22	0.6	0.5
6	30	1.8	1.9
7	30	1.7	2.0
8	30	1.7	2.0
9	30	0.5	0.2
10	17	1.0	0.7
11	28	1.0	0.9
12	30	0.8	0.9
13	29	0.6	0.2
14	30	1.2	0.8
15	29	1.8	1.9
16	30	1.2	1.4
17	29	0.8	0.3
18	23	1.4	1.5
20	29	1.7	1.9
21	29	1.9	1.9
22	30	0.3	0.2
23	29	1.2	1.2
24	30	1.7	1.7
25	29	1.2	1.1
Total	682	1.2 ± 0.5	1.2 ± 0.7

5.2 Shape model for saccadic eye movements

Saccades and microsaccades are often only described by their shared property of high velocity. Since the work of Zuber et al. (1965), the relationship between saccades and microsaccades is commonly presented in the main sequence (cf. Chapter 3.1.1). Concerning the classification as single- and double-saccadic pulse (SSP and DSP), which exists for saccades and microsaccades as well (Abadi & Gowen, 2004), it would be beneficial to have a shape model that can not only separate different patterns but also return a measure of, for example, overshoot width.

To arrive at a shape model that allows the simple collection of typical saccade and microsaccade properties (Chapter 3.7), the main shapes have been identified through principal component analysis, yielding two components whose linear combinations almost completely describe the shapes of microsaccades as well as saccades. The established linear model for microsaccade shapes in Chapter 3.4 agrees with studies by Zuber et al. (1965), which reported the overshoot as a typical property of microsaccades. More recently, by using electromagnetic induction technique with rhesus monkeys, eye movement trajectories of Hafed et al. (2009) also reveal an overshoot in the horizontal and vertical directions, identified as microsaccadic events. Often doubts exist that video-based eye tracking (Chapter 1.5) presents the correct overshoot width, caused by influences of the pupil dilation onto the internal position detection procedure of the device. Performing an experiment with an iris test lens, in which the pupil size remains constant to the camera of the eye tracker, the analysis showed that the overshoot might be overestimated by the video-based eye tracking system. Yet, it still remains a part of the microsaccade (cf. Figures 3.2, 3.4, 3.5, and 3.7). Hence, overshoot cannot be neglected as an artifact though its impact is smaller than thought.

Through the shape coefficients, the saccade and microsaccade shape model can distinguish not only between SSP and DSP but

can also describe intrinsic properties of either event. The model allows simulations of these jump-like events in the eye movement trajectories once the distribution of the shape coefficients is known for different experimental setups.

Properties like amplitude, durations, or velocities have been investigated during the performance, for example, of tasks with different stimuli to affect saccades (for a review, see Weaver, Lauwereyns & Theeuwes, 2011). The novel shape model for saccadic eye movements deviations allows for statistical treatments of the curvature, obtaining shape coefficients to measure differences. Together with the microsaccade shape model, a microsaccade catalog is established and allows for direct access for any subsequent analysis because microsaccades are described by and restorable from these seven parameters.

5.3 Markov models for sequences of microsaccades

Previous studies aimed for a description of microsaccade sequences as patterns in fixational eye movements. Abadi and Gowen (2004) detected and identified them by subjective valuation. Otero-Millan, Serra et al. (2011) separated microsaccades that were aligned in a sequence of two or three subsequent events from single-standing microsaccades. In this thesis, my attempt was not to deliver a neurophysiological model for the generation of microsaccades but to arrive at a stochastic model, the Markov chain. It presents a well-defined framework for the sequences of microsaccades as symbols in fixational eye movements.

Using the microsaccade catalog (Chapter 3.7), microsaccades detected with the scale-invariant wavelet method, were mapped onto symbols, representing their direction. The only assumption made for the stochastic process to generate these sequences was the Markov chain, a process with a certain memory horizon. Using symbolic dynamics (Chapter 4.3) and Bayesian factor model selection, a straight-forward estimator for the Markov order for states of

compound symbols could be proposed and successfully validated (Chapter 4.4).

Earlier findings in the analysis of microsaccades postulate the existence of a statistical coupling of subsequent microsaccade orientations, the square-wave jerks (Chapter 4.1.2) and biphasic square wave intrusions (Chapter 4.1.1). Both have been proposed to coexist between isolated microsaccades. In contrast to these previous works on patterns of subsequent microsaccadic events, I neglected the temporal proximity between the events. According to the Bayes factor analysis (Chapter 4.4), the first-order Markov chain is the best description of most of the experimentally observed microsaccade sequences. Evidence was obtained that both, microsaccades and SWJ, are generated by the same stochastic process. This statistical treatment lends support to the conclusion "that microsaccades and SIs are essentially the same phenomena" (Otero-Millan, Serra et al., 2011, pp. 4386), since they were found to be generated by the same stochastic process.

In the next step, I investigated the loss of memory over time with a time-dynamic model. Here, the Markov chain model changes from first- to zeroth-order; the generating process loses memory over time. The change point from a first- to zeroth-order Markov chain, i. e., the time point around which the memory has faded, is in a range of 214 ± 82 ms across all subjects. Otero-Millan, Serra et al. (2011) reported intra square-wave jerks (SWJ) intervals of 280 ms and 290 ms for healthy and progressive supranuclear palsy patients, However, square-wave jerks consist of two oppositely directed microsaccades in a sequence. Now, with the proposed time-dynamic model, the time interval between two subsequent microsaccades, which are dependent on each other, remains shorter but also includes, for a first-order Markov chain, the probabilities for symbol changes and symbol conservation: for example, to have a word *L*(eft)-*R*ight or *L*eft-*L*eft. The computation of the SWJ-intervals is based on a symbol change.

In their analysis of the saccadic system, Becker and Jürgens (1979) proposed that goal-directed saccades are prepared in two

steps: The direction is decided, requiring a random time delay, and subsequently the calculation of the amplitude. Their conceptual model for the total delay time of the saccadic system included the following components (adapted from Becker & Jürgens, 1979):

- an afferent time delay T_A needed to signal a new target position to the decision-making structure,
- a decision and computing time $T_D + T_W$ as the time for the decision-making structure to decide on a saccade triggering and its amplitude,
- an efferent time delay T_E to transmit the motor signal through the end of the neural pathway to the eye muscles,
- the duration of the saccade t_S.

Additionally, they reported values of $T_D = 100\,\text{ms}$ and $T_W = 120\,\text{ms}$, which together give the computation time in the central decision and computing stage, and $T_A = 40\,\text{ms}$ and $T_E = 35\,\text{ms}$. They also proposed that, around this stage, an outcome can be memorized and directly enter the stage again, while the command for a saccade already travels to the motor system. Holding fixation on a target, the superior colliculus (SC) has been proposed to be the key generator for microsaccadic eye movements. Furthermore, the SC plays a role in the central direction and amplitude computation stage (Hafed et al., 2009; Otero-Millan, Serra et al., 2011; Rolfs et al., 2008).

To further the understanding of the time point at which the Markov chain model switches from first- to zeroth-order, I might assume that for microsaccades the afferent time T_A equals 0 ms because no new target position has to be selected. If a microsaccade were triggered in the SC, then the signal left the SC to the motor neuronal pathway and at the same time, the memory (a copy of the command signal) re-enters the SC. Another run of the decision-computation stage would follow, possibly leading to another saccadic movement – of any amplitude. Each computation in the SC takes around $T_{SC} = T_W + T_D = 220\,\text{ms}$. This time would

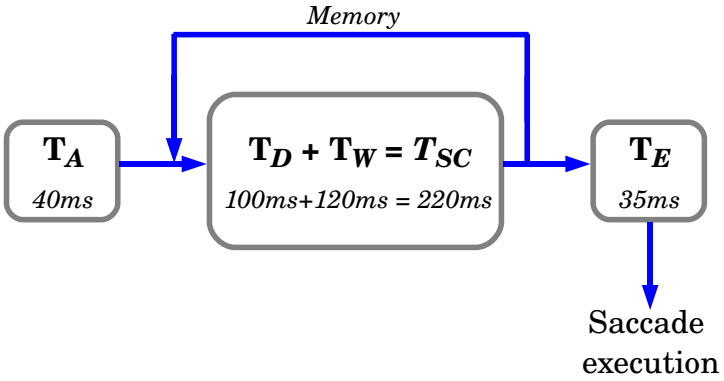

Figure 5.2: Conceptual model of saccade generation in the neural pathway. *The central decision and computing stage is represented by the superior colliculus (SC) in the neural pathway of saccade generation. For microsaccade generation models, the SC plays a key role to trigger microsaccades. The afferent time T_A, decision time T_D, computation time T_D, the sum $T_S C = T_D + T_C$ as time interval for a signal in the SC, and the efferent time T_E are provided. Adapted from (Becker & Jürgens, 1979).*

agree with the estimated threshold time for the time-dynamic model which therefore might provide an explanation for the existence and loss of memory in this time window. An illustration of the proposed pathway and delay times is presented in Figure 5.2.

5.4 Outlook

The detection method for saccades of all amplitude scales should be applied to further experimental data, especially considering the existence of data from primates (Hafed et al., 2009). For monkeys, the horizontal does not dominate the vertical eye movement direction and fixational eye movement data should be analyzed with the wavelet transform method for complex-valued time series. Investigating the selected frequency range, or the zoom, might allow for a decrease of the number of false detections, if only monocular detections are considered. Using the data from the iris test lens experiment, it might be possible to eliminate the effect of pupil

dilation and provide a method for handling the overestimation of the overshoot widths.

Couplings between physiological drift and microsaccades (Engbert et al., 2011; Engbert, 2006b; Poletti, Listorti & Rucci, 2010) could potentially lead to more detailed process assumptions than what is presented here with the Markov chain model for microsaccade directions. This also includes the consideration of amplitudes and displacements. Further experiments, including involuntary and voluntary small amplitude saccades, might allow for investigations of the triggering mechanisms. Furthermore, neurophysiological aspects in the proposed model of memory effects in microsaccades might lead to a more profound model.

While the method for Markov order estimation was demonstrated on examples from fixational eye movements, the Bayesian estimation of the Markov order of a stochastic process underlying the generation of symbol sequences might turn out to be a powerful tool for a broad range of biological systems and could be applied to different systems whose events can be mapped on symbols in a similar manner.

5.5 Final remark

A novel tool for the detection of saccades and microsaccades has been shown to be a well-founded alternative to the already existing methods. A statistical treatment of saccade and microsaccade shapes showed good agreement in both shapes and dissimilarities in the overshoot height. An iris test lens experiment revealed the limitations of video-based eye tracking for investigations of the overshoot, which is prominent for microsaccades. Bayesian inference, stochastic modeling and symbolic dynamics have been combined to present a Markov chain model as a microsaccade-generating process with limited memory of the previous microsaccade symbols in the fixational eye movements.

References

Abadi, R. V., Clement, R. & Gowen, E. (2003). Levels of fixation. *Levels of Perception. New York: Springer*, 213–229.

Abadi, R. V., & Gowen, E. (2004). Characteristics of saccadic intrusions. *Vision Research*, *44*, 2675–2690.

Abadi, R. V., Scallan, C. J. & Clement, R. A. (2000). The characteristics of dynamic overshoots in square-wave jerks, and in congenital and manifest latent nystagmus. *Vision Research*, *40*(20), 2813–2829.

Abrams, R. A., Meyer, D. E. & Kornblum, S. (1989). Speed and accuracy of saccadic eye movements: Characteristics of impulse variability in the oculomotor system. *Journal of Experimental Psychology: Human Perception and Performance*, *15*(3), 529–543.

Adler, F. H., & Fliegelman, M. (1934). Influence of fixation on the visual acuity. *Arch Ophthal*, *12*(4), 475–483.

Antoine, J. P. (2004). *Two-dimensional wavelets and their relatives*. Cambridge University Press, Cambridge, UK.

Aristotle. (384 BC–322 BC). De anima. , *II*.

Arneodo, A., Grasseau, G. & Holschneider, M. (1988). On the wavelet transform of multifractals. *Physical Review Letters*, *61*, 2281–2284.

Bahill, A. T., Clark, M. R. & Stark, L. (1975). The main sequence, a tool for studying human eye movements. *Mathematical Biosciences*, *24*(3–4), 191–204.

Bannerman, R. L., Milders, M. & Sahraie, A. (2009). Processing emotional stimuli: Comparison of saccadic and manual choice-reaction times. *Cognition & Emotion*, *23*(5), 930–954.

Becker, W., & Jürgens, R. (1979). An analysis of the saccadic system by means of double step stimuli. *Vision Research*, *19*(9), 967–983.

Bettenbühl, M., Paladini, C., Mergenthaler, K., Kliegl, R., Engbert, R. & Holschneider, M. (2010). Microsaccade characterization using the continuous wavelet transform and principal component analysis. *Journal of Eye Movement Research*, *3(5)*(1), 1–14.

Bettenbühl, M., Rusconi, M., Engbert, R. & Holschneider, M. (2012). Bayesian selection of markov models for symbol sequences: Application to microsaccadic eye movements. *PLoS ONE*, *7*(9), e43388.

Bolger, C., Bojanic, S., Sheahan, N. F., Coakley, D. & Malone, J. F. (1999). Dominant frequency content of ocular microtremor from normal subjects. *Vision Research*, *39*(11), 1911–1915.

Boyce, P. R. (1967). Monocular fixation in human eye movement. *Proceedings of the Royal Society of London. Series B, Biological Sciences*, *167*(1008), 293–315.

Bridgeman, B., & Palca, J. (1980). The role of microsaccades in high acuity observational tasks. *Vision Research*, *20*, 813–817.

Brien, D. C., Corneil, B. D., Fecteau, J. H., Bell, A. H. & Munoz, D. P. (2009). The behavioral and neurophysiological modulation of microsaccades in monkeys. *Journal of Eye Movement Research*, *3*, 1–12.

Ciuffreda, K. J., & Tannen, B. (1995). *Eye movement basics for the clinician*. St. Louis: Mosby, Maryland, USA.

Cohen, A. S., & Studach, H. (1977). Eye movements while driving cars around curves. *Perceptual and Motor Skills*, *4*(3), 683–689.

Collewijn, H. (1998). Eye movement recording. In Carpenter, R. H. S. and Robson, J. G. (Eds.). *Vision research: A practical guide to laboratory methods*, 245–285.

Collewijn, H., & Kowler, E. (2008). The significance of microsaccades for vision and oculomotor control. *Journal of Vision*, *8*(14), 20.

Collins, T., Semroud, A., Orriols, E. & Doré-Mazars, K. (2008). Saccade dynamics before, during, and after saccadic adaptation in humans. *Investigative Ophthalmology & Visual Science*, *49*(2), 604–612.

Coppola, D., & Purves, D. (1996). The extraordinarily rapid disappearance of entopic images. *Proceedings of the National Academy of Sciences of the United States of America*, *93*, 8001–8004.

Cornsweet, T. N. (1956). Determination of the stimuli for involuntary drifts and saccadic eye movements. *Journal of the Optical Society of America*, *46*(11), 987–988.

Crane, H. D., & Steele, C. M. (1985). Generation-v dual-purkinje-image eyetracker. *Applied Optics*, *24*(4), 527–537.

Cunitz, R. J., & Steinman, R. M. (1969). Comparison of saccadic eye movements during fixation and reading. *Vision Research*, *9*(6), 683–693.

Dambacher, M., & Kliegl, R. (2007). Synchronizing timelines: Relations between fixation durations and n400 amplitudes during sentence reading. *Brain Research*, *1155*, 147–162.

Darwin, R. W., & Darwin, E. (1786). New experiments on the ocular spectra of light and colours. By Robert Waring Darwin, md; Communicated by Erasmus Darwin, md. *Philosophical Transactions of the Royal Society of London*, *76*, 313–348.

Daubechies, I. (1992). *Ten lectures on wavelets*. SIAM.

Daubechies, I., & Teschke, G. (2005). Variational image restoration by means of wavelets: simultaneous decomposition, deblurring and denoising. *Applied and Computational Harmonic Analysis*, *19*, 1–16.

Dell'Osso, L. F., Abel, L. A. & Daroff, R. B. (1977). "Inverse latent" macro square-wave jerks and macro saccadic oscillations. *Annals of Neurology*, *2*(1), 57–60.

Dell'Osso, L. F., & Daroff, R. B. (1975). Congenital nystagmus waveforms and foveation strategy. *Documenta Ophthalmologica*, *39*(1), 155–182.

Dell'Osso, L. F., & Daroff, R. B. (1999). Nystagmus and saccadic intrusions and oscillations. *Neuro-ophthalmology. Baltimore Lippincott, Williams & Wilkins*, 369–401.

Desbordes, G., & Rucci, M. (2007). A model of the dynamics of retinal activity during natural visual fixation. *Visual Neuroscience*, *24*(2), 217.

Deubel, H., & Bridgeman, B. (1995). Perceptual consequences of ocular lens overshoot during saccadic eye movements. *Vision Research*, *35*(20), 2897–2902.

Diallo, M. S., Holschneider, M., Kulesh, M., Scherbaum, F. & Adler, F. (2006). Characterization of polarization attributes of seisimic waves using continuous wavelet transforms. *Geophysics*, *71*, 67–77.

Dimigen, O., Sommer, W., Hohlfeld, A., Jacobs, A. M. & Kliegl, R. (2011). Co-registration of eye movements and EEG in natural reading: Analyses and review. *Journal of Experimental Psychology: General*, *140*, 552–572.

Ditchburn, R. W., & Ginsborg, B. L. (1952). Vision with a stabilized retinal image. *Nature*, *170*, 36–37.

Doslak, M. J., Dell'Osso, L. F. & Daroff, R. B. (1983). Multiple double saccadic pulses occurring with other saccadic intrusions and oscillations. *Neuro-ophthalmology*, *3*(2), 109–116.

Drewes, J., Montagnini, A. & Masson, G. S. (2011). Comparison of reported gaze dynamics between a scleral search coil and a video-based eye tracker. In F. Vitu, E. Castet & L. Goffart (Eds.), *Abstracts of the 16th european conference on eye movements, marseille, 21–25 august 2011* (Vol. 4(3)). Journal of Eye Movement Research.

Drieghe, D., Rayner, K. & Pollatsek, A. (2005). Eye movements and word skipping during reading revisited. *Journal of Experimental Psychology: Human Perception and Performance*, *31*(5), 954.

Eizenman, M., & Hallett, R., P. E.and Frecker. (1985). Power spectra for ocular drift and tremor. *Vision Research*, *25*(11), 1635–1640.

Engbert, R. (2006a). Flick-induced flips in perception. *Neuron*, *49*, 168–170.

Engbert, R. (2006b). Microsaccades: A microcosm for research on oculomotor control, attention, and visual perception. *Progress*

in Brain Research, *154*, 177–192. doi: 10.1016/S0079-6123(06)54009-9

Engbert, R., & Kliegl, R. (2003a). Binocular coordination in microsaccades. In *The mind's eyes: Cognitive and applied aspects of eye movements* (pp. 103–117). J. Hyönä, R. Radach & H. Deubel (Eds.), Elsevier.

Engbert, R., & Kliegl, R. (2003b). Microsaccades uncover the orientation of covert attention. *Vision Research*, *43*(9), 1035–1045.

Engbert, R., & Kliegl, R. (2004). Microsaccades keep the eyes' balance during fixation. *Psychological Science*, *15*, 431–436.

Engbert, R., & Mergenthaler, K. (2006). Microsaccades are triggered by low retinal image slip. *Proceedings of the National Academy of Sciences of the United States of America*, *103*, 7192–7197.

Engbert, R., Mergenthaler, K., Sinn, P. & Pikovsky, A. (2011). An integrated model of fixational eye movements and microsaccades. *Proceedings of the National Academy of Sciences*, *108*, E765–E770.

Farge, M., Schneider, K., Pannekoucke, O. & Nguyen van yen, R. (submitted 09/2010). Multiscale methods for fluid dynamics: fractals, self-similar random processes and wavelets. *Handbook of Environmental Fluid Dynamics*. (http://www.cmi.univ-mrs.fr/∼kschneid/PDF-FILES/wavelets_fractals_sub.pdf)

Feichtinger, H. G., & Strohmer, T. (1998). *Gabor analysis and algorithms: Theory and applications*. Birkhauser, Basel, Switzerland.

Feldon, S. E., & Langston, J. W. (1977). Square-wave jerks: A disorder of microsaccades? *Neurology*, *27*(3), 278.

Findlay, J. (1971). Frequency analysis of human involuntary eye movement. *Kybernetik*, *8*(6), 207–214.

Findlay, J. M., & Gilchrist, I. D. (2003). *Active vision: The psychology of looking and seeing*. Oxford, UK: Oxford University Press.

Frobenius, G. F. (1912). *Über matrizen aus nicht negativen elementen*. Preussische Akademie der Wissenschaften zu Berlin.

Galfano, G., Betta, E. & Turatto, M. (2004). Inhibition of return in microsaccades. *Experimental Brain Research*, *159*, 400–404.

Gowen, E., Abadi, R. V. & Poliakoff, E. (2005). Paying attention to saccadic intrusions. *Cognitive Brain Research*, *25*, 810–825.

Gowen, E., Abadi, R. V., Poliakoff, E., Hansen, P. C. & Miall, R. C. (2007). Modulation of saccadic intrusions by exogenous and endogenous attention. *Brain Res.*, *1141*, 154–167.

Grossmann, A., Kronland-Martinet, R. & Morlet, J. (1989). Reading and understanding continuous wavelet transforms. In *Wavelets: Time-frequency methods and phase space. proceedings of the first international conference on wavelets, marseille, france, december 14–18, 1987.* Combes, J. M. and Grossman, A. and Tchamitchian, P. H. (Eds.), Springer Verlag, Berlin, Germany.

Grossmann, A., & Morlet, J. (1985). Decomposition of functions into wavelets of constant shape, and related transforms. In L. Streit (Ed.), *Mathematics + Physics, Lectures on Recent Results* (Vol. 1). World Scientific.

Hafed, Z. M. (2011). Mechanisms for generating and compensating for the smallest possible saccades. *European Journal of Neuroscience*, *33*(11), 2101–2113.

Hafed, Z. M., & Clark, J. J. (2002). Microsaccades as an overt measure of covert attention shifts. *Vision Research*, *42*, 2533–2545.

Hafed, Z. M., Goffart, L. & Krauzlis, R. J. (2009). A neural mechanism for microsaccade generation in the primate superior colliculus. *Science*, *323*(5916), 940–943.

Harris, C. M., & Wolpert, D. M. (1998). Signal-dependent noise determines motor planning. *Nature*, *394*(6695), 780–784.

Harris, M., & Wolpert, M. (2006). The main sequence of saccades optimizes speed-accuracy trade-off. *Biological Cybernetics*, *95*(1), 21–29.

Hermens, F., & Walker, R. (2010). What determines the direction of microsaccades? *Journal of Eye Movement Research*, *3(4):1*, 1–20.

Hertzsprung, E. (1911). Ueber die verwendung photographischer effektiver wellenlaengen zur bestimmung von farbenaequivalenten. *Publikationen des Astrophysikalischen Observatoriums zu Potsdam*, *63*.

Higgins, K. F., G. C.and Stultz. (1953). Frequency and amplitude of ocular tremor. *Journal of the Optical Society of America*, *43*(12), 1136–1140.

Holschneider, M. (1988). On the wavelet transformation of fractal objects. *Journal of Statistical Physics*, *50*(5), 963–993.

Holschneider, M. (1995). *Wavelets: An analysis tool*. Oxford University Press, Oxford, UK.

Holschneider, M., & Tchamitchian, P. (1991). Pointwise analysis of Riemann's "nondifferentiable" function. *Inventiones Mathematicae*, *105*, 157–175.

Horowitz, T. S., Fencsik, D. E., Fine, E. M., Yurgenson, S. & Wolfe, J. M. (2007). Microsaccades and attention: Does a weak correlation make an index? Reply to Laubrock, Engbert, Rolfs, and Kliegl (2007). *Psychological Science*, *18*, 367–368.

Horowitz, T. S., Fine, E. M., Fencsik, D. E., Yurgenson, S. & Wolfe, J. M. (2007). Fixational eye movements are not an index of covert attention. *Psychological Science*, *18*, 356–363.

Hurst, H., Black, R. & Simaika, Y. (1965). *Long-term storage: An experimental study*. Constable, London, UK.

Jaffard, S. (1989). Construction of wavelets on open sets. In *Wavelets. time-frequency methods and phase space. proceedings of the first international conference on wavelets, marseille, france, december 14–18, 1987.* (Vol. 1, pp. 247–252). Combes, J. M. and Grossman, A. and Tchamitchian, P. H. (Eds.), Springer Verlag, Berlin, Germany.

Javal, L. E. (1879). Essai sur la physiologie de la lecture. *Annales d'Oculistique*, *82*, 242–253.

Jeffreys, H. (1998). *Theory of probability*. Oxford: Oxford University Press.

Jolliffe, I. T. (2002). *Principal component analysis*. Springer Verlag, Berlin/ Heidelberg, Germany.

Jung, R., & Kornhuber, H. H. (1964). Results of electronystagmography in man: the value of optokinetic, vestibular, and spontaneous nystagmus for neurologic diagnosis and research. *The oculomotor system*, 428–488.

Jurin, J. (1738). An essay upon distinct and indistinct vision. *In R.Smith (Ed.): Compleate system of opticks in four books*.

Kapoula, Z. A., Robinson, D. A. & Hain, T. C. (1986). Motion of the eye immediately after a saccade. *Experimental Brain Research*, *61*(2), 386–394.

Kass, R. E., & Raftery, A. E. (1995). Bayes factors. *Journal of the American Statistical Association*, 773–795.

Kliegl, R., Dambacher, M., Dimigen, O., Jacobs, A. M. & Sommer, W. (2011). Eye movements and brain electric potentials during reading. *Psychological Research*, *76*(2), 145–158.

Kohama, T., & Usui, S. (2002). Attentional effects on microsaccadic eye movements. *Cahiers de psychologie cognitive*, *21*(4–5), 377–395.

Kowler, E. (2011). Eye movements: The past 25 years. *Vision Research*, *51*(13), 1457–1483.

Kowler, E., & Steinman, R. M. (1979). Miniature saccades: eye movements that do not count. *Vision Research*, *19*(1), 105.

Krauskopf, J., Cornsweet, T. N. & Riggs, L. A. (1960). Analysis of eye movements during monocular and binocular fixation. *Journal of the Optical Society of America*, *50*, 572–578.

Krauzlis, R. J. (2005). The control of voluntary eye movements: New perspectives. *The Neuroscientist*, *11*(2), 124–137.

Kulesh, M., Diallo, M. S. & Holschneider, M. (2005). Wavelet analysis of ellipticity, dispersion, and dissipation properties of rayleigh waves. *Acoustical Physics (original version Russian with English transl.)*, *51*(4), 425–434.

Lamare, M. (1892). Des mouvements des yeux dans la lecture. *Bulletins et Memoires de la Societe Francaise d'Ophtalmologie*, *10*, 354–364.

Land, M., Mennie, N. & Rusted, J. (1999). The roles of vision and eye movements in the control of activities of daily living. *Perception*, *28*(11), 1311–1328.

Land, M., & Nilsson, D. E. (2002). *Animal eyes*. Oxford University Press, Oxford, UK.

Laubrock, J., Engbert, R., Rolfs, M. & Kliegl, R. (2007). Microsaccades are an index of covert attention: commentary on horowitz, fine, fencsik, yurgenson, and wolfe (2007). *Psychological Science*, *18*, 364–366.

Laubrock, J., Kliegl, R., Rolfs, M. & Engbert, R. (2010). When do microsaccades follow attention? *Attention, Perception, & Psychophysics*, *72*, 683–694.

Laubrock, R., Engbert, R. & Kliegl, R. (2005). Microsaccade dynamics during covert attention. *Vision Research*, *45*, 721–730.

Leigh, R. J., & Zee, D. S. (1999). *The neurology of eye movements* (No. 55). Oxford: Oxford University Press.

Liang, J.-R., Moshel, S., Zivotofsky, A. Z., Caspi, A., Engbert, R., Kliegl, R. & Havlin, S. (2005). Scaling of horizontal and vertical fixational eye movements. *Physical Review E*, *71*, 031909.

Lind, D., & Marcus, M. (1995). *An introduction to symbolic dynamics and coding*. Cambridge University Press.

Liversedge, S., Gilchrist, I. & Everling, S. (2011). *Oxford handbook of eye movements*. Oxford: Oxford University Press, Oxford, UK.

Mallat, S. (1998). *A wavelet tour of signal processing*. Academic Press, New York, USA.

Mallat, S., & Hwang, W. L. (1992). Singularity detection and processing with wavelets. *IEEE Transactions on Information Theory*, *38*, 617–643.

Mammo, D., Kimmel, D. L. & Newsome, W. T. (2011). Tracking eye position non-invasively: Comparing the scleral seach coil and optical techniques. In *Program no. 489.09 2011 neuroscience meeting planner. online.* Washington, DC.

Mandelbrot, B. B. (1982). *The fractal geometry of nature*. New York, USA: W. H. Freedman and Co.

Mandelbrot, B. B., & Van Ness, J. W. (1968). Fractional brownian motions, fractional noises and applications. *SIAM review*, *10*(4), 422–437.

Markov, A. A. (1971). Extension of the limit theorems of probability theory to a sum of variables connected in a chain. In (pp. 552–

577). Reprinted in Howard, R. (Ed.): Dynamic Probabilistic Systems (vol. 1), John Wiley & Sons, Inc., New Jersey, USA.

Marr, D., & Hildreth, E. (1980). Theory of edge detection. *Proceedings of the Royal Society of London. Series B. Biological Sciences*, *207*, 187–217. doi: 10.1098/rspb.1980.0020

Martinez-Conde, S., Macknik, S. L. & Hubel, D. H. (2000). Microsaccadic eye movements and firing of single cells in the striate cortex of macaque monkeys. *Nature Neuroscience*, *3*, 251–258.

Martinez-Conde, S., Macknik, S. L. & Hubel, D. H. (2004). The role of fixational eye movements in visual perception. *Nature Reviews Neuroscience*, *5*, 229–240.

Martinez-Conde, S., Macknik, S. L., Troncoso, X. G. & Dyar, T. A. (2006). Microsaccades counteract visual fading during fixation. *Neuron*, *49*, 297–305.

Martinez-Conde, S., Macknik, S. L., Troncoso, X. G. & Hubel, D. H. (2009). Microsaccades: A neurophysiological analysis. *Trends in Neuroscience*, *32*, 463–475.

Matin, L., Matin, E. & Pearce, D. G. (1970). Eye movements in the dark during the attempt to maintain a prior fixation position. *Vision Research*, *10*(9), 837–857.

McConkie, G. W., Kerr, P. W., Reddix, M. D., Zola, D. & Jacobs, A. M. (1989). Eye movement control during reading: Ii. frequency of refixating a word. *Attention, Perception, & Psychophysics*, *46*(3), 245–253.

Mergenthaler, K. (2009). *The control of fixational eye movements*. PhD thesis, University of Potsdam, Germany. Retrieved from `http://opus.kobv.de/ubp/volltexte/2009/2939/` (URN: urn:nbn:de:kobv:517-opus-29397)

Mergenthaler, K., & Engbert, R. (2007). Modeling the control of fixational eye movements with neurophysiological delays. *Physical Review Letters*, *98*(13), 138104.

Mergenthaler, K., & Engbert, R. (2010). Microsaccades are different from saccades in scene perception. *Experimental Brain Research*, *203*(4), 753–757.

Møller, F., Laursen, M., Tygesen, J. & Sjølie, A. (2002). Binocular quantification and characterization of microsaccades. *Graefe's Archive for Clinical and Experimental Ophthalmology*, *240*(9), 765–770.

Moschovakis, A. K., Scudder, C. A. & Highstein, S. M. (1996). The microscopic anatomy and physiology of the mammalian saccadic system. *Progress in Neurobiology*, *50*(2–3), 133–254.

Mould, M. S., Foster, D. H., Amano, K. & Oakley, J. P. (2011). A simple non-parametric method for classifying eye fixations. *Journal of Vision*, *11*(11), 506.

Munoz, D. P., & Everling, S. (2004). Look away: the anti-saccade task and the voluntary control of eye movement. *Nature Reviews Neuroscience*, *5*(3), 218–228.

Munoz, D. P., & Wurtz, R. H. (1993). Fixation cells in monkey superior colliculus. i. characteristics of cell discharge. *Journal of Neurophysiology*, *70*(2), 559–575.

Nachmias, J. (1959). Two-dimensional motion of the retinal image during monocular fixation. *Journal of the Optical Society of America*, *49*(9), 901–907.

Nyström, M., & Holmqvist, K. (2010). An adaptive algorithm for fixation, saccade, and glissade detection in eyetracking data. *Behavior Research Methods*, *42*(1), 188–204.

Omori, T., Sato, M., Yamauchi, K., Ishikawa, S. & Wakita, T. (2009). Computational modeling of risk-dependent eye movements of car drivers. In *Systems, man and cybernetics, 2009. smc 2009. ieee international conference on advances in neuro-information processing* (pp. 2457–2461).

Oppenheim, A. V., Schafer, R. W., Buck, J. R. et al. (1989). *Discrete-time signal processing* (Vol. 2). Prentice Hall Englewood Cliffs, New Jersey, USA.

Otero-Millan, J., Macknik, S., Serra, A., Leigh, R. & Martinez-Conde, S. (2011). Triggering mechanisms in microsaccade and saccade generation: a novel proposal. *Annals of the New York Academy of Sciences*, *1233*(1), 107–116.

Otero-Millan, J., Serra, A., Leigh, R. J., Troncoso, X. G., Macknik, S. L. & Martinez-Conde, S. (2011). Distinctive features of saccadic intrusions and microsaccades in progressive supranuclear palsy. *The Journal of Neuroscience*, *31*(12), 4379.

Otero-Millan, J., Troncoso, X. G., Macknik, S. L., Serrano-Pedraza, I. & Martinez-Conde, S. (2008). Saccades and microsaccades during visual fixation, exploration, and search: foundations for a common saccadic generator. *Journal of Vision*, *8*(14).

Pearson, K. (1901). On lines and planes of closest fit to systems of points in space. *Philosophical Magazine*, *2*(6), 559–572.

Perron, O. (1907). Zur theorie der matrices. *Mathematische Annalen*, *64*(2), 248–263.

Poletti, M., Listorti, C. & Rucci, M. (2010). Stability of the visual world during eye drift. *The Journal of Neuroscience*, *30*(33), 11143–11150.

Pritchard, R. M. (1961). Stabilized images on the retina. *Scientific American*, *204*, 72–78.

Quiroga, R. Q., Nadasdy, Z. & Ben-Shaul, Y. (2004). Unsupervised spike detection and sorting with wavelets and superparamagnetic clustering. *Neural Computation*, *16*, 1661–1687.

Ratliff, F., & Riggs, L. A. (1950). Involuntary motions of the eye during monocular fixation. *Journal of Experimental Psychology*, *40*(6), 687–701.

Rayner, K. (1978). Eye movement latencies for parafoveally presented words. *Bulletin of the Psychonomic Society*, *11*, 13–16.

Rayner, K., Miller, B. & Rotello, C. M. (2008). Eye movements when looking at print advertisements: the goal of the viewer matters. *Applied Cognitive Psychology*, *22*(5), 697–707.

Rieke, F., Warland, D. & Bialek, W. (1997). *Spikes: Exploring the neural code*. Cambridge, USA: MIT Press.

Riggs, L. A., Ratliff, F., Cornsweet, J. C. & Cornsweet, T. (1953). The disappearance of steadily fixated visual test objects. *Journal of the Optical Society of America*, *43*, 495–501.

Robinson, F. R., & Fuchs, A. F. (2001). The role of the cerebellum in voluntary eye movements. *Annual Review of Neuroscience*, *24*(1), 981–1004.

Rolfs, M. (2009). Microsaccades: small steps on a long way. *Vision Research*, *49*, 2415–2441.

Rolfs, M., Engbert, R. & Kliegl, R. (2005). Crossmodal coupling of oculomotor control and spatial attention in vision and audition. *Experimental Brain Research*, *166*, 427–439.

Rolfs, M., Kliegl, R. & Engbert, R. (2008). Toward a model of microsaccade generation: The case of microsaccadic inhibition. *Journal of Vision*, *8(11)*, 1–23.

Rolfs, M., Laubrock, J. & Kliegl, R. (2006). Shortening and prolongation of saccade latencies following microsaccades. *Experimental Brain Research*, *169*, 369–376.

Rucci, M. (2008). Fixational eye movements, natural image statistics, and fine spatial vision. *Network: Computation in Neural Systems*, *19*(4), 253–285.

Rucci, M., & Casile, A. (2004). Decorrelation of neural activity during fixational instability: Possible implications for the refinement of V1 receptive fields. *Visual Neuroscience*, *21*, 725–738.

Rucci, M., Iovin, R., Poletti, M. & Santini, F. (2007). Miniature eye movements enhance fine spatial detail. *Nature*, *447*, 852–855.

Russell, H. N. (1913). Giant and dwarf stars. *The Observatory*, *36*, 324–329.

Schall, J. D., & Thompson, K. G. (1999). Neural selection and control of visually guided eye movements. *Annual Review of Neuroscience*, *22*(1), 241–259.

Schulz, E. (1984). Binocular micromovements in normal persons. *Graefe's archive for clinical and experimental ophthalmology*, *222*(2), 95–100.

Scudder, C. A., Kaneko, C. R. & Fuchs, A. F. (2002). The brainstem burst generator for saccadic eye movements: a modern synthesis. *Experimental Brain Research*, *142*, 439–462.

Shallo-Hoffmann, J., Petersen, J. & Mühlendyck, H. (1989). How normal are "normal" square wave jerks? *Investigative Ophthalmology & Visual Science*, *30*(5), 1009–11.

Sharpe, J. A., & Fletcher, W. A. (1986). Disorders of visual fixation. In *Neuro-ophthalmology now!* (pp. 267–284). In Lawton Smith, J. (Ed.), Field, Rich and Assoc., Chicago, USA.

Silverman, B. W. (1986). *Density estimation for statistics and data analysis* (Vol. 26). Chapman & Hall/CRC, London, UK.

Sinn, P., & Engbert, R. (2011). Saccadic facilitation by modulation of microsaccades in natural backgrounds. *Attention, Perception, & Psychophysics*, *73*(4), 1029–1033.

Smith, L. I. (2002). *A tutorial on principal components analysis* (Tech. Rep.). Cornell University, USA.

Snellen, H., & Landolt, E. (1874a). Ophthalmometrologie. Die Funktionsprüfung des Auges: I. Eidoptometrie (Bestimmung der Sehschärfe). In *Handbuch der gesamten augenheilkunde (vol.3)* (pp. 1–22). In von Graefe, A. & Saemisch, E. T. (Eds.), Engelmann. Leipzig, Germany.

Snellen, H., & Landolt, E. (1874b). Perioptometrie. In *Handbuch der gesamten augenheilkunde (vol.3)* (p. 52 ff.). In von Graefe, A. & Saemisch, E. T. (Eds.), Engelmann. Leipzig, Germany.

Sparks, D. L. (2002). The brainstem control of saccadic eye movements. *Nature Reviews Neuroscience*, *3*(12), 952–964.

Sparks, D. L., & Mays, L. E. (1990). Signal transformations required for the generation of saccadic eye movements. *Annual Review of Neuroscience*, *13*(1), 309–336.

Spencer, T. S., & Mamalis, N. (2010). The pathology of cataract. In *Cataract surgery, 3rd edition* (pp. 4–5). In Steinert, R. F. (Ed.), Saunders, Philadelphia, USA. Imprint of Elsevier.

Stampe, D. M. (1993). Heuristic filtering and reliable calibration methods for video-based pupil-tracking systems. *Behavior Research Methods*, *25*, 137–142.

Starzynski, C., & Engbert, R. (2009). Noise-enhanced target discrimination under the influence of fixational eye movements and external noise. *Chaos*, *19*, 015112: 1–7.

Taylor, H. M., & Karlin, S. (1984). *An introduction to stochastic modeling*. New York: Academic Press, New York, USA.

't Hart, B. M., & Einhäuser, W. (2011). Eye-tracking in the laboratory and in real life. In *Program no. 176.24 2011 neuroscience meeting planner. online.* Washington, DC.

Theiler, J., Galdrikian, B., Longtin, A., Eubank, S. & Farmer, J. D. (1992). Testing for nonlinearity in time series: the method of surrogate data. *Physica D: Nonlinear Phenomena*, *58*, 77–94.

Thilo, K. V., Santoro, L., Walsh, V. & Blakemore, C. (2004). The site of saccadic suppression. *Nature Neuroscience*, *7*(1), 13–14. doi: 10.1038/nn1171

Torrence, C., & Compo, G. P. (1998). A practical guide to wavelet analysis. *Bulletin of the American Meteorological Society*, *79*(1), 61–78.

Troncoso, X. G., Macknik, S. L. & Martinez-Conde, S. (2008). Microsaccades counteract perceptual filling-in. *Journal of Vision*, *8*(14), 1–9.

Trukenbrod, H. A., & Engbert, R. (2007). Oculomotor control in a sequential search task. *Vision Research*, *47*(18), 2426–2443.

Trukenbrod, H. A., & Engbert, R. (2012). Eye movements in a sequential scanning task: Evidence for distributed processing. *Journal of Vision*, *12*(1), 5.

Tu, C., Hwang, W. & Ho, J. (2005). Analysis of singularities from modulus maxima of complex wavelets. *IEEE Transactions on Information Theory*, *51*(3), 1049–1062.

Van Gisbergen, J. A., Robinson, D. A. & Gielen, S. (1981). A quantitative analysis of generation of saccadic eye movements by burst neurons. *Journal of Neurophysiology*, *45*(3), 417–42.

Van Horn, M. R., & Cullen, K. E. (2012). Coding of microsaccades in three-dimensional space by premotor saccadic neurons. *The Journal of Neuroscience*, *32*(6), 1974–1980.

von Helmholtz, H. (1867). *Handbuch der physiologischen optik: mit 213 in den text eingedruckten holzschnitten und 11 tafeln* (Vol. 9). Leipzig, Germany: Voss.

Wade, N., & Tatler, B. (2005). *The moving tablet of the eye: The origins of modern eye movement research*. Oxford University Press, USA.

Weaver, M. D., Lauwereyns, J. & Theeuwes, J. (2011). The effect of semantic information on saccade trajectory deviations. *Vision Research*, *51*(10), 1124–1128.

Witkin, A. P. (1983). Scale-space filtering. In *Ijcai'83: Proceedings of the eighth international joint conference on artificial intelligence* (pp. 1019–1022).

Wurtz, R. H., & Goldberg, M. (1989). *The neurobiology of saccadic eye movements*. Elsevier Publishing Company, Amsterdam, Netherlands.

Wurtz, R. H., Goldberg, M. E. & Robinson, D. L. (1982). Brain mechanisms of visual attention. *Scientific American*, *246*(6), 124–135.

Wurtz, R. H., & Optican, L. M. (1994). Superior colliculus cell types and models of saccade generation. *Current Opinion in Neurobiology*, *4*(6), 857–861.

Zuber, B. L., Stark, L. & Cook, G. (1965). Microsaccades and the velocity-amplitude relationship for saccadic eye movements. *Science*, *150*, 1459–1460.

The first thing we do upon waking is open our eyes. Rotating them in our eye sockets, we scan our surroundings and collect the information into a picture in our head. Eye movements can be split into saccades and fixational eye movements, which occur when we attempt to fixate our gaze. The latter consists of microsaccades, drift and tremor. Before we even lift our eye lids, eye movements – such as saccades and microsaccades that let the eyes jump from one to another position – have partially been prepared in the brain stem. Saccades and microsaccades are often assumed to be generated by the same mechanisms. But how saccades and microsaccades can be classified according to shape has not yet been reported in a statistical manner. Research has put more effort into the investigations of microsaccades' properties and generation only since the last decade. Consequently, we are only beginning to understand the dynamic processes governing microsaccadic eye movements. Within this thesis, the dynamics governing the generation of microsaccades is assessed and the development of a model for the underlying processes. Eye movement trajectories from different experiments are used, recorded with a video-based eye tracking technique, and a novel method is proposed for the scale-invariant detection of saccades (events of large amplitude) and microsaccades (events of small amplitude). Using a time-frequency approach, the method is examined with different experiments and validated against simulated data. A shape model is suggested that allows for a simple estimation of saccade- and microsaccade related properties. For sequences of microsaccades, in this thesis a time-dynamic Markov model is proposed, with a memory horizon that changes over time and which can best describe sequences of microsaccades.

ISSN 2190-4545
ISBN 978-3-86956-122-6